Université du Québec
Institut national de la recherche scientifique
Centre Armand-Frappier Santé Biotechnologie

Exploiting furan-maleimide Diels-Alder linkages for the functionalization of organoruthenium complexes

Par

Hoang-Van Tran

Mémoire présenté pour l'obtention du grade de
Maître ès Sciences (M. Sc.)
en sciences de Sciences expérimentales de la santé

Jury d'évaluation

Président du jury et examinateur interne	Prof. Charles Gauthier INRS - Centre Armand-Frappier Santé Biotechnologie
Examinateur externe	Prof. Jung Kwon (John) Oh Concordia University
Directrice de recherche	Prof. Annie Castonguay INRS- Centre Armand Frappier Santé Biotechnologie

ACKNOWLEDGEMENTS

Foremost, I would like to express my sincere gratitude to my supervisor **Prof. Annie Castonguay** for the continuous support for my Master's study and research, for her patience, motivation, and enthusiasm. Her guidance helped me in almost the time of research and writing of this thesis.

I am very grateful to **Prof. Charles Gauthier** for sharing the materials and instruments necessary for carrying out my experiments and for evaluating this thesis and **Prof. John Oh** for his acceptance of judging this thesis as an external examiner.

My sincere thanks also go to professors **David Chatenet** and **Isabelle Plante** for providing human cancer cell lines for biological experiments, professors **Charles Ramassamy**, **Nicolas Doucet**, **Steve Laplante**, and **Salim Islam** for sharing their lab and instruments with us.

I thank all my fellow labmates in the Castonguay group: **Dr. Mohammad Mehdi Hagdoost**, **Dr. Golara Golbaghi**, **Dr. Hala Elsamy**, **Robin Vidal** and **Dr. Ahmed Shabana**, and the scientists at INRS, especially **Myriam Letourneau**, **Marianne Piochon** and **Sylvain Milot** for their technical, scientific, and moral contributions during my study at INRS.

This thesis is dedicated to:

My mother, **my father**, and **my sister**, for their understanding, belief, and support during my study at INRS.

And **Quynh**, **my love**, for her continuous support and helping me prepare the manuscripts and this thesis.

RÉSUMÉ

Les cycloadditions de Diels-Alder (DA) de furanes et maléimides sont largement utilisées en chimie de synthèse. La réversibilité thermique de cette réaction a été exploitée depuis de nombreuses années en synthèse organique et des matériaux, utilisant des températures élevées. Récemment, des groupes de recherches, incluant le nôtre, ont montré que la réaction de rétro Diels-Alder (rDA) des adduits endo peut se produire à la température du corps, faisant des liaisons de type DA une avenue prometteuse pour le développement de systèmes de livraison thermo-stimulés. Ces systèmes pourraient donc faciliter le transport de molécules thérapeutiques fonctionnalisées avec des agents de ciblage ou de pénétration cellulaire pour l'atteinte d'une cible biologique. Ce domaine de recherche en est encore à un stade embryonnaire et, à notre connaissance, le potentiel des médicaments à base de métaux contenant une liaison de type DA n'a jusqu'à présent que rarement été examiné. Étant donné que des complexes d'organoruthénium ont engendré des avancées intéressantes pour le traitement du cancer, l'objectif de ce mémoire est d'explorer la possibilité d'utiliser la liaison DA comme un outil pour moduler les propriétés biologiques de tels complexes. Les résultats rapportés dans ce mémoire fournissent des informations importantes qui pourront ouvrir la porte au développement et à la conception de nouveaux médicaments conjugués plus efficaces ou à des systèmes de livraison thermo-stimulés comportant des médicaments à base de ruthénium ou d'autres métaux.

Mots-clés : complexes organoruthénium, médicaments anticancéreux, réaction de Diels-Alder, réaction de rétro Diels-Alder, liaison thermo-sensible, système de livraison de médicaments thermo-stimulé, libération de médicaments contrôlée.

ABSTRACT

Diels-Alder cycloadditions involving furans and maleimides are extensively used in synthetic chemistry. The thermoreversibility of this reaction has been widely exploited for many years in organic and material synthetic chemistry using elevated temperatures. More recently, we and others have shown that retro Diels-Alder (rDA) reactions of endo adducts can take place at biologically-relevant temperatures, making DA-type linkages a promising tool for the stimuli-responsive delivery of drugs/drug candidates functionalized with targeting or cell-penetrating agents. This field of research is still in its infancy, and to our knowledge, the potential of DA-containing metal-based drugs/drug candidates has so far only scarcely been examined. Given the promising advances of organoruthenium complexes in cancer therapy, this thesis aims to explore the possibility of exploiting DA linkages as a means to modulate the biological properties of such complexes. The research findings reported in this thesis provide important information that will pave the way to the development/design of improved drug conjugates or delivery systems involving ruthenium- or other metal-based drugs/drug candidates.

Keywords: organoruthenium complex, anticancer drug, Diels-Alder reaction, retro Diels-Alder reaction, thermosensitive linkage, stimuli-responsive drug delivery, controlled-release drug.

SOMMAIRE RÉCAPITULATIF

Les cycloadditions de Diels-Alder (DA) impliquant des furanes et des maléimides sont largement utilisées en chimie de synthèse. De plus, les furanes et les maléimides font partie de la structure de divers médicaments. Parmi de nombreux exemples, les composés contenant le groupe maléimide dans leur structure peuvent mener à l'épuisement intracellulaire de glutathion, un mode d'action anticancéreux bien connu. La réversibilité thermique de cette réaction a été exploitée depuis de nombreuses années en synthèse organique et des matériaux utilisant des températures élevées. Plus récemment, diverses équipes de recherche incluant la nôtre ont montré que la réaction de rétro Diels-Alder (rDA) des adduits endo peut se produire à la température du corps humain, rendant les liaisons de type DA très prometteuses pour le développement de systèmes de livraison thermo-stimulés pouvant faciliter le transport de molécules thérapeutiques fonctionnalisées couplées à un agent de ciblage ou de pénétration cellulaire pour permettre l'atteinte de leur cible. Ce domaine de recherche en est encore à un stade embryonnaire et, à notre connaissance, le potentiel des médicaments à base de métal contenant des liaisons de type DA n'a jusqu'à présent que rarement été examiné.

Les complexes d'organoruthénium ont généré des avancées encourageantes pour le traitement du cancer et l'objectif de ce mémoire est d'explorer la possibilité d'utiliser la liaison DA comme un outil pour moduler les propriétés biologiques de tels complexes. Tout au long de cette étude, nous avons développé des voies de synthèse vers des complexes de Ru portant des liaisons DA à base de furanes et de maléimides et également étudié leur réactivité/stabilité dans des conditions biologiques.

Dans la première voie synthétique, nous avons préparé d'abord le ligand *N*,*N*-triazole **1** contenant du furane qui a été préparé par une cycloaddition d'alcyne et d'azide catalysée par le Cu (CuAAC). Par la suite, la réaction du ligand **1** avec $[Ru(\eta^6\text{-}C_6H_6)Cl_2]_2$ et NH_4BF_4 dans l'éthanol à reflux (Schéma 1) a conduit à la formation du complexe cationique de ruthénium **3**, qui a été isolé avec un rendement élevé. La réaction pouvait également se poursuivre à température ambiante, mais avec un temps de réaction prolongé. Le complexe s'est avéré soluble dans la plupart des solvants organiques. Notamment, **3** s'est également avéré stable lorsque que maintenu à 65 °C pendant cinq

jours dans de l'acétone ou de l'acétonitrile (9 mM), car seules des traces de benzène libre ont été détectées par RMN-^{1}H.

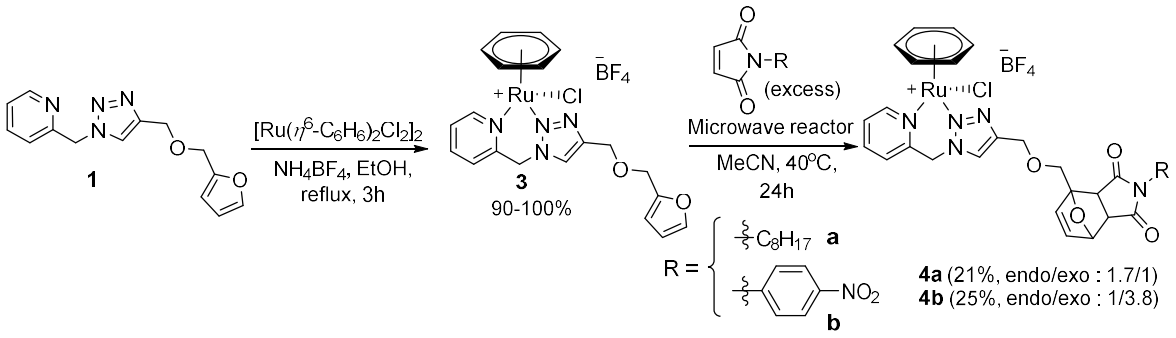

Schéma 1. Voie synthétique initiale utilisée pour l'obtention des complexes de ruthénium **4a** et **4b** : cycloaddition de Diels-Alder réalisée sur le complexe (comme étape finale).

Ensuite, une réaction de DA entre ce complexe et des maléimides portant deux substituants différents, notamment une chaîne alkyle, considérée comme un groupement à effet inductif donneur, et un cycle phényle substitué par un groupement nitro, considéré comme un groupement à effets mésomères attracteurs, a été entreprise. En fait, nous avons estimé que la sélection de maléimides d'une nature électronique différente pourrait aider à confirmer l'impact de tels substituants sur la capacité des maléimides à subir une réaction DA, mais permettrait également d'évaluer leur influence sur le désassemblage (la réaction rDA) des complexes qui se produit dans des conditions biologiques. La réaction du complexe **3** avec un grand excès (30 eq) de maléimide de *N*-octyle et de maléimide de *N*-*p*-nitrophényle, respectivement, a été suivie à l'aide de la spectroscopie RMN-^{1}H et des rendements de réaction ont été obtenus à l'aide d'un étalon interne. Lorsque la réaction a été réalisée à température ambiante dans l'acétone-d_6 pendant un jour, les complexes **4a** et **4b** (schéma 1) ont été obtenus avec des rendements très faibles (**4a** : 17 %, **4b** : 15 %). L'augmentation de la température à 65 °C a considérablement amélioré le rendement de réaction pour les deux complexes (**4a** : 75 %, **4b** : 70 %). Comme prévu, un mélange des adduits endo et exo a été observé aux deux températures. L'endo-régio-isomère (produit cinétique) s'est avéré prédominant dans les deux cas lorsque la réaction a été réalisée à température ambiante (**4a$_{endo}$/4a$_{exo}$** : 3, **4b$_{endo}$/4b$_{exo}$** : 5), considérant que l'exo régio-isomère (produit thermodynamique) s'est avéré prédominant lorsque la réaction a été effectué à des températures plus élevées (**4a$_{endo}$/4a$_{exo}$** : 0,8, **4b$_{endo}$/4b$_{exo}$** : 0,3). Il convient de noter que la prédominance de l'isomère examinée ci-dessus s'est avérée plus prononcée pour le

diénophile porteur d'un substituant à effet attracteur, à savoir le *N*-*p*-nitrophényle, tel qu'indiqué dans les rapports précédents. Quand ces réactions ont été effectuées à 40 °C dans l'acétone pendant cinq jours, le rendement réactionnel des deux complexes a été doublé (83 %) par rapport aux réactions réalisées en un jour dans les mêmes conditions. Parmi les solvants qui sont généralement utilisés pour effectuer des réactions de DA, il a été noté que l'acétone et l'acétonitrile entraînaient des rendements plus élevés que le chloroforme ou le méthanol (temps de réaction d'un jour). Une solubilité plus élevée des substrats dans ces solvants pourrait peut-être expliquer cette observation. De plus, il a été constaté qu'un rendement relativement élevé pouvait être obtenu en seulement une journée lorsque la réaction était réalisée dans un réacteur à micro-ondes (6,5 W) dans de l'acétonitrile à 40 °C **(4a** : 75 %, **4b** : 70 %). Cependant, malgré les conversions élevées observées par RMN du proton, l'isolement des complexes est resté très difficile, car l'utilisation de méthodes chromatographiques a conduit à une perte importante du produit dans les deux cas (**4a** : 21 %, **4b** : 25 %), et les tentatives de séparation des complexes endo et exo n'ont pas été couronnées de succès.

Une stratégie alternative pour la synthèse de **4a** et **4b** a donc été tentée en effectuant la réaction DA sur les ligands avant leur complexation (Schéma 2). En suivant cette voie, les ligands **2a** et **2b** ont pu être obtenus avec des rendements élevés (**2a** : 93 %, **2b** : 82 %) en faisant réagir le ligand **1** avec le maléimide de *N*-octyle ou de *N*-*p*-nitrophényle en utilisant les conditions réactionnelles DA précédemment optimisées pour l'irradiation aux micro-ondes. Il est à noter que la conversion plus élevée et la légère augmentation du rapport endo/exo régio-isomère constatées après 24h lorsque la réaction DA a été réalisée sur le ligand (Schéma 2) par rapport à lorsqu'elle a été réalisée sur le complexe dans les mêmes conditions indique que le centre cationique du ruthénium pourrait potentiellement exercer un effet d'attraction d'électrons au niveau du groupement furane. Les complexes **4a** et **4b** ont ensuite été synthétisés (**4a** : 90 %, **4b** : 85 %) en faisant réagir le $[Ru(\eta^6\text{-}C_6H_6)Cl_2]_2$ avec les ligands DA **2a** et **2b**, respectivement, à température ambiante, en présence du sel de NH_4BF_4. Aucun désassemblage considérable du ligand DA (rDA) n'a été observé. En dépit de l'avantage des rendements réactionnels plus élevés obtenus, un autre avantage considérable de l'utilisation de cette stratégie alternative est que la synthèse directe des complexes endo et exo de **4a** pourrait également être réalisée, car les adduits endo et exo du ligand **2a** pourraient être isolés par HPLC semi-préparative en phase inverse avant la préparation

de **4a**. De manière intéressante, l'analyse HPLC des adduits endo et exo de **4a** et **4b** (avec de l'acide trifluoroacétique à 0,1 %) a révélé la présence d'un mélange équimolaire de deux espèces distinctes dans le cas de l'endo **4a**. Ces pics ont été attribués à un mélange de deux endo-stéréo-isomères de **4a** (tel que montré par ESI-MS) pour lequel le contre-ion a été remplacé par du trifluoroacétate au cours de l'analyse, un processus corroboré par l'absence de signal dans le spectre RMN-^{19}F enregistré après l'analyse.

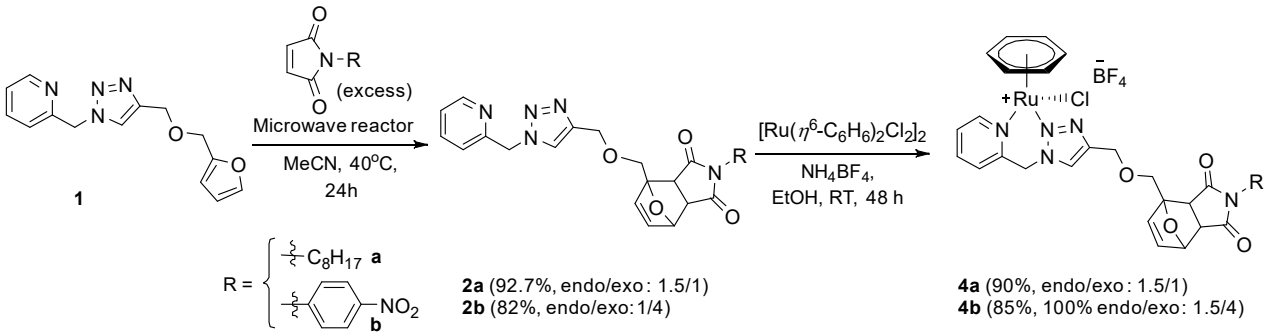

Schéma 2. Voie synthétique alternative utilisée pour la synthèse des complexes de ruthénium **4a** et **4b** : cycloaddition de Diels-Alder réalisée sur le ligand **1** (comme étape initiale).2

Tous les complexes ont été caractérisés par RMN-^{1}H-, -^{13}C et -^{19}F et HR-ESI-MS. Par rapport au ligand **1**, le spectre RMN-^{1}H du complexe **3** (dans l'acétone-d_6) présentait *i)* un décalage significatif vers le bas des fréquences pour plusieurs pics, notamment pour celles à proximité du centre cationique du ruthénium (voir figure 1 : le proton H_k de la fraction pyridine, les deux protons H_g du groupe méthylène et le H_f du cycle triazole), *ii)* l'apparition d'un singulet à 6,24 ppm, caractéristique des protons équivalents d'un cycle arène coordonné, et *iii)* l'émergence d'un système de spin AB (δ 5,96 et 6,30 ppm, 2 d, J = 15,8 Hz) pour les protons H_g du groupe méthylène. Lors de la formation des complexes **4a** et **4b** (réaction DA avec chaque maléimide), le proton H_a (δ 7,54 ppm, dd, J = 1,9, 0,8 Hz) du cycle furane du complexe **3** a été remplacé par de nouveaux signaux dans la région 5,0-5,5 ppm, qui ont été attribués respectivement aux adduits DA endo et exo. Ces changements chimiques se sont avérés en bon accord avec la littérature. La stéréochimie des produits a été attribuée sur la base d'une analogie avec des systèmes précédemment publiés, en utilisant les constantes de couplage entre les protons $H_{a'}$ et $H_{l'}$ ($^{3}J_{Ha'Hl' endo}$ = 5,8 Hz et $^{3}J_{Ha'Hl' exo}$ = 1,6 Hz). Il est à noter que deux séries de pics ont été observées par RMN-^{1}H pour l'endo **4a** (en accord avec les deux stéréoisomères précédemment observés par HPLC). Les composés **4a** et **4b** sont très

solubles et stables dans des solvants organiques tels que l'acétone, l'acétonitrile et le DMSO (solutions 30 mM, évaluées par RMN-^{1}H après 48h), ainsi que dans l'eau contenant 0,5 % DMSO, un milieu typiquement utilisé pour évaluer l'activité biologique de tels complexes.

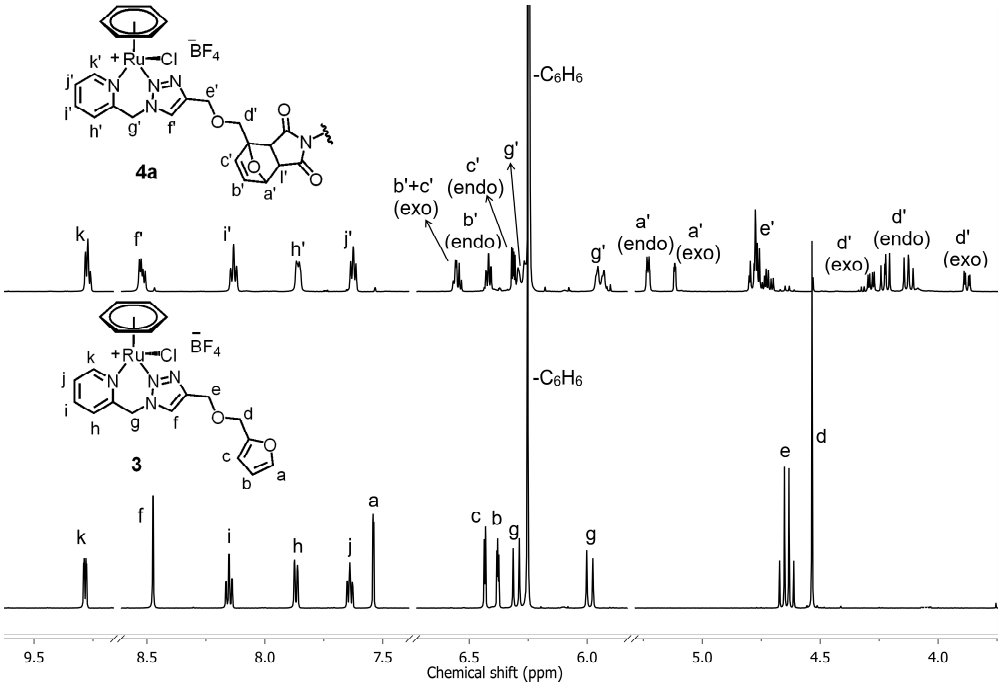

Figure 1. Illustration de certains des changements spectraux observés par RMN-^{1}H lors de la cycloaddition DA (ex: 40°C dans l'acétone-d_6) du complexe **3** et du *N*-octylmaléimide pour former **4a** (**4a$_{exo}$** : **4a$_{endo}$** = 1 : 2).

La nature/conformation de **3** et **4a$_{exo}$** a été confirmée par analyse aux rayons X de monocristaux. La figure 2 présente une vue ORTEP des structures à l'état solide, et un résumé des données cristallographiques est fourni dans les tableaux S2 et S3. Les deux complexes de Ru adoptent une géométrie octaédrique déformée (structure piano-selles) avec un cycle benzénique de coordination 6, un fragment donneur N,N bidenté et un ligand chlorure. Toutes les distances de liaison métal-ligand se trouvent dans la plage attendue pour de tels complexes. Elles sont similaires pour les deux complexes à l'exception de Ru-N2 qui est plus court dans **4a$_{exo}$** que dans **3**.

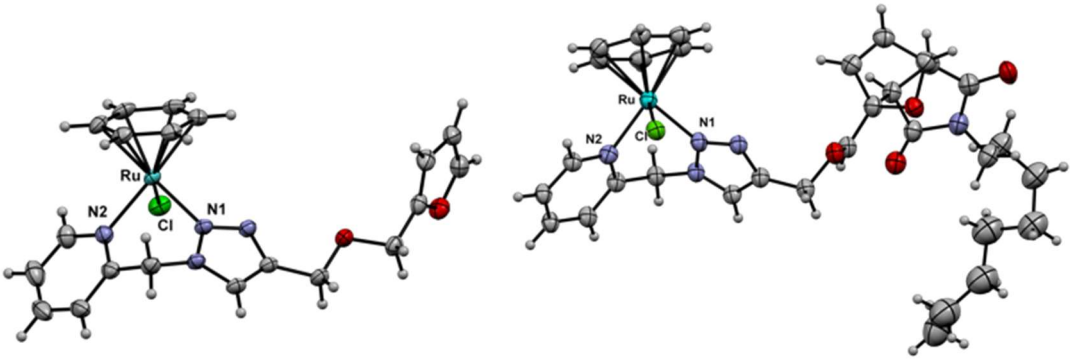

Figure 2. Dessin ORTEP de **3** (à gauche) et **4a$_{exo}$** (à droite) illustrant le schéma de numérotation atomique à des ellipsoïdes de probabilité de 50 %. Pour plus de clarté, le contre-ion BF_4^- n'est pas affiché et seule la position avec le facteur d'occupation le plus élevé est affichée. Longueurs de liaisons sélectionnées : **3** : Ru–Cl, 2.3849 (5); Ru–N1, 2.0863 (15); Ru–N2, 2.1301 (17); Ru-benzene, 1.677 Å; **4a$_{exo}$** : Ru–Cl, 2.385 (2); Ru–N1, 2.075 (7); Ru–N2, 2.096 (7); Ru-benzene, 1.668 Å.

La stabilité des deux différents types de liaisons DA qui sont étudiées dans cette étude, incluant leur désassemblage DA, a été évaluée dans des conditions biologiquement pertinentes à des températures différentes. Ceci a été réalisé en enregistrant des spectres RMN du proton dans des solutions aqueuses de NaCl (110 mM) (D_2O contenant 1 % de DMSO-d_6) pour les adduits endo ou exo de **4a** et **4b** après une incubation à une température située entre 37 et 50 °C (plage de température physiologique ou pathologique et pouvant correspondre aux conditions locales induites par hyperthermie) pendant 48h (tableau 1).

Tableau 1. Évaluation du désassemblageDA (réaction rDA) des complexes Ru DA **4a** et **4b** dans des conditions biologiquement pertinentes (D_2O- 1% DMSO-d_6-110 mM NaCl) par RMN-^{1}H après 48h.

	Réaction rétro Diels-Alder (%)[a]		
	37°C	**42°C**	**50°C**
4a$_{endo}$	18	28	59
4a$_{exo}$	0	1	3
4b$_{endo}$	72	81	100
4b$_{exo}$	11	18	41

[a]Le désassemblage DA (%) a été calculé sur la base de l'intégration du proton triazole du complexe furane **3** à 8,53 ppm et des protons DA des complexes Ru DA **4a** et **4b** à ~5,3 ppm.~

Comme prévu, **4a** s'est avéré beaucoup moins enclin à subir une réaction rDA que **4b**. En effet, il a déjà été démontré que la présence d'un substituant à effet attracteur sur le groupe maléimide des adduits DA peut améliorer la réaction de rDA alors que le contraire a plutôt été observé en présence d'un substituant à effet donneur.

Il est important de noter que le désassemblage DA n'a pas été observé exclusivement pour les isomères endo de **4a** et **4b**. Alors qu'un désassemblage DA négligeable a été observé pour **4a$_{exo}$** à toutes les températures étudiées, un résultat attendu pour un adduit exo de type furane-maléimide DA, un désassemblage DA significatif a été noté pour **4b$_{exo}$**.

Comme le pH physiologique (7,4) est connu pour améliorer les réactions de rDA entre le furane et les maléimides (hydrolyse plus rapide du groupe maléimide libéré), et que le maléimide libéré pourrait facilement réagir avec la pléthore de thiols ou d'amines présents dans les environnements biologiques (contribuant également à déplacer l'équilibre vers les produits rDA), nous nous sommes intéressés à effectuer quelques expériences préliminaires *in vitro* impliquant des lignées cellulaires humaines, afin d'évaluer une potentielle activité antiproliférative pour les isomères DA endo et exo. Pour cette étude, **4a** a été sélectionné en fonction de son caractère lipophile plus élevé par rapport au complexe **3**, d'autant plus qu'aucune réaction rDA n'était attendue pour l'adduit exo. L'activité antiproliférative de **4a** a été évaluée avec deux lignées de cellules tumorales du sein (MCF-7 et T47D) par une analyse de SRB. Les résultats présentés sous la forme d'IC_{50} sont présentés au tableau 2.

Tableau 2. Valeurs déterminées d'IC_{50} pour des complexes de ruthénium contre des variétés de cellules humaines MCF-7 et T47D de cancer du sein.

Endo : exo		**IC_{50} (µM)[a]**	
		MCF-7	**T47D**
3		>300	>300
4a	Endo	59,5 ± 1,9	70,1 ± 3,5
	Exo	57,2 ± 3,0	72,8 ± 4,9
5a	Endo	51,3 ± 3,0	78,0 ± 1,2
	Exo	54,7 ± 8,1	73,5 ± 4,5

[a]L'activité inhibitrice a été déterminée par l'exposition des lignées cellulaires à des solutions de chaque complexe pendant 48 h et exprimée comme la concentration requise pour inhiber la viabilité cellulaire de 50 % (IC_{50}). Les erreurs correspondent à l'écart type de deux à trois expériences indépendantes. IC_{50} de maleimide de *N*-octyle = 26,1 ± 5,1 µM et 24,4 ± 6,1 µM pour les lignées cellulaires MCF-7 et T47D, respectivement.

Le complexe **4a** a montré une activité antiproliférative nettement augmentée contre les deux variétés de cellules de cancer en comparaison du précurseur **3**. Cette amélioration pourrait être attribuée à la lipophilicité plus élevée de ce complexe de DA. Ce qui était

inattendu à partir des résultats obtenus est l'absence de différence significative entre l'activité des formes exo et endo du complexe **4a**, ce qui suggère que les deux isomères n'ont subi aucun désassemblage DA ou tout au plus un désassemblage négligeable. Le désassemblage partiel ou complet de DA des deux isomères (dans la même mesure) n'a pas pu être exclu, mais serait improbable en raison des différents profils de rDA notés précédemment, et de l'activité antiproliférative considérable du maléimide de *N*-octyle (IC_{50} = 26,1 ± 5,1 µM et 24,4 ± 6,1 µM pour les variétés de cellule MCF-7 et T47D, respectivement).

Pour répondre à la question de savoir si le désassemblage du **4a** pourrait avoir lieu dans l'environnement biologique *in vitro* décrit ci-dessus, et en supposant que la réduction de la double liaison impliquée dans la réaction de rDA entraînerait un complexe avec une cytotoxicité similaire à celle du **4a** intact en empêchant tout désassemblage DA de se produire, nous avons synthétisé une version thermostable du complexe **4a** (schéma 3). Le complexe thermostable **5a** a été obtenu avec un rendement quantitatif par hydrogénation directe d'un mélange **4a** d'isomères endo et exo. Le complexe **5a** a été caractérisé par RMN et HR-ESI-MS. Tel qu'attendu, nous avons observé l'absence des deux signaux à 5,09 et 5,19 ppm dans son spectre RMN-^{1}H, qui étaient respectivement attribués aux protons endo et exo alcényle (voir figure 1, $H_{b'}$ et $H_{c'}$) de l'adduit de **4a**. Lorsqu'il a été testé sur les deux mêmes lignées cellulaires de cancer du sein humain, **5a** présentait une IC_{50} qui n'était pas significativement différente de celle des deux isomères de **4a**, après 48h (tableau 2). Ce résultat appuie l'hypothèse que la rDA de ce système spécifique pourrait ne pas avoir lieu dans le cadre biologique étudié.

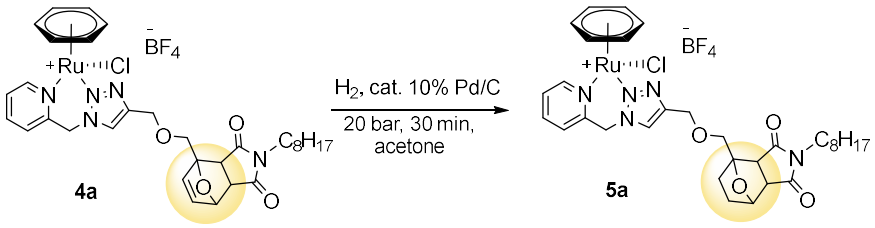

Schéma 3. Hydrogénation de la double liaison de **4a**.

Les résultats de recherche rapportés dans ce mémoire fournissent des informations importantes qui pourront ouvrir la porte au développement et à la conception de nouveaux médicaments conjugués plus effectifs ou de systèmes de délivrance thermo-stimulés portant des médicaments à base de ruthénium ou d'autres métaux.

TABLE OF CONTENTS

LIST OF FIGURES

LIST OF SCHEMES

LIST OF TABLES

LIST OF ABBREVIATIONS

- ALP: Alkaline phosphate
- AMF: Alternating magnetic field
- ASCs: Adipose-derived stem cells
- Boc: *tert*-butyloxycarbonyl
- CuAAc: Catalyzed alkyne azide cycloaddition
- COSY: Correlation spectroscopy
- DOX: Doxorubicin
- DIMs: Doxorubixin-Indocyanine-loading nanoparticles
- DCC: *N*,*N*'-Dicyclohexylcarbodiimide
- DA: Diels-Alder
- DCM: Dichloromethane
- DMF: Dimethylformamide
- DMSO: Dimethyl sulfoxide
- EWG: Electron-withdrawing groups
- EDG: Electron-donating groups
- EPR: Enhanced permeability and retention effect
- Et_2O: Diethyl ether
- Fu-Ma: Furan-maleimide
- FMO: Frontier molecular orbitals
- FRET: Foster resonance electron transfer
- GEM: Gemcitabine
- GSH: Reduced glutathione
- HR-ESI-MS: High resolution-electrospray ionization-mass spectrometry
- HMSCs: Human mesenchymal stem cells
- HNPs: Iron oxide/Au core-shell hybrid nanoparticles
- HA: Hyaluronic acid
- HMBC: Heteronuclear Multiple Bond Correlation spectroscopy
- HSQC: Heteronuclear Single Quantum Correlation spectroscopy
- HPLC-MS: High Performance Liquid chromatography–Mass Spectrometry

- HOMO: Highest occupied molecular orbital
- IGC: Indocyanine green
- IONPs: Magnetic iron oxide nanoparticles
- ICP-MS: Inductively coupled plasma mass spectrometry
- LUMO: Lowest unoccupied molecular orbital
- MES: 2-(*N*-morpholino)ethanesulfonic acid
- MRI: Magnetic resonance imaging
- NIR: Near-infrared
- NMR: Nuclear Magnetic Resonance spectrometry
- NPs: Nanoparticles
- ORTEP: Oak Ridge Thermal Ellipsoid Plot
- Pd/C: Palladium/carbon catalyst
- PBS: Phosphate Buffered Saline
- PEG: Polyethylene glycol
- PNA: Peptide nucleic acids
- PPy: Polypyrrole nanoparticles
- POA: Pyrene-oxabicycloheptene-alkyne
- rDA: Retro Diels-Alder
- Ru: Ruthenium complex
- RAFT: Reversible addition−fragmentation chain-transfer
- SPIONs: Super-paramagnetic iron oxide nanoparticles
- SRB: Sulforhodamine B assay
- THF: Tetrahydrofuran
- UV/Vis: Ultraviolet/visible

1. INTRODUCTION

Diels-Alder cycloadditions involving furans and maleimides are extensively used in synthetic chemistry. Moreover, furan and maleimide moieties are part of the structure of various drugs/drug candidates. Among numerous examples, maleimide-containing compounds can lead to intracellular glutathione depletion, a well-known anticancer mode of action. When allowed to react together under certain conditions, furan and maleimide moieties undergo a [4 + 2] Diels-Alder (DA) cycloaddition. The thermoreversibility of this reaction has been widely exploited for many years in organic and material synthetic chemistry using elevated temperatures. More recently, we and others have shown that retro Diels-Alder (rDA) reactions of endo adducts can take place at biologically-relevant temperatures, making DA-type linkages a promising tool for the stimuli-responsive delivery of drugs/drug candidates functionalized with targeting or cell-penetrating agents. This field of research is still in its infancy, and to our knowledge, the potential of DA-containing metal-based drugs/drug candidates has so far only scarcely been examined.

The first chapter of this thesis consists of a complete literature review of the studies that were so far reported for the use of furan-maleimide DA linkages for the development of stimuli-responsive drug delivery systems. This review offers an overview of the range of biological applications derived from such drug delivery systems and the factors that influence such DA and rDA reactions, proposing avenues for designing more innovative drug delivery systems using these types of stimuli-responsive linkages.

1.1 Stimuli-responsive furan-maleimide Diels-Alder linkages: a promising tool for the development of drug delivery systems (a review article: publication 1)

Liaisons furane-maléimide Diels-Alder sensibles aux stimuli : un outil prometteur pour le développement de systèmes de délivrance de médicaments.

Hoang-Van Tran and **Annie Castonguay***

INRS-Centre Armand-Frappier Santé Biotechnologie, Université du Québec, Laval, QC H7V 1B7, Canada

Corresponding author: *annie.castonguay@inrs.ca

Contribution of authors:

Hoang-Van Tran participated in conceptualization, writing the original draft, and editing the manuscript.

Prof. Annie Castonguay obtained the research funding and participated in conceptualization, writing, and revising the manuscript.

The article is in preparation and will shortly be submitted to a journal for publication.

Abstract

Various stimuli-responsive strategies hold great promise for the development of drug delivery systems that can efficiently overcome multiple obstacles in cancer treatment. In such system, local delivery of drug candidates is controlled by reversible process via physical, chemical, or mechanical stimulations. For instance, thermosensitive linkages such as Diels-Alder reaction (DA) has recently appeared as a simple but powerful tool for controlling drug release at the desired location in the body either by a variation of temperature in the physiologically relevant condition or by utilizing local-heat-induction. Recent studies show that such stimuli-responsive drug delivery systems are not only nontoxic for the healthy cells but also enhance the cellular uptake and selectivity of therapeutic agents. However, using DA linkages for this strategy has so far only scarcely been examined. In this literature review, we aim to provide an overview of the release mechanism and the range of applications of stimuli-responsive drug delivery systems bearing DA linkages. The summary and highlights from this review will offer insight into the important role of the DA linkage in particularly or other covalent bonds in general that would enable to develop the more appropriated (or smarter) drug delivery systems adapting with specific diseases.

List of keywords:

Thermosensitive linkages, stimuli-responsive drug delivery system, controlling drug release, Diels-Alder reaction, exogenous stimulation-triggered heating.

REVIEW

Stimuli-responsive furan-maleimide Diels-Alder linkages: a promising tool for the development of drug delivery systems

Hoang-Van Tran,[a] and Annie Castonguay*[a]

Entry for the Table of Contents

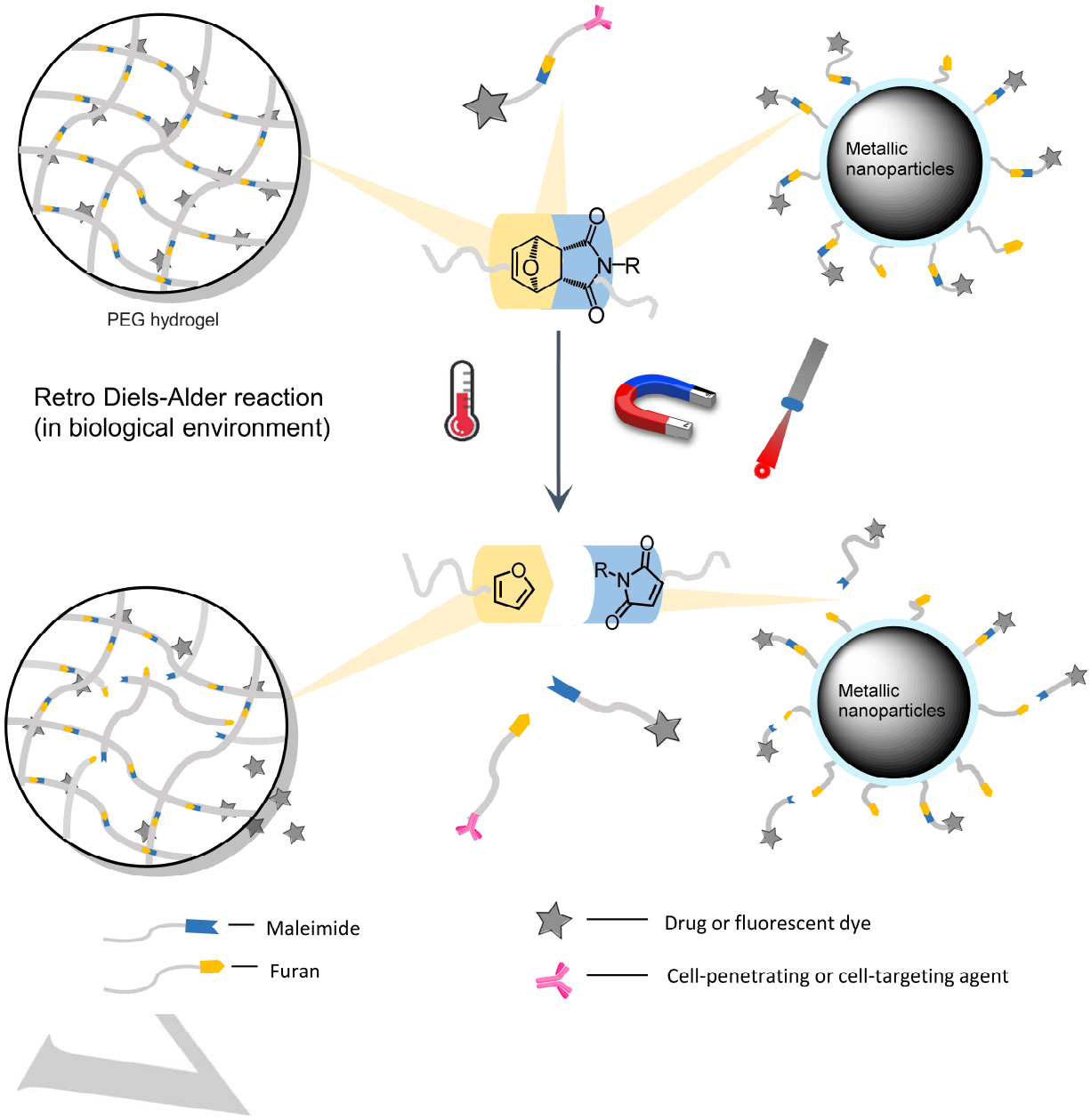

[a] INRS-Centre Armand-Frappier-Santé Biotechnologie, Université du Québec, Laval, Québec
Correspondant: Prof. Annie Castonguay
E-mail: annie.castonguay@inrs.ca

Abstract: Stimuli-responsive strategies hold promise for the development of drug delivery systems that can efficiently overcome multiple obstacles in therapy. In such systems, the local delivery of drug candidates is controlled by a reversible process via physical, chemical, or mechanical stimulations. Given their thermo-reversibility, furan-maleimide Diels-Alder (DA) linkages have recently caught some attention for their potential to allow the local release of drug candidates under biologically-relevant conditions (with or without the aid of local heat-inducting tools). Although the development of such systems is still in its infancy, recent studies have shown that some can enhance the cellular uptake and/or the selectivity of therapeutic agents. This review aims at providing an overview of the wide range of applications of such drug delivery systems, and at offering insights to prompt the development of novel strategies for the treatment of various diseases.

1. Introduction

Stimuli-responsive drug delivery systems have received increasing attention in the last years given their ability to improve the effectiveness and selectivity of various anticancer, antimicrobial and antiviral drugs.[1] Systems that are thermo-sensitive are among the most studied stimuli-responsive strategies and have been extensively exploited in oncology.[2] As their disassembly specifically depends on the thermal lability of the linkages used, selecting systems with the most appropriate drug release profile is crucial. Thermally-labile linkages can *i*) allow the slow release of a drug payload at physiological temperature without the use of an external stimulus, but can *ii*) also remain stable under biological conditions (with no or limited leakage of the drug payload), requiring the use of a local heat-inducting tool (such as a laser or a magnetic field). The latter is exploited when a specific target needs to be reached by the delivery system before allowing the drug to be released at the target location. For such systems, the increase in local temperature needs to be managed to prevent thermal damage of healthy tissues. Indeed, in all cases, the linkages chosen must be biocompatible and not toxic in their inactivated or activated form.[3] Among the various thermally-sensitive drug delivery systems reported (mainly based on hydrogen bonds, π-π interactions, etc.),[2] the ones based on covalent linkages such as Diels-Alder (DA) cycloadditions hold promise due to their high tuneability and their ability to prevent extensive premature degradation or disassembly in biological settings.[4] Besides, DA reactions are coveted transformations as they are atom efficient (no tedious purification needed), can take place in water, and do not require the use of heat or catalysts.[5],[6] Since their discovery at the beginning of the 20th century by Otto Diels and Kurt Alder,[7] DA cycloadditions have evolved as some of the most powerful synthetic tools for the preparation of unsaturated six-membered rings.[8] [9] Interestingly, we and others have reported that the reverse reaction of furan and maleimide (Fu-Ma) [4+2] normal demand DA reactions, referred to as retro Diels-Alder (rDA),[10] [11] can take place at temperatures as low as 50-80°C,[5, 12] and in some cases, at physiologically-relevant temperatures.[13] However, the potential of such systems has up to now only been scarcely examined. This literature review aims at providing an overview of what has been achieved in the field, and at providing insights on the applicability of Fu-Ma DA linkages for the development of superior stimuli-responsive drug delivery systems.

1.1 Reversible Fu-Ma Diels-Alder linkages

Whereas maleimide is straightforward to substitute at the *N*-terminus by condensation of maleic anhydride with functionalized amines, furan can be functionalized from low-cost commercial precursors such as furfural, furfuryl alcohol, or 2,5-dimethylfuran.[14] Therefore, Fu-Ma DA reactions were exploited in various synthetic processes including reversible cross-linkable polymeric materials,[12a] reversible interpenetrating hybrid networks,[15] thermally-responsive dendrimers[13a, 16] and modular printing and lithography.[17]

Normal electron demand Fu-Ma DA reactions usually take place more efficiently when the furan (diene) bears an electron-donating substituent (increasing the energy of its HOMO, highest occupied molecular orbital) and when the maleimide (dienophile) bears an electron-withdrawing substituent (lowering the energy of its LUMO, lowest unoccupied molecular orbital), allowing an enhanced overlap between the two frontier molecular orbitals (FMO) (Figure 1).[9],[10, 12b, 18] [19] [14] [12a] The electronic properties of both partners also greatly influence the reverse process (rDA), [12b, 18b] which makes DA linkages very tunable for diverse drug delivery applications.

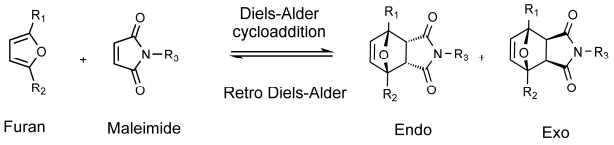

Figure 1. DA/rDA reactions between a (substituted) furan and a maleimide.

A variety of different factors can affect Fu-Ma rDA reactions (Table 1). Some studies demonstrated that the disassembly of DA adducts is favored in the presence of an electron-withdrawing group on the maleimide part, whereas it is unfavored in the presence of an electron-withdrawing group (EWG) at the 2- or 3-position of the furan ring.[12b] In addition, it has been reported that Fu-Ma rDA reactions can be accelerated in presence of a nucleophile (e.g. thiol).[12b]

Importantly, DA reactions result in the formation of two diastereoisomers, endo and exo cycloaddition products. The cyclo-reversion (rDA) temperature of endo adducts has been reported to be lower than that of their exo counterparts.[12b] Based on the study of Woodward and Baer, the exo adduct is more thermodynamically stable (less sterically strained) whereas the endo adduct forms more rapidly and corresponds to the kinetic product (favored by secondary orbital interactions or "endo-rule").[10] Although it would seem logical to favour endo adducts for the design of stimuli-responsive drug delivery systems, it is

important to note that the rDA reaction rate of each type of addition product would yet have to be further investigated under biological conditions.

Fortunately, the formation of endo or exo adduct can be modulated by different factors (Table 1). For example, introducting an electron-withdrawing group (EWG) on the N-terminal of maleimide or an electron-donating group (EDG) at the 2-, 3- positions of the furan ring,[18b] using low temperatures[12b, 18b] or a catalyst[20] was reported to favor the formation of the endo adduct.

Table 1. Examples of factors that have an impact on the kinetics of DA/rDA reactions and their endo/exo isomer ratio.

N°	Factors		Endo/exo ratio	DA reaction rate	rDA reaction rate
1	Electronic nature of substituents on diene/dienophile[12b, 18b]	EWG on maleimide	>1	↑	↑
		EDG at 2, -3 position on furan	<1	↑	n.d.
		EWG on furan	>1	↓	↓
2	Temperature[12b, 18b]		>1 when temperature is decreased	↑	↑
3	pH[21], [22]		n.d.	n.d.	Faster when pH is increased
4	Presence of nucleophile in the solution[12b], [23]		n.d.	n.d.	↑
5	Pressure[24]		n.d.	↑	n.d.
6	Catalysts: Lewis acid or Brønsted acid ($Co(NO_3)_2$; $Ni(NO_3)_2$; $Cu(NO_3)_2$; $Zn(NO_3)_2$; HCl)[20]		>1	n.d	↑
7	The rate of maleimide hydrolysis[21], [22]		n.d.	n.d.	↑

[a] ↑: reaction kinetics is increased; ↓: reaction kinetics is decreased.

2. Applications

This literature review is divided into three main sections, according to the various ways of exploiting Fu-Ma rDA reactions: untriggered, photothermally-triggered, and magnetothermally-triggered systems.

2.1. Systems that are untriggered

2.1.1. Systems without cell-targeting/-penetrating agents

Dendrimers have attracted significant attention in the past years for the development of drug carriers, vehicles for gene delivery or diagnostic agents, due to the numerous functional groups located at their surface. The introduction of Fu-Ma DA linkages within their structure could allow the delivery of multiple units of biologically-active compounds.[25] This approach was exploited by Castonguay et *al.* (2011),[13a] following their previous work[16] on the development of synthetic strategies combining Cu-catalyzed alkyne-azide (CuAAC) and Diels-Alder cycloadditions to afford thermally-responsive dendrimers. In this study, many units of lipoic acid, a powerful antioxidant, were linked at the periphery of such a dendrimer using Fu-Ma DA linkages (Figure 2). NMR studies (3 mM DMSO-d_6) revealed that the resulting DA linkages were not stable over time in the 22-42°C range. Although the release profile of the drug was not investigated in biological settings, *in vitro* studies have shown that the dendrimer could rescue microglial cells from paraquat-induced oxidative stress after 24h (at 12.5 µM).

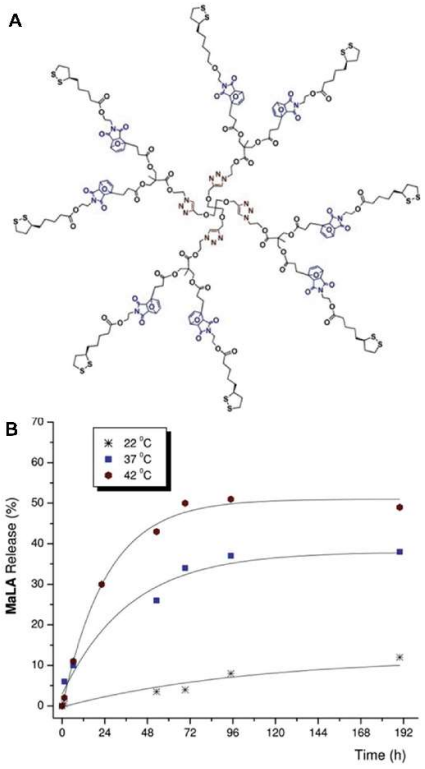

Figure 2. Maleimide-functionalized-lipoic acid (MaLA) was conjugated to furan-functionalized dendrimers, creating multiple DA thermosensitive linkages. A) Structure of the DA dendrimer; B) Release of MaLA via simultaneous rDA reactions at different temperatures, as followed by ^{1}H NMR spectroscopy (3 mM DMSO-d_6 solutions). (Adapted from [13a])

Hydrogels are also widely exploited in drug delivery,[26] as they can protect the loaded drugs from degradation or rapid excretion from the body, providing a sustained or triggered drug release.[26] Fu-Ma DA linkages were previously used as effective cross-linking agents for the formation of hydrogels.[26-27] In 2010, Wei et *al.* reported the preparation of hydrogels performed via Fu-Ma DA cross-linking reactions between linear furan-functionalized polymer chains based on poly(furfuryl amine maleic acid monoamide-co-N-isopropyl-acrylamide) and bismaleimide.[28] Results from these studies showed that the gelation time, cross-

linking, and swelling capacity were affected by the furan intake (the content of furan in the copolymer) and maleimide concentration.[29] However, the kinetics of depolymerization of these hydrogels via rDA reactions was very slow, as only a negligible extent of DA disassembly was detected in water at 100°C after 12h.[28-30]

Other reports have shown that hydrogels can also be prepared by allowing two linear polymers functionalized with furan and maleimide moieties to react via DA cycloadditions, respectively.[31] In these examples, biodegradable hydrogels were formed via the DA reaction between furan- and maleimide-functionalized hyaluronic acid (HA) in aqueous solutions at 37°C. The hydrogels were successfully used to encapsulate two model proteins, insulin and lysozyme, for which the release was monitored in PBS over 21 days at 37°C. An *in vitro* assay revealed that these hydrogels were not cytotoxic and could preserve the viability of human adipose-derived stem cells after five days (3 wt% solutions).[31a] Despite the several advantages of preparing hydrogels using Fu-Ma DA reactions, a major drawback of these systems is that sufficient disassembly of the DA linkages was only observed at quite high temperatures, limiting their applications in biological settings.[32]

In 2013, Goepferich et *al.* reported a hydrogel that could disassemble under biologically-relevant conditions (Figure 3Error! Reference source not found.).[13b, 21] In this study, two monomers were initially prepared by functionalizing star-shaped polyethylene glycol (PEG) with furyl and maleimide moieties before cross-linking DA reactions were performed in water at 37°C. The concentration, the branching level, and the molecular weight of the monomers were the main factors affecting the gelation time which was found to rapidly take place, ranging from 14 to 170 min. The degradation of hydrogels takes place from two days to several weeks at human body temperature (37°C).[13b, 21] Importantly, the fast OH^- catalyzed ring-opening hydrolysis of the maleimide group was found to be the main factor affecting the degradation rate of these hydrogels under the conditions used, leading to the formation of unreactive maleamic acid. Due to a decrease in concentration of free maleimide-containing monomers, the dynamic equilibrium was shifted in favor of the disassembly of these hydrogels.[21] Therefore, hydrogels with a higher number of active chains (8armPEG10k-hydrogel) displayed the highest longevity. In contrast, hydrogels with a lower number of active chains (4armPEG10k-hydrogel or 8armPEG20k-hydrogel) were more prone to undergo faster disassembly, due to their lower concentration of functional groups per branching point. This finding is important as it demonstrates the potential of modulating the rate of hydrogel disassembly by a careful selection of macromonomers' branching factors and molecular weights. In 2017, the same research group exploited this strategy for controlling the release of bevacizumab, an antibody currently used to treat neovascular age-related macular degeneration that might potentially benefit from a long-term controlled release.[33] Indeed, three different hydrogels were tailored using different 8armPEG10k-hydrogel/4armPEG10k-hydrogel ratios to adjust the antibody release rate, which was monitored at 37°C over 7, 21, and 115 days in phosphate buffer (pH 7.4). As expected, the antibody release was completed after only 7 and 21 days, respectively, for the hydrogel mixtures with a higher content of the 4armPEG10k-hydrogel (0:3) and (1:5). Increasing the content of the highly branched 8armPEG10k-hydrogel (1:2) could also lead to the full release of the antibody, but only after 115 days.

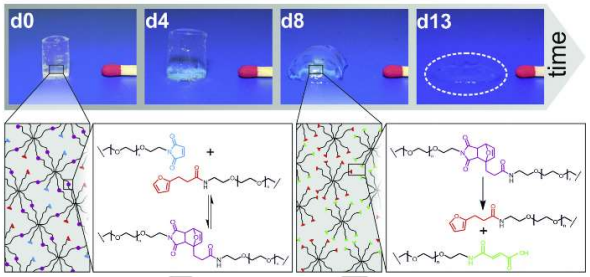

Figure 3. Degradation under physiological conditions over 13 days of 10% (w/v) 8armPEG10k–hydrogels that were prepared by reacting equimolar amounts of 8armPEG10k–furan (114.3 mg) and 8armPEG10k–maleimide (110.7 mg) in 4500 µL of water. (Adapted from [21])

In 2013, Bowman et *al.* exploited a different strategy using a hydrogel containing pendant DA reaction sites to control the release of drug candidates from an irreversibly cross-linked network.[34] Rather than constructing a DA cross-linked degradable polymer as previously done by other groups, the hydrogel in this study was prepared by a Michael addition between maleimide and thiol PEG macromers in which the maleimide was used in excess to create hydrogel networks with pendant Diels–Alder compatible tethering sites (maleimide). In addition, a fluorescently-labeled furan-RGDS sequence (Arg–Gly–Asp–Ser) was incorporated into the hydrogel network with pending maleimide functionalities via Fu-Ma DA reactions (Figure 4), allowing a study of the DA disassembly by fluorescence measurements. A release profile of 40%-100% was found to take place over several days in PBS buffer at temperatures ranging from 37 to 80°C. A reaction-diffusion model was used to support the experimental release data and assess the impact of altering the number of potential maleimide binding sites in the hydrogel. In this study, lowering the hydrogel maleimide concentration was predicted to result in a faster release rate.

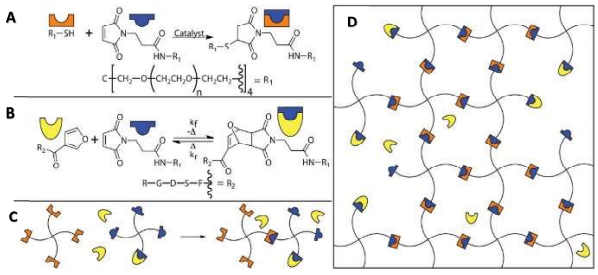

Figure 4. Creation of a PEG hydrogel with Diels–Alder compatible tethering sites. (A) The hydrogel was created by an off-stoichiometric thiol-Michael addition reaction between multifunctional maleimide and thiol PEG macromers. The maleimide was used in excess to create hydrogel networks with pendant Diels–Alder compatible tethering sites (maleimide). (B) Diels–Alder reaction between the furan-functionalized peptide and the excess maleimide within hydrogel networks. (C) This diagram depicts a schematic representation of the Michael addition and Diels-Alder reaction used to create the hydrogel release platform. (D) Portrayal of the overall polymer network cross-linked via Michael addition. Furan peptide sequences are present in both their bound and unbound states. (Adapted from [34])

In an additional study reported in 2013, the authors prepared an analogous hydrogel containing a furan-bearing dexamethasone peptide that could induce osteogenic differentiation of human mesenchymal stem cells (hMSCs).[35] Dexamethasone can also be used to induce the adipogenic differentiation of MSCs, with the concentration used to induce adipogenesis being higher than for osteogenic differentiation.[36] Therefore, they first performed a predictive model to identify the dexamethasone release and achieve a concentration suitable for inducing osteogenic differentiation of hMSCs. The release profile of the furan-containing dexamethasone peptide from the hydrogel was quantitatively assessed in both 2D (in 24 well plates) and 3D cultures (when the dexamethasone-releasing hydrogel was encapsulated within an hMSC-laden hydrogel) by staining for alkaline phosphatase (ALP) and mineral deposition. As a result, the furan-containing dexamethasone peptide induced a robust osteogenic differentiation in both cell culture conditions with a significantly increased ALP activity and mineral deposition compared to the dexamethasone-free treatment. More interestingly, ALP activity exceeded the dexamethasone positive control after 5 and 10 days, suggesting the potential benefit of a constant release in 3D cultures. This finding might be applicable for bone tissue engineering applications.

More recently, Taimoory et *al.* (2018) reported computational studies to support experimental results obtained for DA reactions between 4-substituted α-furfuryl alcohols and N-substituted maleimides to establish a library of end-caps for a new class of self-immolative polymers.[37] Self-immolative polymers are stabilized with an “end-cap” to one end of the polymer after they are made. When their end-cap is removed, those polymers can begin to disassemble. The authors have shown that the rDA reaction of several Fu-Ma DA cycloadducts could occur at a wide range of temperatures, from physiologically-relevant temperatures (40°C) to 110°C, suggesting their potential use for the design of valuable materials for biomedical or industrial applications.

2.1.2. System with cell-targeting/ -penetrating agents

Shoichet et *al.* (2007) successfully used Fu-Ma DA cycloadditions to introduce Herceptin (trastuzumab), an antibody that targets HER2 cancer cell receptors, at the surface of micellar NPs. Accordingly, the furan-functionalized micellar NPs were first obtained through the self-assembly of biodegradable graft copolymers of poly(2-methyl-2-carboxytrimethylene carbonate-*co*-$_{D,L}$-lactide)-*graft*-poly(ethylene glycol)-furan (poly(TMCC-*co*-LA)-*g*-PEG-furan in aqueous solution (Figure 5). [38] The micellar NPs then reacted with maleimide-modified anti-HER2 antibody via a DA reaction in MES buffer (pH 5.5) at 37°C. *In vitro* studies demonstrated that introducing a maleimide group within the antibody structure did not alter its biological activity. Moreover, a cytometry analysis showed that, compared to furan-functionalized NPs alone, conjugated NPs led to a higher binding affinity with the human HER2-overexpressing cancer cell line SKBR3, making it a promising construct for immune-targeted breast cancer therapy.

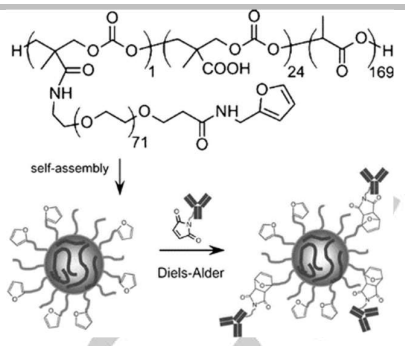

Figure 5. Self-assembly of furan-functionalized NPs and their conjugation with maleimide-modified antibodies. (Adapted from [38])

In 2009, this strategy was further exploited by the same authors in combination with chemotherapy.[39] In this study, the HER2-targeting antibodies and doxorubicin (DOX), a chemotherapeutic used for cancer therapy, were attached at the surface of micellar NPs via Fu-Ma DA reactions for the targeted and delivery of DOX. The NPs-antibodies-DOX formulation exhibited an enhanced cellular uptake, resulting in a more significant level of apoptosis in HER2-overexpressing human breast cancer cells SKBR-3 than for NP formulations with either DOX or antibodies alone. Notably, the NPs-antibodies-DOX formulation showed a higher selectivity for SKBR-3 cancer cells than HMEC-1 healthy cells when compared to DOX alone.[39]

The Fu-Ma DA reaction has also been used to functionalize drugs/drug candidates with cell-penetrating agents. It is well precedented that the efficient cellular delivery of biologically-active molecules or nanocarriers is often affected by their ability to cross cellular membranes. Introducing cell-penetrating agents into their structure (e.g., lipophilic molecules or cell-penetrating peptides) was reported as an efficient method to enhance their cellular uptake and, as a result, their biological activity.[40] The first example of using this strategy with Fu-Ma DA linkages was documented by Graham and coworkers (2008). In this study, the authors developed an effective method for conjugating oligonucleotides with cell-penetrating peptides through Fu-Ma DA reactions, enhancing their cellular uptake via protein-transduction domains.[41]

Metal-based complexes have lately received increasing attention due to their outstanding biological activities. For instance, ruthenium complexes are among the most investigated and advanced metallodrugs due to their significant anti-proliferative and antimetastatic activity against a wide range of cancer cells. Recently, Castonguay et *al.* (2021) reported microwave-assisted synthetic pathways to functionalize a cationic furan-containing organoruthenium complex via DA linkages with two maleimides of a different electronic nature, one of which included a lipophilic aliphatic carbon chain that could potentially act as a cell-penetrating agent (Figure 6).[13c] In this study, the stability of the Fu-Ma DA constructs at biologically-relevant temperatures was assessed (using ^{1}H NMR), and the conformation of the exo and endo isomers was taken into account. As expected, the complex prepared using the most electron-withdrawing maleimide substituent was found to be much more prone to undergo a rDA reaction. Importantly, not only the endo, but even the exo DA isomers (usually known to undergo rDA at higher temperatures than their endo counterparts, *vide*

supra) of both systems could disassemble at these temperatures. The complex based on the maleimide with the most lipophilic substituent (aliphatic alkyl chain) was found to display an improved anti-proliferative activity against two human breast cancer cell lines MCF-7 and T47D compared to the free furan-containing organoruthenium complex, attributed to its probable enhanced ability to penetrate the cell membrane.[42] Interestingly, no difference was noted between the activity of the exo and endo forms of this complex, suggesting that both isomers could not undergo any disassembly under the assay conditions. This hypothesis was further supported by the fact that a similar anti-proliferative activity profile was observed for a thermostable analogue of this complex, for which the double bond involved in the DA linkage was hydrogenated and thus, for which DA disassembly could not occur.

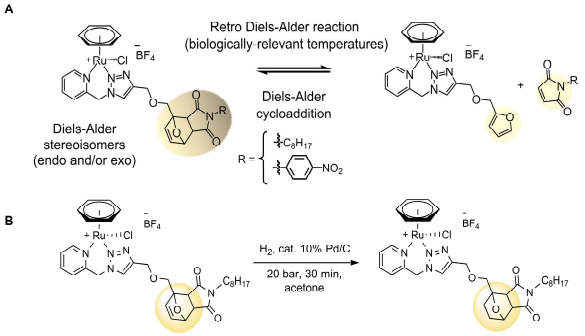

Figure 6. (A) Functionalization of organoruthenium complexes using furan/maleimide DA linkages and the reversibility reaction (rDA) under biologically-relevant conditions. (B) Hydrogenation of the DA linkage double bond of the ruthenium Fu-Ma DA adduct bearing an alkyl chain. (Adapted from [13c])

The kinetics of drug release via Fu-Ma DA linkages at body temperature can be locally enhanced using heat-inducing tools. External stimuli such as light and magnetism have been investigated for that purpose, as presented in the following sections.

2.2. Photothermally triggered system

The light-triggered generation of heat using NPs has been widely exploited for the thermally-induced release of drugs.[43] Thus, some attention was recently devoted to the development of NPs that can efficiently generate heat under laser irradiation.[43-44] Thermosensitive Fu-Ma DA linkages were exploited for their potential to disassemble [5, 12b, 45] in combination with both metallic- and organic-based NPs, allowing a faster or more efficient rDA-induced release of therapeutics.

2.2.1. Metal-based nanoparticles

AuNPs display a highly light-to-heat generation efficiency and have by far been the most studied NPs for photothermal therapies. Indeed, due to their surface plasmon resonance band, these metallic-based NPs have a strong ability to absorb light at a specific range of wavelengths.[4, 44] Moreover, they are attractive candidates to be exploited for drug delivery purposes as they display a high-level chemical inertness,[46] are not highly toxic,[47] and are straightforward to functionalize through the formation of Au-S covalent bond.[48] Under laser irradiation at their SPR peak of absorption, the local generation of heat could reach up 60 to 70°C at the surface of AuNPs via the photothermal effect.[49] This local increase of temperature is believed to enable the release of therapeutic payloads from NP vehicles via rDA reactions. It is worth noting that core-shell silica AuNPs and Au nanorods are more coveted AuNPs for drug delivery applications than their counterparts that absorb in the visible region, as they allow a deeper laser penetration into the tissues, minimizing damage.[44]

In 2009, Bakhtiari et *al.* studied the photothermal release of a furan-functionalized dye (fluorescein) using core-shell AuNPs (Figure 7).[45] A DA cycloaddition was performed between the furan-bearing fluorescein and a thiol-functionalized maleimide molecule. The resulting construct was then conjugated onto the surface of AuNPs via a Au-S covalent bond.[50] FRET (Foster resonance electron transfer) was exploited in this system to investigate the kinetics of the dye release.[51] When AuNPs were activated under laser irradiation in the SPR absorption region of the AuNPs (from 400 to 1100 nm), local heat was generated around the NPs, triggering the DA linkage disassembly of the construct. The release of fluorescent dye could be monitored over time, as it led to an increase in the fluorescence emission of the solution. Notably, the photothermally-induced drug release from silica-Au core/shell NPs was almost completed under laser irradiation after only 30 min. In contrast, incubating NPs in a water bath at 60°C (the temperature at which cells would be significantly damaged) only resulted in a 25% release of the dye. It is important to note that laser irradiation only led to a local temperature increase at the surface of silica core-shell AuNPs whereas a negligible temperature increase was observed in the surrounding environment.[45] A faster drug release kinetics was observed for the solid spherical NPs, for which a complete release was noted after only 15 min. However, a closer look at those results revealed the occurrence of some Au-S bond breakage, which did not take place in the case of core-shell NPs and nanorods.[45, 52] It is important to note that the breakage of Au-S bonds is considered as detrimental to the biological system due to the occurrence of unwanted side-reactions from free thiols.[45] Thus, core-shell NPs and nanorods were found to be more advantageous for drug delivery purposes using the photothermal effect. In addition, this study investigated the difference in conformation of both endo and exo isomers. As expected, results from ^{1}H NMR studies demonstrated that both endo and exo adducts were stable at room and body (37°C) temperatures. However, some disassembly could take place (63% for the endo adduct and 33% for the exo adduct)[45] after incubation in a water bath at 60°C.[45]

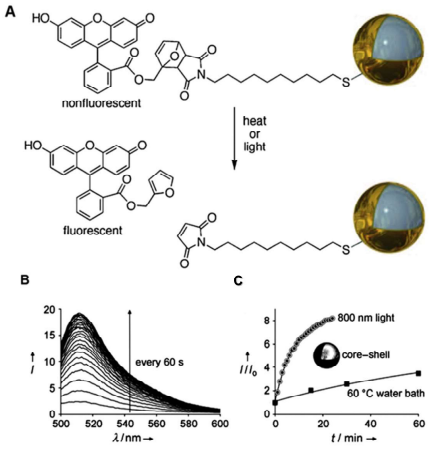

Figure 7. (A) Photothermal release of a furan-functionalized fluorescein dye via a Fu-Ma rDA reaction from the surface of a silica–gold core–shell nanoparticles. (B) Representative spectra show changes in the fluorescence intensity when an aqueous dispersion of gold-coated silica nanoparticles functionalized with the fluorescein dye (200 nm diameter) is irradiated with NIR light (800 nm, 1 kHz, 700 mW, 100 fs), and (C) Fluorescence intensity increases when aqueous dispersions of core-shell decorated with the fluorescein dye (200 nm diameter) are heated in a water bath at 60°C (■) or irradiated with 800 nm light (1 kHz, 700 mW, 100 fs) (**O**). (Adapted from [45])

In 2011, Yamashita et *al.* reported the use of Au nanorods functionalized with PEG chains through Fu-Ma DA linkages[53] which absorb in the near-infrared (NIR) region (preferred for biological applications). The DA disassembly of the adducts was induced by irradiating the construct with NIR light to photothermally release the PEG chains. Notably, the release of the PEG chain under laser irradiation could also increase the heat-inducing efficiency of the Au nanorods due to their subsequent aggregation at the irradiation site.

In 2012, Branda et *al.* also investigated the stability of AuNPs decorated with a fluorescein derivative via Fu-Ma DA linkages, and studied their *in vivo* photothermal release profile after injection in the oocytes of frogs.[54] Whereas the fluorescent dye remained bound to the AuNPs under cellular physiological conditions before laser irradiation, an increase in luminescence was observed following the pulsed laser irradiation, indicating the successful photothermal release of the drug payload within the cells. Cellular uptake studies in Chinese hamster ovary (CHO)-K1 cells suggested that the AuNPs did not internalize via receptor-mediated endocytosis, a common mechanism of cell adsorption for AuNPs. It is more likely that the emission measured from the released fluorescein derivative throughout the cytosol was due to its rapid diffusion through the endosomal membrane prior to fixation with paraformaldehyde.[54] Furthermore, the authors also showed that cell proliferation was not affected by AuNPs or laser exposure.

In 2013, Kitamura et *al.* reported a probing technique to monitor the kinetics of the Fu-Ma DA disassembly of a fluorinated molecule-functionalized AuNPs in phosphate buffer (pH = 7.0). Indeed, ^{19}F NMR spectroscopy measurements could be used for the detection of reduced glutathione (GSH), a biomolecule involving in many crucial biological processes in the human body.[55] Fluorinated groups, -CF_3, were incorporated onto AuNPs via Fu-Ma Diels-Alder reactions (Figure 8). Before exposing the AuNPs to heat, the CF_3-containing maleimide moiety, the binding site for GSH, was inactivated by its DA reaction with a furan-containing linker, and the ^{19}F NMR signal from the CF_3 group was suppressed. After heating the AuNPs-based probe, the CF_3-containing maleimide was released via rDA reactions, and thus, the ^{19}F NMR signal could be observed. GSH could then react with the probe through a Michael addition with the CF_3-containing maleimide moiety, resulting in a new peak in the ^{19}F NMR spectrum. The reaction rates of DA disassembly of fluorinated molecule-functionalized AuNPs or Michael addition of GSH were evaluated quantitatively from the signal intensity change. Compared to the fluorescence FRET technique, the use of fluorinated molecules might be more promising for monitoring the DA disassembly *in vitro* or *in vivo* conditions due to the high sensitivity of the isotropic chemical shift of fluorine resonances in different chemical environments, even when the fluorinated moiety is distant from the reaction site.[56]

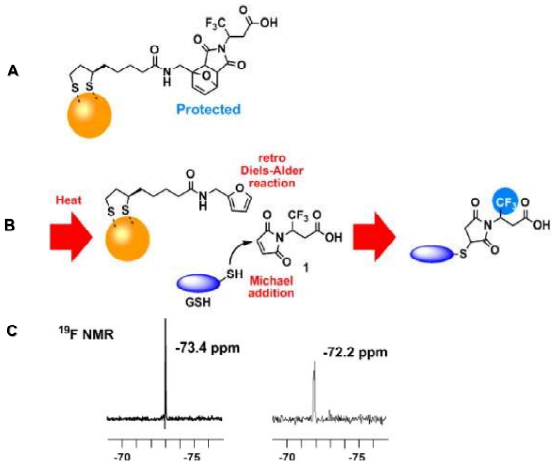

Figure 8. (A) Structure of fluorinated molecule-functionalized AuNPs**.** (B) The proposed scheme of DA disassembly in phosphate buffer and Michael addition for the detection of GSH. (C)^{19}F NMR spectra of **1** were recorded before (left) and after (right) the GSH treatment. (Adapted from [55])

In 2017, Hoskin et *al.* reported the preparation of a Fu-Ma DA Gemcitabine (GEM) delivery system based on iron oxide/Au core-shell hybrid NPs (HNPs) to treat pancreatic cancer.[49b, 57] GEM, used as a first-line chemotherapeutic for pancreatic cancer, was modified with the thermally labile Fu-Ma linkage (L-GEM). The attachment of L-GEM to the HNPs surface occurred through the dative covalent binding between the thiol residue on L-GEM with the gold surface of HNPs (Figure 9). The HPLC data showed that the gemcitabine analogue binding occurred (5 mg GEM:1 mg HNP). The HNPs were prepared by coating a 30 nm-diameter iron oxide core with Au, using the seeding technique with a polyethylenimine intermediate layer. HNPs were covered by a layer of PEG, which is biocompatible and enhanced their stability in biological settings. Interestingly, the iron oxide core of the HNPs could allow the use of magnetic resonance imaging (MRI) to track the drug release.[49b] The light-triggered heating experiment demonstrated that the hybrid NPs had a similar heating efficiency compared to the silica-Au core-shell NPs under the pulsed laser irradiation, for which the temperature was found to be in the 65-70°C range at the surface of the HPNs. [49b] The *in vitro* drug release of the HPNs-GEM formulation was carried out at 20, 37,

and 44°C (temperature that can be reached by the light irradiation of the NPs) at different pH (pH 7, water; pH 5.6 and 7.4, cell media) in order to evaluate the impact of pH changes on the drug release rate via DA disassembly. However, results from this study suggested that the temperature was the primary factor affecting the rDA reaction, not the pH. The release of the drug from the NPs was considerably fast, with about 80% of the free drug being detected by HPLC analysis when samples were incubated at 44°C after only 60s.[57] In addition, the cytotoxicity of GEM, HNPs, the prodrug (maleimide-functionalized GEM, Mal-GEM), and the HNPs-GEM formulation was assessed against pancreatic adenocarcinoma (BxPC-3) cells using the MTT assay. Cancer cells were treated with the HPNs-GEM formulation (0.01 - 100 µg/mL) and then incubated at 44°C for 30 min. The HNPs-GEM formulation resulted in a 56% increase in cytotoxicity after heating compared with standard conditions, whereas GEM and Mal-GEM did not display any significant change in cytotoxicity with or in the absence of applied heat. Although heat-activated HNPs-GEM were found to be 26% less cytotoxic than the free drug (GEM) *in vitro*, *in vivo* studies carried out using NIR laser irradiation in the presence of HNPs-GEM resulted in a 62% reduction in tumor weight, a 1.6-fold more significant decrease than when the same experiment was performed with GEM alone.

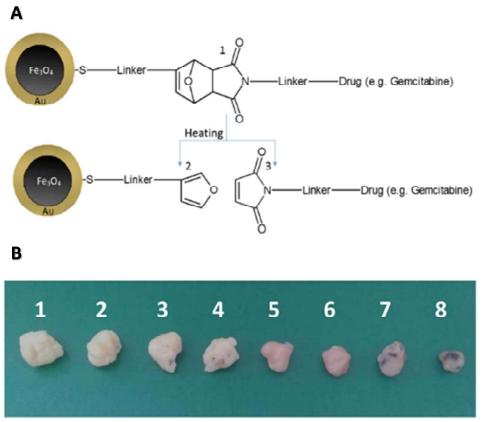

Figure 9. (A) Schematic representation of the mechanism of drug loading/release from the hybrid nanoparticle surface via heat-initiated reversal of the Diels Alder reaction. (B) Comparison of tumors after excision: 1) control, 2) control with laser irradiation, 3) HNP, 4) HNP with laser irradiation, 5) GEM, 6) GEM with laser irradiation, 7) HNP-L-GEM, 8) HNP-L-GEM with laser irradiation. The tumor was irradiated at 1064 nm as for 20 s using a ML-LASER-YB5 Q-switched Nd:YAG Laser Treatment System. Pulse width: 10 ns, pulse repetition frequency: 6 Hz, laser spot diameter: 3 mm, cooling system: water-cooled with airflow cooling. (Adapted from [57])

Peptide nucleic acids (PNA)- conjugated AuNPs were so far widely reported for biosensing, gene delivery, and *in vivo* imaging applications in the literature.[59] Cadoni et *al.* (2020) demonstrated that Fu-Ma DA reactions can be exploited to graft PNA onto the surface of AuNPs (Figure 10).[58] Results showed that attaching PNA to AuNPs through DA linkages could overcome the challenges associated with the conventional thiol-exchange-based technique, while retaining the ability to target DNA and to release the duplex chain system from AuNPs. However, this study presented some limitations: the use of laser irradiation to trigger the release of DNA from AuNPs was not investigated, and the impact of the temperature on the stability and activity of the PNA chain were not assessed.

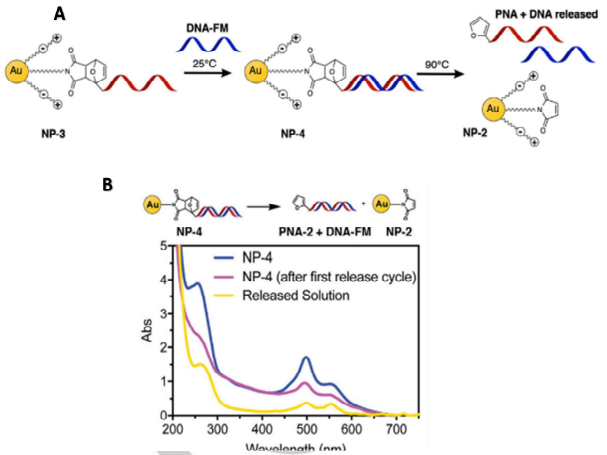

Figure 10. (A) Schematic representation of hybridization and release experiments with DNA. (B) UV-vis spectra of NPs-4 after thermal release. (Adapted from [58])

2.2.2. Organic-based nanomaterials

Light-absorbing organic-based NPs have attracted increasing attention in the last few years. Inspired by pioneering studies of light-to-heat conversion of polyaniline conductive polymers,[60] organic-based NPs have also been used for developing stimuli-responsive drug delivery systems. For instance, FDA-approved indocyanine green (ICG)-based NPs were exploited for many clinical imaging applications with an efficient light-to-heat conversion.[44, 61] Other approaches allowed the use of ICG as a photothermal agent for drug delivery systems, such as those proposed by Li et *al.* (2015).[62] The NIR photothermal effect-triggered drug delivery micellar platform based on doxorubicin (DOX) and ICG were synthesized, and encapsulated into thermoresponsive block copolymer micelles (Figure 11). The poly(oligo(ethylene glycol) methacrylate)-block-poly(furfuryl methacrylate) (POEGMA-b-PFMA) micelles were first prepared by a sequential reversible addition fragmentation chain-transfer (RAFT) polymerization reaction, and then conjugated with *N*-octyl maleimide through Diels–Alder (DA) reactions. The resulting amphiphilic block copolymer POEGMA-b-POMFMA could undergo self-assembly via nano-precipitation in the presence of the DOX and ICG.

Similarly to some metal-based NPs, these nanostructures of 34±15 nm displayed an absorption in the NIR region.[62] Upon NIR laser exposure, the local temperature increase at the micellar core led to a partial DA disassembly and a 80% DOX release. An *in vitro* cytotoxicity assay performed using Hela cells revealed a remarkably low cytotoxicity of the DOX-ICG NPs (DIMs) (at various concentrations of DOX). Upon NIR laser exposure, DIMs displayed an enhanced cytotoxicity, which was also found to be more considerable than that of NIR-activated ICG NPs (IMs). An intracellular distribution study performed after 4h of incubation showed that DOX alone could quickly enter cells and localize in the nucleus, most likely due to its high affinity with DNA. In contrast, DIMs were mainly found in the cytoplasm. Upon laser irradiation (5 min) and incubation (2h), increased DOX amounts were found in the nucleus, suggesting that DIMs can effectively deliver and photothermally release drugs within cells using NPs.

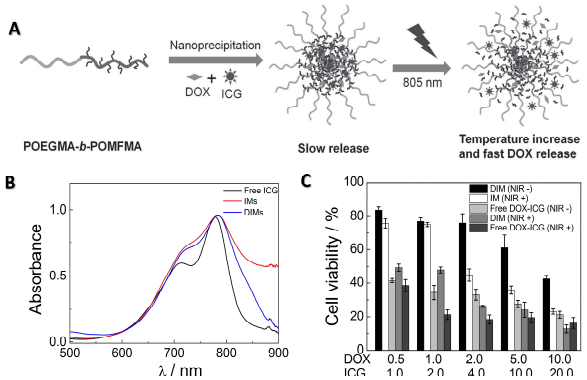

Figure 11. (A) Schematic illustration of ICG and DOX encapsulation and NIR photothermal-triggered drug release. (B) UV-Vis absorbance spectra of DIMs, IMs, and free ICG in aqueous solution. (C) HeLa cell survivals after treatment with DIMs, IMs, free ICG-DOX with or without 5 min NIR irradiation at various ICG or DOX concentrations. (Adapted from [62])

More recently, organic NPs based on polypyrrole (PPy) conductive polymers with a strong absorbance in the NIR region were found to display photothermal properties at relatively low power intensities. Interestingly, the laser power required to achieve similar light-triggered heating efficiencies than that of AuNPs was found to be lower.[44, 63] In 2016, Zhang et *al*. exploited PPy NPs for the development of a stimuli-responsive drug delivery system decorated with fluorescent dyes via Fu-Ma DA linkages.[64] In this study, a PEGlated pyrrole/azide-containing bottle-brush copolymer was simultaneously functionalized with pyrene-oxabicycloheptene-alkyne (POA, pyrene being a fluorescent dye) and sodium propynesulfonate (to enhance water-solubility and to act as a self-doping group for conjugated PPy) (Figure 12).[64] Free pyrrole molecules were allowed to copolymerize with the PEG-POA polymer's pendant pyrrole groups, forming a crosslinked PPy core layer, and consequently, PEG-POA PPy NPs (50±5 nm from TEM analysis). A light-induced heating assessment of the NPs showed an efficient heat generation upon NIR irradiation (at 808 nm, 2 W.cm^{-2}) that increased the temperature of the solution up to 70-80°C within 30 min. In contrast, the temperature of the solution containing the PEG-POA PPy bottle-brush precursor in the absence of the PPy layer was only found to be in the 35-40°C range, demonstrating the efficacy of the photothermal conversion of PEG-POA PPy NPs. The dye release profile of PEG-POA PPy NPs upon NIR laser exposure was quantified by UV-Vis. A 89% dye release via rDA reactions was observed after an irradiation time of 60 min. This result suggests that PPy NPs could be promising candidates for the development of photothermally-triggered drug delivery systems. However, further investigations on the activity and cell viability of such systems under biologically-relevant conditions would be required.

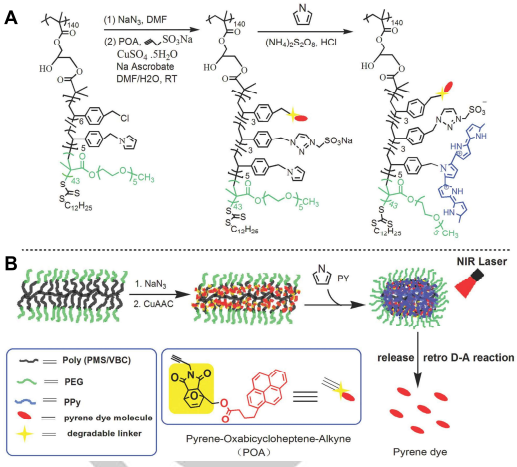

Figure 12. (A) Synthetic route of PEG-POA PPy nanoparticles. (B) Graphic showing the synthesis of PEG-POA PPy nanoparticles and photothermal-induced release of pyrene dye by the retro D–A reaction under NIR irradiation. (Adapted from [64])

2.3. Magnetothermally triggered system

In recent years, magnetic iron oxide NPs (IONPs) have been investigated for various biological applications such as magnetic resonance imaging (MRI), hyperthermia therapy, and drug delivery.[65] Upon exposure to an alternating magnetic field (AMF), IONPs can induce the generation of thermal energy due to a combination of independent mechanisms (such as the Néel relaxation, Brownian relaxation and hysteresis loss).[65a, 66] Therefore, this phenomenon has been exploited for selective hyperthermia, [66b, 67] as well as for the controlled drug delivery systems in which the heat generated upon AMF exposure can trigger the remote release of suitable therapeutic agents.[68]

Only a few examples of the use of Fu-Ma DA linkages for the development of stimuli-responsive drug release systems based on IONPs are found in the literature. In 2013, Nguyen et *al*. reported the first study involving Fu-Ma DA linkages for the development of a stimuli-responsive drug delivery system based on IONPs to control the release of fluorescent dyes upon exposure to an alternating magnetic field.[69] IONPs were prepared by a co-precipitation method, whereas a versatile multifunctional ligand containing a phosphonic acid, a furan and an alkyne was synthesized using a Kabachnok-Field reaction.[69-70] The alkyne moiety was used to link an azide-PEG chain to the ligand via a CuAAC reaction to improve the dispersibility/stability and biocompatibility of the system in biological settings. The multifunctional ligand was then linked to IONPs by exploiting the strong affinity of the phosphonic acid group for iron oxide surfaces. A maleimide-functionalized fluorescent dye (tetramethyl rhodamine) was then allowed to react (DA reaction) with the pendant furan of the ligand in water at 40°C (Figure 13).[69] The size of IONPs (13 ± 1.0 nm) was measured by transmission electron microscopy and X-ray diffraction, and was optimized using the size-sorted maghemite ferrofluid to enable an efficient bond-cleavage induced by the magnetism-thermal effect. Interestingly, the use of small IONPs has been reported to require a lower intensity of the stray magnetic field, decreasing the potential health risks caused by magnetic fields.[71] The UV/Vis

spectroscopy was used to measure the iron oxide concentration as well as to confirm the presence of fluorescence dyes on the IONPs (at 552 nm). A FRET quenching effect was observed between the dye and the iron oxide NPs,[69] offering a method to monitor the drug release (potentially intracellularly) from IONPs-based delivery systems via DA disassembly. Diluting the IONPs dispersion to 2.5 × 10^{-3} and 2.5 × 10^{-2} wt%, resulted in a temperature increase of 0.0014°C and 0.014°C every minute, respectively, limiting the undesired increase in temperature in the medium. As expected, incubating IONPs in a NaCl aqueous solution for 22 mins at 30°C with no AMF exposure did not result in any significant release of the dye. In contrast, after AMF exposure, IONPs (dye concentration of 1.8 mM) resulted in a 3 nM (2 min at 2.5 × 10^{-3} wt%) and 105 nM (10 min at 2.5 × 10^{-2} wt%) release of the dye, repectively (this range of concentrations matches the IC_{50} of many anticancer drugs). This result demonstrates that such a drug delivery system based on IONPs could be useful to selectively treat different types of cancers, given the ability of tumors to preferentially accumulate NPs via the EPR effect.

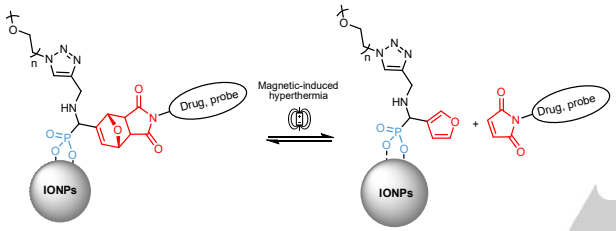

Figure 13. IONPs bearing a multifunctional ligand. The magnetism-induced localized heating initiates the rDA reaction to release drugs/drug candidates. (Adapted from [69])

In 2015, Yang Lia et *al.* developed other classes of IONPs by using magnetic organic-based hyaluronic acid (HA) nanospheres for the vectoring delivery of adipogenic factors.[72] Indeed, HA is the main glycosaminoglycan and the backbone of proteoglycans in the extracellular matrix. Because of its excellent properties, HA has been applied in cell scaffolds for tissue regeneration.[72] Magnetic hyaluronic acid (HA) nanospheres were prepared using a combined emulsification-precipitation polymerization via the aqueous DA chemistry between furan and maleimide HA derivatives[72]. IONPs with a Fe_3O_4 core were prepared by a co-precipitation method, and then encapsulated into the HA nanospheres to produce magnetic HA NPs. Subsequently, a furan-functionalized-dexamethasone (Dex)-peptide was attached to the HA nanospheres via the Fu-Ma DA reaction. As previously mentioned, Dex has been used as an adipogenic factor to induce adipogenesis for adipose regeneration (Figure 14). The magnetic-HA-NPs showed high stability in the biological system, and the super-paramagnetism of IONPs was retained after encapsulation in the HA nanosphere. An MTT assay performed using human adipose-derived stem cells (ASCs) showed that magnetic HA NPs did not influence the growth of ASCs at various concentrations. Upon AMF exposure, Dex-furan peptide-loaded NPs showed a higher cell viability than the untreated NPs samples, demonstrating that Dex-furan peptide could be successfully released via rDA reactions triggered by an external magnetic field.

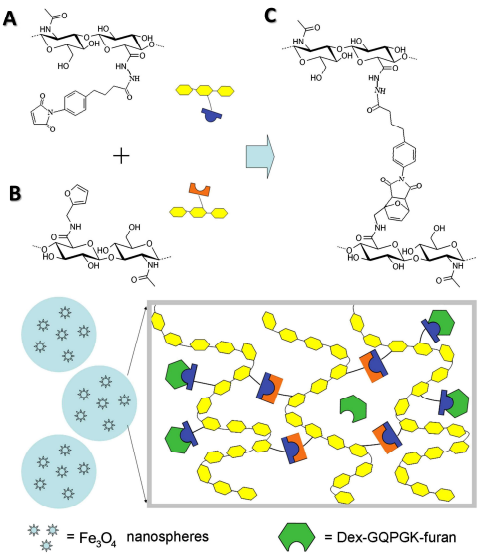

Figure 14. Schematic of magnetic hyaluronic acid (HA) nanosphere bearing dexamethasone immobilization via the DA linkage. (A) furan-modified HA macromers. (B) maleimide-modified HA macromers. (C) HA nanosphere system was generated by conjugating HA-furan and Dex-GQPGK-furan with HA-maleimide. (Adapted from [72])

Hempelmann and coworkers (**2017**) recently reported the development of functionalized bi/magnetic core-shell NPs to control the release of Doxorubicin (DOX), a chemotherapy medication used to treat several cancers.[73] This new class of IONPs has a reduced surface energy and optimum size for NPs due to the interfacial exchange interaction between hard and soft magnetic faces, thus enhancing the heating efficiency of IONPs. The maleimide modified-DOX was then attached to the surface of furan-functionalized IONPs via Fu-Ma DA linkages. As expected, the DOX-loaded IONPs showed excellent stability in PBS medium and no significant toxicity against either Hela cancer cells or HepG2 nontumorigenic cells. However, DOX-conjugated IONPs induced cell death up to 80% after AMF exposure. This result could be explained by the synergistic effect of magnetically-induced hyperthermia and magnetically-triggered drug release, suggesting that the localized heat caused by IONPs upon AMF exposure successfully activated the release of DOX via rDA, inducing cancer cell death. However, this study did not compare the cytotoxicity of drug-conjugated IONPs with the non-conjugated drug on cancer cells.

This was further investigated later on by Ott et *al.* (**2017**). The study reported the development of a drug delivery system using a commercial IONPs-MAGSILICA® containing a ferritic core (mixture of maghemite Fe_2O_3 and magnetite Fe_3O_4), a silica shell for tumor-selective drug delivery and release of toxins.[74] This class of IONPs was shown to have many advantages, including *i*) rendering the super-paramagnetic properties of IONPs, *ii*) enhancing the chemical resistance of iron cores, and *iii*) allowing chemical functionalization. Accordingly, furan-functionalized ansamitosin drugs were linked to the surface of maleimide-modified IONPs via Fu-Ma DA reactions that were carried out at 62°C for three days. The supernatant was then decanted by fixation of IONPs with an external magnet. The LC/MS analysis of the suspended solution of IONPs in methanol revealed an efficient

drug-loading, with about 60% of ansamitosin being successfully attached at the surface of IONPs (Figure 15). Drug-conjugated IONPs showed excellent stability in cell media in the presence or absence of serum albumin. In addition, neither IONPs nor drug-conjugated IONPs (20 nM) exhibited any cytotoxicity in Huh-7 hepatocarcinoma cells after 24 h, 48 h, and 72 h of treatment without AMF exposure, whereas both furan-functionalized ansamitosin and ansamitosin alone showed a very considerable anti-proliferative activity in the same cell line, with an IC_{50} ~ 1.5 nM. The release of drugs from IONPs was completed within 30 min, after exposure to a high-frequency magnetic field (778 Mhz, 5kW). Interestingly, the IC_{50} value of the magnetically-induced drug release was found to be 18.7 nM, a much higher value than that of the drug alone (1.5 nM). This result reveals that the drug is released under inductive heating conditions from the drug-conjugated IONPs resulting in the diminution of the cell viability in a dose-dependent manner. Furthermore, an additional *in vivo* study on mice demonstrated that the heat-induced release of drugs from IONPs effectively prevents cancer tumor growth.

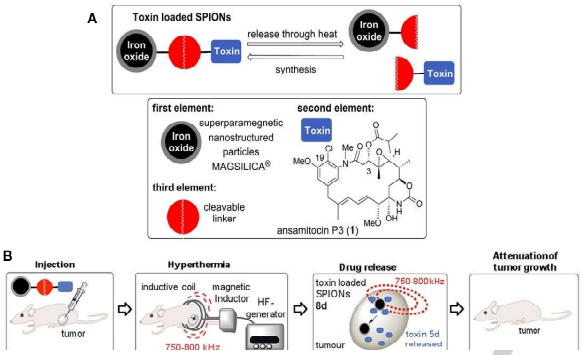

Figure 15. (A) Concept for the combination of hyperthermia with chemotherapy using drug-nanostructured particle conjugates. (B) Magnetic-Nanoparticle/Ansamitocin Conjugates—Inductive Heating Leads to Decreased Cell Proliferation *In Vitro* and Attenuation of Tumor Growth *In Vivo*. (Adapted from [74])

3. Summary and Outlook

This section (currently in progress) will also be part of the review.

Acknowledgements

This work was supported by the Natural Sciences and Engineering Research Council of Canada (NSERC), the Fonds de Recherche du Québec Santé (FRQS) and the Institut national de la recherche scientifique (INRS).

Conflict of Interest

The authors declare no conflict of interest.

Keywords: Thermosensitive linkages, stimuli-responsive drug delivery system, drug delivery, Diels-Alder cycloaddition, retro Diels-Alder reaction, exogenous stimulation-triggered heating.

[1] S. Mura, J. Nicolas, P. Couvreur, *Nature materials* **2013**, *12*, 991.

[2] M. Bikram, J. L. West, *Expert Opinion on Drug Delivery* **2008**, *5*, 1077-1091.

[3] V. P. Torchilin, *Nature reviews Drug discovery* **2014**, *13*, 813.

[4] S. K. Sharma, N. Shrivastava, F. Rossi, L. D. Tung, N. T. K. Thanh, *Nano Today* **2019**, *29*, 100795.

[5] M. Gregoritza, F. P. Brandl, *European Journal of Pharmaceutics and Biopharmaceutics* **2015**, *97*, 438-453.

[6] a) Y. G. Shtyrlin, D. G. Murzin, N. A. Luzanova, G. G. Iskhakova, V. D. Kiselev, A. I. Konovalov, *Tetrahedron* **1998**, *54*, 2631-2646; b) A. Kumar, *Chemical Reviews* **2001**, *101*, 1-20; c) T. Inukai, T. Kojima, *The Journal of Organic Chemistry* **1966**, *31*, 1121-1123; d) S. Otto, J. B. Engberts, *Tetrahedron letters* **1995**, *36*, 2645-2648.

[7] O. Diels, K. Alder, *Justus Liebigs Annalen der Chemie* **1928**, *460*, 98-122.

[8] a) F. Fringuelli, A. Taticchi, *The Diels-Alder reaction: selected practical methods*, John Wiley & Sons, **2002**; b) J. Sauer, *Angewandte Chemie International Edition in English* **1967**, *6*, 16-33.

[9] R. B. Woodward, R. Hoffmann, *Journal of the American Chemical Society* **1965**, *87*, 395-397.

[10] I. Fleming, *Molecular orbitals and organic chemical reactions*, John Wiley & Sons, **2011**.

[11] a) N. Kuramoto, K. Hayashi, K. Nagai, *Journal of Polymer Science Part A: Polymer Chemistry* **1994**, *32*, 2501-2504; b) L. Engle, K. Wagener, *Journal of Macromolecular Science, Part C: Polymer Reviews* **1993**, *33*, 239-257.

[12] a) A. Gandini, *Progress in Polymer Science* **2013**, *38*, 1-29; b) V. Froidevaux, M. Borne, E. Laborbe, R. Auvergne, A. Gandini, B. Boutevin, *RSC Advances* **2015**, *5*, 37742-37754.

[13] a) A. Castonguay, E. Wilson, N. Al-Hajaj, L. Petitjean, J. Paoletti, D. Maysinger, A. Kakkar, *Chemical Communications* **2011**, *47*, 12146-12148; b) S. Kirchhof, F. P. Brandl, N. Hammer, A. M. Goepferich, *Journal of Materials Chemistry B* **2013**, *1*, 4855-4864; c) H.-V. Tran, M. M. Haghdoost, S. Poulet, P. Tcherkawsky, A. Castonguay, *Dalton Transactions* **2021**; d) Z. Wei, J. H. Yang, X. J. Du, F. Xu, M. Zrinyi, Y. Osada, F. Li, Y. M. Chen, *Macromolecular Rapid Communications* **2013**, *34*, 1464-1470; e) A. Oluwasanmi, W. Al-Shakarchi, A. Manzur, M. H. Aldebasi, R. S. Elsini, M. K. Albusair, K. J. Haxton, A. D. Curtis, C. Hoskins, *Journal of Controlled Release* **2017**, *266*, 355-364.

[14] A. Gandini, M. N. Belgacem, *Progress in Polymer Science* **1997**, *22*, 1203-1379.

[15] Y. Imai, H. Itoh, K. Naka, Y. Chujo, *Macromolecules* **2000**, *33*, 4343-4346.

[16] A. Vieyres, T. Lam, R. Gillet, G. Franc, A. Castonguay, A. Kakkar, *Chemical Communications* **2010**, *46*, 1875-1877.

[17] B. J. Adzima, C. J. Kloxin, C. A. DeForest, K. S. Anseth, C. N. Bowman, *Macromolecular rapid communications* **2012**, *33*, 2092-2096.

[18] a) S. N. Pieniazek, K. N. Houk, *Angewandte Chemie International Edition* **2006**, *45*, 1442-1445; b) R. C. Boutelle, B. H. Northrop, *The Journal of organic chemistry* **2011**, *76*, 7994-8002.

[19] H. Kwart, I. Burchuk, *Journal of the American Chemical Society* **1952**, *74*, 3094-3097.

[20] a) S. Otto, J. B. Engberts, J. C. Kwak, *Journal of the American Chemical Society* **1998**, *120*, 9517-9525; b) K. N. Houk, R. W. Strozier, *Journal of the American Chemical Society* **1973**, *95*, 4094-4096.

[21] S. Kirchhof, A. Strasser, H.-J. Wittmann, V. Messmann, N. Hammer, A. M. Goepferich, F. P. Brandl, *Journal of Materials Chemistry B* **2015**, *3*, 449-457.

[22] M. Sortino, V. Cechinel Filho, R. Corrêa, S. Zacchino, *Bioorganic & Medicinal Chemistry* **2008**, *16*, 560-568.

[23] a) J. K. Andersen, J. Q. Mo, D. G. Hom, F. Y. Lee, P. Harnish, R. W. Hamill, T. H. McNeill, *Journal of Neurochemistry* **1996**, *67*, 2164-2171; b) A. H. Jansen, B. J. Russell, V. Chernick, *Canadian Journal of Physiology and Pharmacology* **1975**, *53*, 726-733.

[24] F. Benito-Lopez, A. J. Kettelarij, R. J. Egberink, A. Velders, R. M. Tiggelaar, J. G. Gardeniers, D. Reinhoudt, W. Verboom, *Chimica oggi= Chemistry today* **2010**, *28*, 56-59.

[25] a) E. Abbasi, S. F. Aval, A. Akbarzadeh, M. Milani, H. T. Nasrabadi, S. W. Joo, Y. Hanifehpour, K. Nejati-Koshki, R. Pashaei-Asl, *Nanoscale Research Letters* **2014**, *9*, 247; b) E. R. Gillies, J. M. J. Fréchet, *Drug Discovery Today* **2005**, *10*, 35-43; c) T. Barrett, G. Ravizzini, P. L. Choyke, H. Kobayashi, *IEEE Engineering in Medicine and Biology Magazine* **2009**, *28*, 12-22.

[26] T. Vermonden, R. Censi, W. E. Hennink, *Chemical Reviews* **2012**, *112*, 2853-2888.

[27] J. L. Drury, D. J. Mooney, *Biomaterials* **2003**, *24*, 4337-4351.

[28] H.-L. Wei, Z. Yang, Y. Chen, H.-J. Chu, J. Zhu, Z.-C. Li, *European Polymer Journal* **2010**, *46*, 1032-1039.

[29] H.-L. Wei, Z. Yang, H.-J. Chu, J. Zhu, Z.-C. Li, J.-S. Cui, *Polymer* **2010**, *51*, 1694-1702.

[30] C. Toncelli, D. C. De Reus, F. Picchioni, A. A. Broekhuis, *Macromolecular Chemistry and Physics* **2012**, *213*, 157-165.

[31] a) H. Tan, J. P. Rubin, K. G. Marra, *Macromolecular Rapid Communications* **2011**, *32*, 905-911; b) C. García-Astrain, A. Gandini, D. Coelho, I. Mondragon, A. Retegi, A. Eceiza, M. A. Corcuera, N. Gabilondo, *European Polymer Journal* **2013**, *49*, 3998-4007.

[32] a) B. J. Adzima, H. A. Aguirre, C. J. Kloxin, T. F. Scott, C. N. Bowman, *Macromolecules* **2008**, *41*, 9112-9117; b) H.-L. Wei, K. Yao, H.-J. Chu, Z.-C. Li, J. Zhu, Y.-M. Shen, Z.-X. Zhao, Y.-L. Feng, *Journal of Materials Science* **2012**, *47*, 332-340.

[33] M. Gregoritza, V. Messmann, K. Abstiens, F. P. Brandl, A. M. Goepferich, *Biomacromolecules* **2017**, *18*, 2410-2418.

[34] K. C. Koehler, K. S. Anseth, C. N. Bowman, *Biomacromolecules* **2013**, *14*, 538-547.

[35] K. C. Koehler, D. L. Alge, K. S. Anseth, C. N. Bowman, *Biomaterials* **2013**, *34*, 4150-4158.

[36] F. Mosna, L. Sensebe, M. Krampera, *Stem cells and development* **2010**, *19*, 1449-1470.

[37] S. M. Taimoory, S. I. Sadraei, R. A. Fayoumi, S. Nasri, M. Revington, J. F. Trant, *The Journal of Organic Chemistry* **2018**, *83*, 4427-4440.

[38] M. Shi, J. H. Wosnick, K. Ho, A. Keating, M. S. Shoichet, *Angewandte Chemie* **2007**, *119*, 6238-6243.

[39] M. Shi, K. Ho, A. Keating, M. S. Shoichet, *Advanced functional materials* **2009**, *19*, 1689-1696.

[40] R. Zhang, X. Qin, F. Kong, P. Chen, G. Pan, *Drug Deliv* **2019**, *26*, 328-342.

[41] V. Steven, D. Graham, *Organic & biomolecular chemistry* **2008**, *6*, 3781-3787.

[42] M. Haghdoost, G. Golbaghi, M. Létourneau, S. A. Patten, A. Castonguay, *Eur J Med Chem* **2017**, *132*, 282-293.

[43] X. Huang, P. K. Jain, I. H. El-Sayed, M. A. El-Sayed, *Lasers in medical science* **2008**, *23*, 217-228.

[44] D. Jaque, L. Martínez Maestro, B. del Rosal, P. Haro-Gonzalez, A. Benayas, J. L. Plaza, E. Martín Rodríguez, J. García Solé, *Nanoscale* **2014**, *6*, 9494-9530.

[45] A. B. S. Bakhtiari, D. Hsiao, G. Jin, B. D. Gates, N. R. Branda, *Angewandte Chemie* **2009**, *121*, 4230-4233.

[46] C. Abbruzzese, P. Fornari, R. Massidda, F. Vegliò, S. Ubaldini, *Hydrometallurgy* **1995**, *39*, 265-276.

[47] a) I. Fratoddi, I. Venditti, C. Cametti, M. V. Russo, *Nano Research* **2015**, *8*, 1771-1799; b) N. Khlebtsov, L. Dykman, *Chemical Society Reviews* **2011**, *40*, 1647-1671.

[48] P. Jonkheijm, D. Weinrich, H. Schröder, C. M. Niemeyer, H. Waldmann, *Angewandte Chemie International Edition* **2008**, *47*, 9618-9647.

[49] a) M. Alrahili, V. Savchuk, K. McNear, A. Pinchuk, *Scientific Reports* **2020**, *10*, 18790; b) C. Hoskins, Y. Min, M. Gueorguieva, C. McDougall, A. Volovick, P. Prentice, Z. Wang, A. Melzer, A. Cuschieri, L. Wang, *Journal of nanobiotechnology* **2012**, *10*, 1-12.

[50] Z. Huang, F. Chen, P. A. Bennett, N. Tao, *Journal of the American Chemical Society* **2007**, *129*, 13225-13231.

[51] S. Mayilo, B. Ehlers, M. Wunderlich, T. A. Klar, H.-P. Josel, D. Heindl, A. Nichtl, K. Kürzinger, J. Feldmann, *Analytica Chimica Acta* **2009**, *646*, 119-122.

[52] S. Yamashita, H. Fukushima, Y. Akiyama, Y. Niidome, T. Mori, Y. Katayama, T. Niidome, *Bioorganic & medicinal chemistry* **2011**, *19*, 2130-2135.

[53] S. Yamashita, H. Fukushima, Y. Niidome, T. Mori, Y. Katayama, T. Niidome, *Langmuir* **2011**, *27*, 14621-14626.

[54] W. F. Zandberg, A. B. S. Bakhtiari, Z. Erno, D. Hsiao, B. D. Gates, T. Claydon, N. R. Branda, *Nanomedicine: Nanotechnology, Biology and Medicine* **2012**, *8*, 908-915.

[55] N. Kitamura, K. Tanaka, Y. Chujo, *Bioorganic & medicinal chemistry letters* **2013**, *23*, 281-286.

[56] C. Dalvit, E. Ardini, G. P. Fogliatto, N. Mongelli, M. Veronesi, *Drug Discovery Today* **2004**, *9*, 595-602.

[57] A. Oluwasanmi, W. Al-Shakarchi, A. Manzur, M. H. Aldebasi, R. S. Elsini, M. K. Albusair, K. J. Haxton, A. D. M. Curtis, C. Hoskins, *Journal of Controlled Release* **2017**, *266*, 355-364.

[58] E. Cadoni, D. Rosa-Gastaldo, A. Manicardi, F. Mancin, A. Madder, *Frontiers in Chemistry* **2020**, *8*.

[59] E. Boisselier, D. Astruc, *Chemical Society Reviews* **2009**, *38*, 1759-1782.

[60] a) J. F. Lovell, C. S. Jin, E. Huynh, H. Jin, C. Kim, J. L. Rubinstein, W. C. W. Chan, W. Cao, L. V. Wang, G. Zheng,

Nature Materials **2011**, *10*, 324-332; b) M. A. Albota, C. Xu, W. W. Webb, *Applied optics* **1998**, *37*, 7352-7356.

[61] J. Yu, D. Javier, M. A. Yaseen, N. Nitin, R. Richards-Kortum, B. Anvari, M. S. Wong, *Journal of the American Chemical Society* **2010**, *132*, 1929-1938.

[62] H. Li, J. Li, W. Ke, Z. Ge, *Macromolecular Rapid Communications* **2015**, *36*, 1841-1849.

[63] L. Cheng, K. Yang, Q. Chen, Z. Liu, *ACS nano* **2012**, *6*, 5605-5613.

[64] H. Zhang, L. Xiong, X. Liao, K. Huang, *Macromolecular Rapid Communications* **2016**, *37*, 149-154.

[65] a) L. H. Reddy, J. L. Arias, J. Nicolas, P. Couvreur, *Chemical reviews* **2012**, *112*, 5818-5878; b) Z. Cheng, A. Al Zaki, J. Z. Hui, V. R. Muzykantov, A. Tsourkas, *Science* **2012**, *338*, 903-910; c) E. Amstad, M. Textor, E. Reimhult, *Nanoscale* **2011**, *3*, 2819-2843.

[66] a) A. E. Deatsch, B. A. Evans, *Journal of Magnetism and Magnetic Materials* **2014**, *354*, 163-172; b) C. S. Kumar, F. Mohammad, *Advanced drug delivery reviews* **2011**, *63*, 789-808.

[67] a) D. Yoo, H. Jeong, C. Preihs, J.-s. Choi, T.-H. Shin, J. L. Sessler, J. Cheon, *Angewandte Chemie International Edition* **2012**, *51*, 12482-12485; b) S. Laurent, S. Dutz, U. O. Häfeli, M. Mahmoudi, *Advances in colloid and interface science* **2011**, *166*, 8-23; c) J.-H. Lee, J.-t. Jang, J.-s. Choi, S. H. Moon, S.-h. Noh, J.-w. Kim, J.-G. Kim, I.-S. Kim, K. I. Park, J. Cheon, *Nature nanotechnology* **2011**, *6*, 418-422.

[68] a) J. Dobson, *Nature nanotechnology* **2008**, *3*, 139-143; b) A. K. Gupta, M. Gupta, *biomaterials* **2005**, *26*, 3995-4021; c) S. Mornet, S. Vasseur, F. Grasset, E. Duguet, *Journal of materials chemistry* **2004**, *14*, 2161-2175.

[69] T. T. N'Guyen, H. T. Duong, J. Basuki, V. Montembault, S. Pascual, C. Guibert, J. Fresnais, C. Boyer, M. R. Whittaker, T. P. Davis, *Angewandte Chemie* **2013**, *125*, 14402-14406.

[70] L. Ménard, L. Fontaine, J.-C. Brosse, *Reactive Polymers* **1994**, *23*, 201-212.

[71] M. Jeon, M. V. Halbert, Z. R. Stephen, M. Zhang, *Advanced Materials* **2021**, *33*, 1906539.

[72] Y. Jia, M. Fan, H. Chen, Y. Miao, L. Xing, B. Jiang, Q. Cheng, D. Liu, W. Bao, B. Qian, *Journal of colloid and interface science* **2015**, *458*, 293-299.

[73] M. Hammad, V. Nica, R. Hempelmann, *Colloids and Surfaces B: Biointerfaces* **2017**, *150*, 15-22.

[74] K. Seidel, A. Balakrishnan, C. Alexiou, C. Janko, R. M. Komoll, L. L. Wang, A. Kirschning, M. Ott, *Chemistry–A European Journal* **2017**, *23*, 12326-12337.

1.2 Ruthenium-based compounds for cancer therapy

Metal-based complexes have received increasing attention due to their outstanding biological activities. Compared to purely organic compounds, inorganic complexes have unique properties and can offer excellent opportunities to the field of chemotherapy. Currently, platinum-based complexes such as *cis*-platin are widely used to treat distinct types of cancer.[1] Indeed, *cis*-platin, the most well-known metal-based anticancer drug, is included in about 50% of all cancer regimens,[1] and is used for over 90% of testicular cancer cases. Inspired by the discovery of anticancer activity of *cis*-platin in 1960, the medicinal properties of a large number of metal-based compounds have been explored. Further, despite the numerous chemotherapeutic agents synthesized to date, platinum-based complexes remain some of the most effective anticancer drugs (Figure 3).[2]

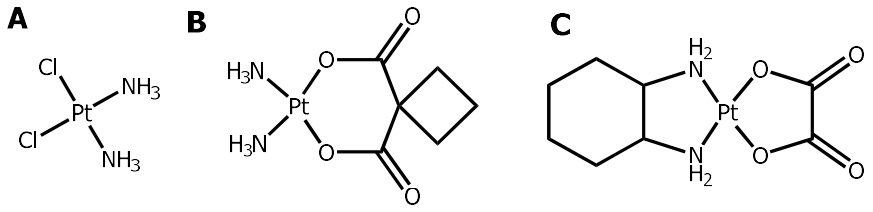

Figure 3. Structure of platinum-based therapeutic agents: A) *cis*-platin, B) carboplatin, C) oxaliplatin.

Despite its important success in clinics, *cis*-platin has also been shown to cause numerous side effects. Since the main mode of action of platinum drugs is DNA interaction, they are toxic to cancer cells and normal cells.[3] Because of this lack of selectivity, cancer patients usually suffer from important side effects, including kidney and nerve damage, hearing difficulties, and others.[3] In addition, cancer cells can develop resistance to platinum-based drugs that limit their clinical use. This phenomenon can be explained through two mechanisms:[3] *i*) decreased cellular drug accumulation or enhancement of cell-repair DNA damage caused by *cis*-platin; *ii*) increased intracellular thiol levels leading to *cis*-platin deactivation by coordination.

In recent years, considerable efforts have been devoted to replacing platinum drugs with other transition metal-based agents, specifically with ruthenium (Ru).

1.2.1 Chemotherapeutic agents based on ruthenium

Among various organometallic therapeutic agents mainly designed for replacing platinum-based drugs, ruthenium (Ru) has attracted increasing attention during the last few years. Accordingly, some highly potent and selective anticancer Ru-based compounds have proven beneficial compared to other metal-based antitumor drugs, including the currently clinically-used drug *cis*-platin.[4] Furthermore, many studies have reported that some Ru-based compounds are active against platinum-resistant cell lines, particularly breast cancer cells such as T47D and ovarian cancer cells such as A2780cisR.[5] In addition, the importance of anticancer ruthenium complexes is highlighted by the fact that two Ru(III) complexes have already entered phase II of clinical trials (Figure 4).[6]

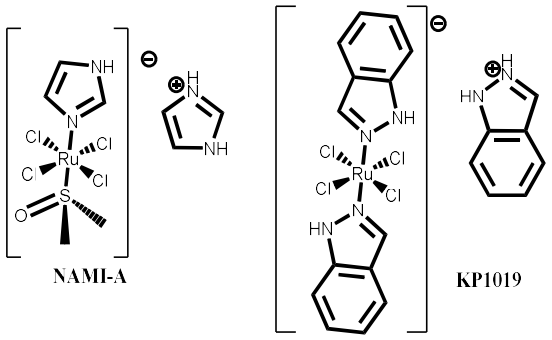

Figure 4. Structure of NAMI-A and KP1019

Like *cis*-platin, ruthenium complexes interact with DNA but, as anticipated, interact differently, and some ruthenium compounds bind even more strongly, leading to an adduct that is more resistant to cell repair mechanisms. [7] [8]

It is also believed that Ru drugs can induce cancer cell death by various mechanisms. For example, they can enter cells by mimicking iron through their interaction with transferrin at the surface of the cell,[9] binding to human serum albumin,[10] or by interacting with mitochondria.[11] In addition, Ru(III) complexes have often been reported to be more selective towards cancer cells than Ru(II) complexes.[12]

It has been proposed that the mode of action of some of these Ru(III)-based drugs involves their "activation by reduction". Due to the lower oxygen content and higher acidity or cancer cells/tumors compared to normal tissues, inert Ru(III) complexes are then selectively being reduced to Ru(II) species, which are more toxic than their Ru(III) counterparts.[13]

Although various Ru-based drug candidates have been synthesized, ruthenium arene complexes have attracted increased interest in recent years.[8] Ru(II) arene complexes bearing a neutral arene ring showed higher stability to displacement in bioassay media than the cyclopentadienyl (Cp) Ru complexes.[8] A review of the literature on these half-sandwich "piano-stool" Ru(II)-arene complexes exposed the great potential of these organometallic complexes as an alternative to conventional platinum-based therapeutic agents (Figure 5).[8, 13]

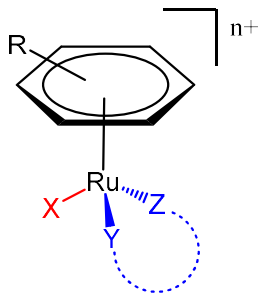

Figure 5. Structure of ruthenium-arene complexes

In addition, these half-sandwich ruthenium–based compounds can potentially undergo a modification of various arene derivatives, and their substituents include leaving group (X), chelating ligand (YZ), and overall charge of the complex (n^+). Consequently, it offers an ability to refine the chemical reactivity of complexes and control their pharmacological properties such as cell uptake, bio-distribution, interaction with biomolecules, and more.

The first possibility is based on the nature of the arene ring of ruthenium(II)-arene complexes which have exhibited a profound impact on the cytotoxicity of complexes. For instance, the increased hydrophobicity of the arene ring may facilitate transportation through the cancer cell membrane and, therefore, enhance these complexes' anticancer activity.[14]

The second possibility is, in referred to the mode of action above-mentioned of the ruthenium-based compound, the leaving group (X), which strongly influenced the cytotoxicity of ruthenium complexes. For instance, in the case of $[(\eta^6\text{-arene})Ru(en)Cl]^+$, hydrolysis is largely suppressed outside the nucleus where high chloride concentration is found. However, under low chloride concentration inside the tumor site, the anticancer activity of Ru complex can also be activated through hydrolysis with water molecules in the environment.[8] The nature of X can also influence the rate and extent of hydrolysis of Ru-X bond. It has been reported that the difference in the hydrolysis of Ru complexes bearing X=Cl or X=Br is negligible but was 3- to 7-fold slower in the case of X=I or wholly blocked when X is pyridine.[15] Thus this effect can lead to the reduction of anticancer activity of Ru complexes.

The third possibility concerns the nature of the YZ chelating ligand, which has been reported to influence the reactivity of Ru(II)-arene complexes.[8] For example, the modification of the neutral chelate with an anion O,O-chelator acetylacetonate can significantly enhance the rate of Ru complexes' hydrolysis.[8] In addition, the coordination of hydrogen-bond donor chelating ligands such as ethylenediamine to Ru complexes influences the rate of binding to DNA nucleobase and affects nucleobase selectivity.[8]

Finally, bringing modifications to the chelating ligands can also provide an ability to refine the chemical reactivity of Ru complexes, therefore allowing to control over their anticancer activity and selectivity. Indeed, our research group has recently reported the influence of substituents of the chelating ligands on the antiproliferative activity of Ru(II)η^6-arene complexes bearing N, O-bidentate ligands. It was shown that increasing the hydrophobicity of the substituents on N, O-bidentate ligands can enhance the cellular uptake of Ru complexes and thus lead to an improvement of their anticancer activity (Figure 6).[16]

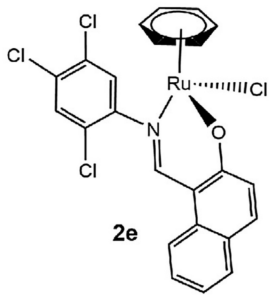

IC_{50} values of ligand **1e**, complexes **2e** and *cis*-platin against SH-SY5Y, MCF-7 and A2780 cancer cell lines.

	IC_{50} (μM)[a]		
	MCF-7	SH-SY5Y	A2780
1e	>50	>50	>50
2e	23.0 (±2.0)	16.1 (±3.5)	12.6 (±1.0)
cis-platin	27.2 (±2.3)	4.1 (±0.1)	1.3 (±0.3)

[a] Inhibitory activity was determined by exposure of cell lines to the complex for 48 h and expressed as a concentration required to inhibit the cell metabolic activity by 50% (IC_{50}). Values in parentheses represent the standard deviation of two to four independent experiments.

Figure 6. IC_{50} values of complexes **2e** and *cis*-platin against several cancer cell lines.[16]

Although metal-based drug candidates in general (or ruthenium organometallic anticancer drug in particularly) have shown tremendous potential in cancer therapy, their development has unfortunately raised some issues related to their pharmacological deficiencies such as poor bioavailability, non-specific distribution, development of multiple drug resistance, and non-specific targeting, rapid blood clearance and also poor solubility in the physiological environment.[17]

1.2.2 Examples of functionalization of metal-based drug candidates by Diels-Alder linkages

Although Diels-Alder linkages have been widely used for the development of drug delivery systems, however, the potential of this linkage to modulate has been rarely applied to functionalize ruthenium- or metal-based based drug candidates with bioactive molecules to modulate the biological activities of complexes.

For example, the research group of Rudolf reported a few studies using the Diels-Alder reaction to functionalize metal-based complexes.[18] In 1997, the authors demonstrated a performing Diels-Alder reaction on a $CpFe(CO)_2$(N-maleimidato) complex that was reacted with 1,3-diphenylisobenzofuran to afford the Diels-Alder adduct in nearly quantitative yield. (Figure 7. B). The reaction between the maleimide containing-metal complex with 1,3-diphenylisobenzofuran furan is indicated much more slowly than the parent maleimide. This result could be explained by the donating electron effect of $CpFe(CO)_2$ group towards the maleimide substituents resulting in a slower DA reaction than the reaction of the maleimide ligand.[18c]

In another study reported in 2009, they also performed the DA reaction of metallocarbonyl complexes of Fe, W, and Mo with a less reactive diene, cyclopentadiene, compared to the 1,3-diphenylisobenzofuran in the previous study (Figure 7. C). [18a] The DA reaction was carried out in CH_2Cl_2 under conditions mimicking biological labeling (water-methanol 9:1 to 3:1) at room temperature in only 30 minutes to afford stable complexes with 50–80% yield. Accordingly, the kinetic of DA reaction of these metallocarbonyl complexes with cyclopentadiene is much more slowly than with 1,3-diphenylisobenzofuran.

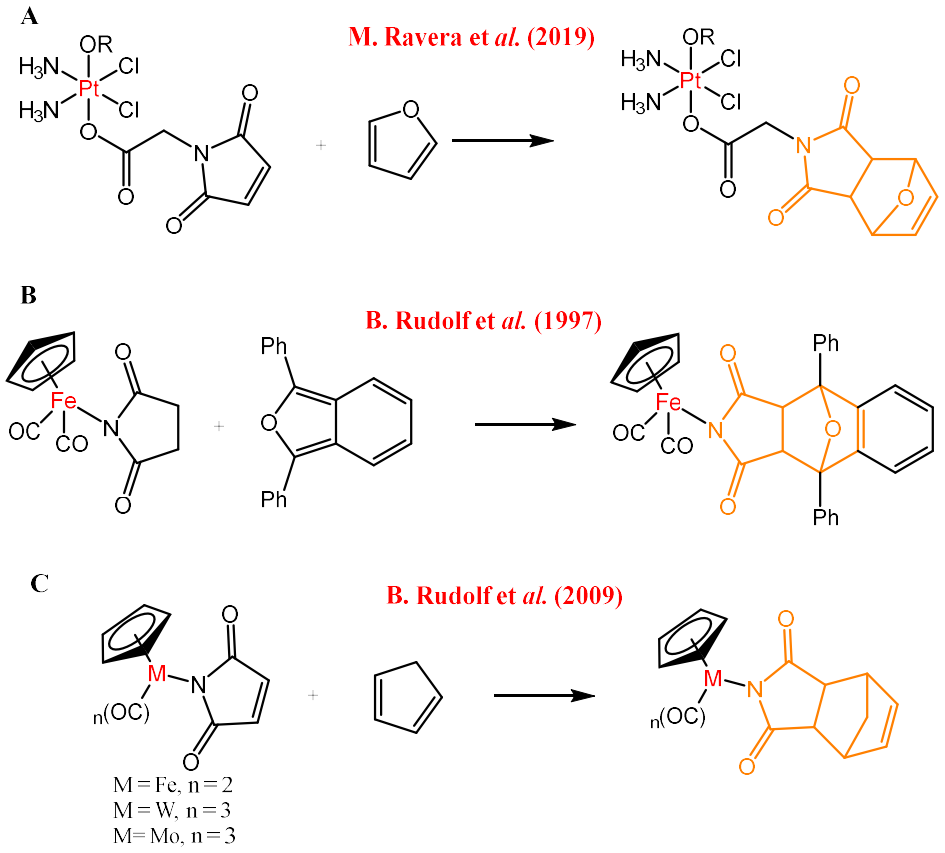

Figure 7. Examples of functionalization of metal-based drug candidates by DA linkages. (adapted from [19],[18c])

More recently, Gabano and coworkers reported the functionalization of Pt(IV) complexes, which act as antitumor prodrugs, with silica nanoparticles via furan-maleimide DA reactions (Figure 7. A).[19] Pt(IV) complexes containing axial maleimide were prepared by oxidation of cisplatin and oxidized with hydrogen peroxide in ethanol that was reacted with maleimide-containing ligand by using N N'-

dicyclohexylcarbodiimide, DCC). Pt(IV) complexes containing axial maleimide were then attached to the silica-NPs by the DA reaction with the furan groups on the surface of silica NPs.

Based on the research in the literature, DA linkages, to our knowledge, have not yet been exploited for the delivery of ruthenium-based drug candidates. In addition, it is important to note that these examples as mentioned above only discussed the synthetic methods and characterization of complexes but did not provide any background information about their behaviors in biological condition and their biological activity, particularly cytotoxicity towards cancer cells.

2. HYPOTHESES AND OBJECTIVES

2.1 Hypotheses

- Diels-Alder reactions will take place on furan-containing Ru drug candidates.
- Functionalizing Ru-based drug candidates with highly lipophilic agents via DA linkages will enhance their activity against cancer cells.
- Kinetic endo and thermodynamic exo DA adducts, known to undergo disassembly at different temperatures, will display a different antiproliferative activity against cancer cells.
- Ru thermo-sensitive and thermostable complexes (for which the double bond of the DA linkage was reduced) will show a different antiproliferative activity against cancer cells.

2.2 Objectives

Main objective: The main goal of this project is to develop synthetic pathways to Ru complexes bearing furan/maleimide DA linkages and study their reactivity/stability under biologically relevant conditions, which will help pave the way to the development of improved drug candidates and stimuli-responsive drug delivery systems involving Ru- or other metal-based drugs/drug candidates.

- **Specific objective 1**: To prepare Ru drug candidates including furan/maleimide DA thermo-sensitive linkages and their thermo-stable analogues.
  - Objective 1a: To synthesize, purify and characterize a furan-containing Ru drug candidate and maleimides of a different electronic nature.
  - Objective 1b: To link maleimides to the furan-functionalized Ru drug candidate via a DA reaction.
  - Objective 1c: To prepare Ru thermo-stable analogues of the complexes prepared in 1b.
- **Specific objective 2:** To evaluate the solubility and stability of the furan-containing Ru complex, Ru DA adducts and their thermo-stable analogues under the conditions used to perform biological assays.

- **Specific objective 3:** To assess the stability of Ru complex DA linkages under biologically-relevant conditions.
- **Specific objective 4:** To investigate and compare the antiproliferative activity of all Ru complexes against two human breast cancer cell lines, MCF-7 and T47D.

3. PUBLICATION 2

Exploiting exo and endo furan-maleimide Diels-Alder linkages for the functionalization of organoruthenium complexes.

Exploitation des linkages thermosensitives de Diels-Alder de furanes-maléimides endo et exo pour la fonctionnalisation de complexes d'organoruthénium.

Hoang-Van Tran, Mohammad Mehdi Haghdoost, Sylvain Poulet, Paul Tcherkawsky and Annie Castonguay*

INRS-Centre Armand-Frappier Santé Biotechnologie, Université du Québec, Laval, QC H7V 1B7, Canada

Corresponding author: * annie.castonguay@inrs.ca

Contribution of authors:

Hoang-Van Tran designed and performed the chemistry and biology experiments, the statistical analyses and wrote the original draft of the manuscript.

Dr. Mohammad Mehdi Haghdoost designed and performed the synthesis of furan-containing ruthenium complexes and were involved in some other chemistry experiments done for this project.

Sylvain Poulet and **Paul Tcherkawsky** were summer trainee students who worked under the supervision of Dr. Haghdoost and involved in some chemistry experiments done for this project.

Prof. Annie Castonguay obtained the research funding, supervised the project, and participated in conceptualization, writing, and revising the manuscript.

This article was accepted and published in *Dalton Transactions* (October 2021).

https://doi.org/10.1039/D1DT02766B

3.1 RÉSUMÉ

This third chapter presents the fundamental knowledge acquired in the course of this thesis regarding the synthesis, characterization and biological activity of organoruthenium complexes that include a furan-maleimide DA linkage. More specifically, synthetic pathways to afford cationic furan-containing half-sandwich ruthenium arene complexes (bearing an N,N-donor ligand) with two maleimides of a different electronic nature via a DA-type linkage are reported and compared. Their relative potential to disassemble (rDA) under biologically-relevant conditions is also discussed, taking into account the regioselectivity of the DA cycloaddition products (endo or exo). Notably, although it is well precedented that exo DA linkages disassemble at temperatures that are too high for being relevant in a drug delivery context, the results presented in this chapter demonstrate that the choice of substituent on the maleimide DA partner has such a drastic effect on the linkage properties that under certain conditions, exo linkages can also possibly undergo a rDA reaction at biologically-relevant temperatures (not only endo linkages). Moreover, functionalizing the furan precursor complex with the most lipophilic of both maleimides (which could potentially act as a cell-penetrating agent) resulted in a complex that displayed an improved anticancer activity against two human breast cancer cell lines, MCF-7 and T47D.

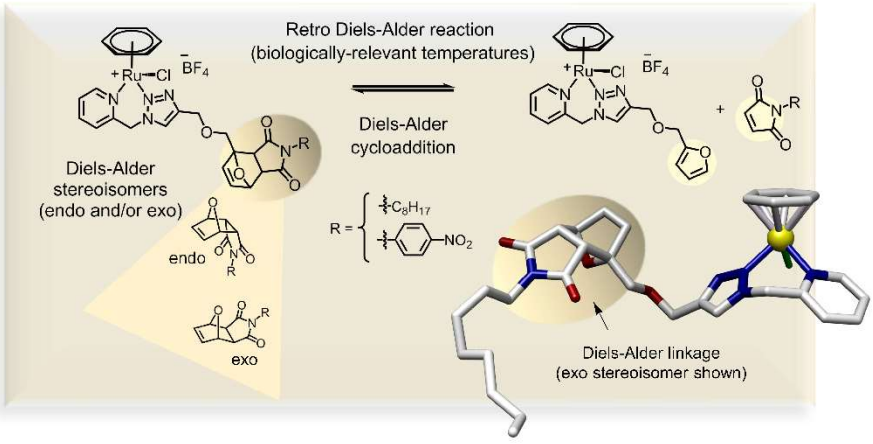

3.2 ARTICLE

COMMUNICATION

Exploiting exo and endo furan-maleimide Diels-Alder linkages for the functionalization of organoruthenium complexes

Received 00th January 20xx,
Accepted 00th January 20xx

DOI: 10.1039/x0xx00000x

Hoang-Van Tran,[a] Mohammad Mehdi Haghdoost,[a] Sylvain Poulet,[a] Paul Tcherkawsky[a] and Annie Castonguay*[a]

Diels-Alder cycloadditions involving furans and maleimides are extensively used in organic chemistry and materials synthesis. Given the promising advances of organoruthenium complexes in therapy, we explored the possibility of exploiting such Diels-Alder linkages as a mean to modulate their biological properties.

Furan and maleimide moieties are part of the structure of various drugs. When allowed to react together under certain conditions, they undergo a normal demand [4 + 2] Diels-Alder (DA) cycloaddition.[1] This type of cycloaddition is regioselective, leading to kinetic (endo) and/or thermodynamic (exo) adducts, depending on various factors. The thermoreversible nature of this reaction has been widely exploited in organic and material synthetic chemistry using elevated temperatures (>90°C).[2] For such applications, no distinction is usually made between the thermal behaviour of both regioisomers, often perpetuating the erroneous assumption that they are similar or identical. In fact, endo adducts do undergo retro Diels-Alder (rDA) reactions (DA disassembly) at lower temperatures than their corresponding exo counterparts.[3] We and others have previously shown that rDA reactions of DA adducts can even take place at biologically-relevant temperatures.[4,5] Thus, the use of DA-type linkages holds promise as a useful tool for the functionalization of drugs/drug candidates with targeting or cell-penetrating agents, but has so far surprisingly only scarcely been examined. Therefore, it would be of interest to get a better understanding of the factors that influence the behavior of DA-containing drugs/prodrugs in biological settings.[6]

Metal-based complexes have recently received increasing attention due to their outstanding biological activities.[7] For instance, ruthenium (Ru) complexes are among the most investigated and advanced metallodrugs due to their significant antiproliferative and antimetastatic activity against a wide range of cancer cells.[8] It was previously shown that the biological activity of Ru complexes strongly depends on their ancillary ligands,[9] and that the introduction of hydrophobic ligands (such as pyrene, phenanthroline, CF_3, octyl, etc) [10,11] enhanced cellular uptake through a passive diffusion mechanism.[10] In the past years, our research group has focused on the synthesis of various half-sandwich "piano-stool" Ru(II)-arene complexes, and also found their biological activity to be strongly dependent on the nature of their ligands, particularly their lipophilicity. By investigating the structure-activity relationship of a series of structurally related Ru(II) complexes bearing bidentate N,O-donor Schiff-base ligands, we observed that enhancing their lipophilicity resulted in a more considerable cellular uptake, leading to a higher cytotoxicity against cancer cells.[12] Therefore, developing straightforward and atom-efficient ways to functionalize ruthenium complexes (or other metallodrug candidates) with specific chemical fragments would be highly desirable, and we reasoned that thermoresponsive DA linkages could be exploited in this regard. Herein, we report synthetic pathways to afford cationic furan-containing half-sandwich Ru(η^6-C_6H_6) complexes (bearing an N,N-donor ligand) with two maleimides of a different electronic nature via a DA-type linkage. We also discuss our preliminary results on their relative potential to disassemble (undergo a rDA reaction) under biologically-relevant conditions. Moreover, we show that functionalizing the furan precursor with the most lipophilic of both maleimides (which can potentially act as a cell-penetrating agent) resulted in a complex that displayed an improved anticancer activity against two human breast cancer cell lines, MCF-7 and T47D.

To exploit DA linkages for the functionalization of organoruthenium complexes, an N,N-donor-type ligand was selected. The thermal stability of arene complexes formed with this type of ligand could allow the use of heat for the formation of DA linkages of distinct endo/exo regioisomer ratios directly from metal complexes. Besides, the ability of such ligands to react with Ru arene dimers at room temperature could alternatively allow the functionalization of furan or maleimide ligands prior to their complexation,[13] thus limiting ligand disassembly (rDA) during the complex synthesis. Furan-containing N,N-triazole ligand **1** was then prepared via a Cu-catalyzed alkyne azide cycloaddition (CuAAC). Its reaction with $[Ru(\eta^6\text{-}C_6H_6)Cl_2]_2$ and NH_4BF_4 in refluxing ethanol (Scheme 1) led

[a] *INRS-Centre Armand-Frappier Santé Biotechnologie, Université du Québec, Laval, QC H7V 1B7, Canada.*
* Corresponding author.
E-mail address: annie.castonguay@inrs.ca (A. Castonguay)
Electronic Supplementary Information (ESI) available: Experimental Section, figures, crystallographic data, etc. See DOI: 10.1039/x0xx00000x

to the formation of cationic ruthenium complex **3**, which was isolated in high yield. The reaction could also proceed at room temperature, but over a longer time period. The complex was found to be soluble in most organic solvents. Notably, **3** was also found to be stable when heated up to 65°C for 5 days in acetone or acetonitrile (9 mM), as only trace amounts of free benzene were detected by ^{1}H NMR.

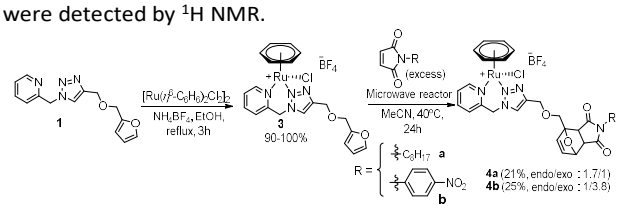

Scheme 3. Initial synthetic route employed for the obtention of ruthenium complexes **4a** and **4b**: Diels-Alder cycloaddition performed on complex **3** (as the final step).

Performing a DA reaction between this complex and maleimides bearing two different substituents was attempted, notably an electron-donating alkyl chain (octyl) and an electron-withdrawing nitro-substituted phenyl ring. We reasoned that selecting maleimides of a different electronic nature would be relevant to confirm the impact of such substituents on the ability of the maleimides to undergo a DA reaction,[14,15] but also to assess their influence on the linkage disassembly (rDA reaction) of the resulting complexes under biologically-relevant conditions.[16] The high lipophilicity of the *N*-octyl maleimide and its potential effect on the biological activity of its Ru DA adduct[12] is also among the reasons it was included in this study. The reaction of complex **3** with a large excess (30 eq) of *N*-octyl maleimide and *N*-*p*-nitrophenyl maleimide, respectively, was monitored using ^{1}H NMR spectroscopy and reaction yields were obtained with the aid of an internal standard. When the reaction was performed at ambient temperature in acetone-d_6 for 1 day, complexes **4a** and **4b** (Scheme 1) were obtained in very low yields (**4a**: 17%, **4b**: 15%; Table S1). Increasing the temperature to 65°C drastically improved the reaction yield for both complexes (**4a**: 75%, **4b**: 70%; Table S1). As expected, a mixture of the endo and exo adducts was observed at both temperatures. The endo regioisomer (kinetic product) was found to be predominant in both cases when the reaction was performed at ambient temperature (**4a$_{endo}$**/**4a$_{exo}$**: 3, **4b$_{endo}$**/**4b$_{exo}$**: 5; Table S1), whereas the exo regioisomer (thermodynamic product) was found to be predominant when the reaction proceeded at higher temperatures (**4a$_{endo}$**/**4a$_{exo}$**: 0.8, **4b$_{endo}$**/**4b$_{exo}$**: 0.3; Table S1). It is noteworthy that the isomer predominance discussed above was found to be more pronounced for the dienophile bearing the electron-withdrawing substituent, namely *N*-*p*-nitrophenyl, as also noted in previous reports.[15,17] Allowing these reactions to proceed at 40°C in acetone for 5 days resulted in a two-fold increase in the reaction yield of both complexes (83%, Table S1), when compared to 1-day reactions performed under the same conditions. Among solvents that are typically used to perform DA reactions,[15] acetone and acetonitrile led to higher yields than chloroform or methanol (for 1 day), possibly due to the higher solubility of the substrates in these solvents (Table S1). Finally, it was found that a relatively high yield could be obtained, after only 1 day, when the reaction was performed in a microwave reactor (6.5 W) in acetonitrile at 40°C (**4a**: 70%, **4b**: 86%; Table S1). However, despite the high conversions observed by ^{1}H NMR, the isolation of the complexes remained very challenging, as the use of chromatographic methods led to an important loss of the product in both cases (**4a**: 21%, **4b**: 25%), and attempts at separating the endo and exo complexes were not successful.

As an alternate strategy, the synthesis of **4a** and **4b** was attempted by performing the DA reaction on the ligands, prior to their complexation (Scheme 2). Following this route, ligands **2a** and **2b** could be obtained in high yields (**2a**: 93%, **2b**: 82%) by allowing ligand **1** to react with *N*-octyl and *N*-*p*-nitrophenyl maleimide, respectively, using the DA reaction conditions previously optimized using microwave irradiation. It is noteworthy that the higher conversion and the slight increase in endo/exo regioisomer ratio noted after 24h when the DA reaction was performed on the ligand (Scheme 2) compared to when performed on the complex under the same conditions (Table S1, entry 5) is indicative that the cationic ruthenium center might possibly exert an electron-withdrawing effect on the furan moiety. **4a** and **4b** were then synthesized (**4a**: 90%, **4b**: 85%) by reacting the $[Ru(\eta^6\text{-}C_6H_6)Cl_2]_2$ with DA ligands **2a** and **2b**, respectively, at room temperature, in the presence of NH_4BF_4. No considerable DA disassembly (rDA) was observed. In addition to the higher reaction yields obtained, another considerable advantage of using this alternate strategy is that the direct synthesis of the endo and exo forms of **4a** could also be achieved, as endo and exo ligand adducts **2a** could be successfully isolated by reversed phase semi-preparative HPLC prior to the preparation of **4a** (Figures S1 and S2). Interestingly, independent HPLC analysis of pure endo and exo regioisomers of **4a** and **4b** (with 0.1% trifluoroacetic acid) revealed the presence of an equimolar mixture of two distinct species in the case of **4a$_{endo}$** (Figure S3). These peaks were attributed to a mixture of two endo isomers of **4a** (as supported by ESI-MS, Figure S4) for which the counterion was replaced by trifluoroacetate during the analysis (as supported by the absence of signal in the ^{19}F NMR spectrum recorded post-analysis).

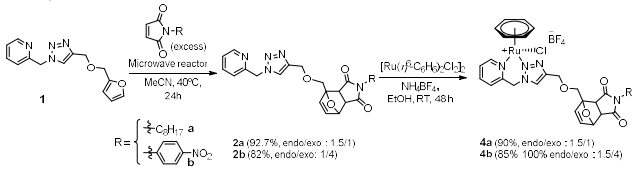

Scheme 4. Alternate synthetic route employed for the obtention of ruthenium complexes **4a** and **4b**: Diels-Alder cycloaddition performed on ligand **1** (as the initial step).

All complexes were carefully characterized by NMR spectroscopy, HR-MS and elemental analysis (see ESI). In comparison to ligand **1**, the ^{1}H NMR spectrum of complex **3** (acetone-d_6) displayed *i)* a significant downfield shift for several resonances, notably for the ones in proximity to the cationic ruthenium center (Figure 1: the H_k proton of the pyridine moiety, the two H_g protons of the methylene group and the H_f

of the triazole ring), *ii*) the appearance of a singlet at 6.24 ppm, characteristic for equivalent protons of a coordinated arene ring, and *iii)* the emergence of an AB spin system (δ 5.94 and 6.29 ppm, 2 d, J = 15.7 Hz) for the H_g protons of the methylene group.[13] Upon formation of complexes **4a** and **4b** (DA reaction with each maleimide), the H_a proton (δ_H 7.54 ppm, dd, J = 1.9, 0.8 Hz) of the furan ring of complex **3** was replaced by new signals in the 5.0-5.5 ppm region, which were assigned to the endo and exo DA adducts, respectively. These chemical shifts were found to be in good agreement with literature reports.[15] The stereochemistry of the products was assigned based on analogy with previously published systems, using the coupling constants between the $H_{a'}$ and the $H_{l'}$ protons ($^3J_{Ha'Hl'\ endo}$ = ~5.8 Hz and $^3J_{Ha'Hl'\ exo}$ = ~1.6 Hz). It is noteworthy that two sets of peaks were observed by ^{1}H NMR for **4a$_{endo}$** (in line with the two isomers previously observed by HPLC). **4a** and **4b** are highly soluble and stable in organic solvents such as acetone, acetonitrile and DMSO (30 mM solutions, assessed by ^{1}H NMR after 48h, Figure S5), as well as in water/0.5% DMSO, a medium typically used for assessing the biological activity of such complexes (Figure S6).

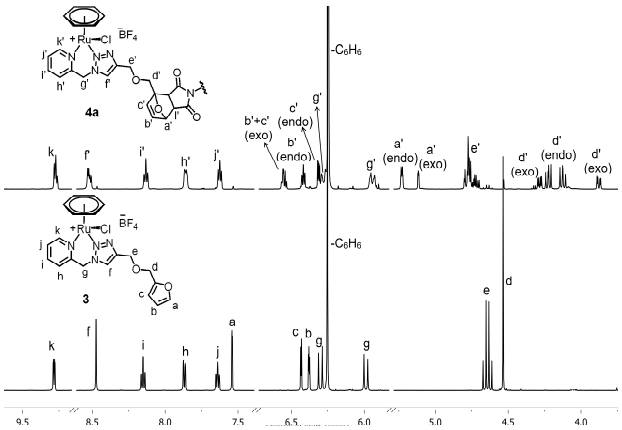

Figure 1. Illustration of some of the ^{1}H NMR spectral changes observed upon the DA cycloaddition (ex: 40°C in acetone-d_6) of complex **3** and *N*-octyl maleimide to yield **4a** (**4a$_{exo}$**:**4a$_{endo}$** = 1:2).

The nature/conformation of **3** and **4a$_{exo}$** was confirmed by single crystal X-ray analysis. Figure 2 presents an ORTEP view of the solid-state structures, and a summary of the crystallographic data is provided in Table S2 and S3. Both Ru complexes adopt a distorted octahedral geometry (piano-stool structure) with η^6-coordination benzene ring, a bidentate N,N-donor moiety, and a chloride ligand. All metal-ligand bond distances are found within the expected range for such complexes.[18] They are similar for both complexes except for Ru-N_2 , which is shorter in **4a$_{exo}$** than in **3**.

The stability of the two different types of DA linkages reported in this study (extent of their rDA disassembly) was assessed under biologically-relevant conditions at different temperatures. This was achieved by recording ^{1}H NMR spectra of NaCl (110 mM) aqueous solutions (D_2O containing 1% DMSO-d_6) of both the endo or exo adducts of **4a** and **4b** after incubation at 37°C-50°C (physiological/pathological/locally-induced hyperthermia temperature range) for 48h (Table 1 and see ESI).

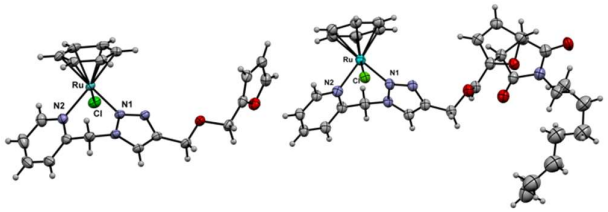

Figure 2. ORTEP diagram of **3** (left) and **4a$_{exo}$** (right), showing 50% and 20% probability level, respectively. For clarity, counterions and solvent molecules are not displayed. Selected bond lengths and angles: 3: Ru–Cl, 2.3849(5); Ru–N1, 2.0863(15); Ru–N2, 2.1301(17); Ru-benzene (centroid), 1.6764(8) Å; N1–Ru–Cl, 86.50(5); N1–Ru–N2, 84.91(6); N2–Ru–Cl, 84.06(5); 4a$_{exo}$: Ru–Cl, 2.385(2); Ru–N1, 2.075(7); Ru–N2, 2.096(7); Ru-benzene (centroid), 1.669(4) Å; N1–Ru–Cl, 85.58(19); N1–Ru–N2, 84.0(3); N2–Ru–Cl, 85.4(2).

Table 1. DA disassembly (rDA reaction) assessment of Ru DA complexes **4a** and **4b** under biologically-relevant conditions (D_2O - 1% DMSO-d_6-110 mM NaCl) by ^{1}H NMR after 48h.

	retro Diels-Alder reaction (DA disassembly) (%)[a]		
	37°C	**42°C**	**50°C**
4a$_{endo}$	18	28	59
4a$_{exo}$	0	1	3
4b$_{endo}$	72	81	100
4b$_{exo}$	11	18	41

[a]The rDA disassembly (%) was calculated based on the integration of the triazole proton of the furan complex **3** at 8.53 ppm and the DA protons of Ru DA complexes **4a** and **4b** at ~5.3 ppm.

As expected, **4a** was found to be much less prone to undergo DA disassembly (rDA reaction) than **4b**. Indeed, the presence of an electron-withdrawing substituent on the maleimide part of DA adducts was previously shown to enhance their DA disassembly whereas the contrary was noted in the presence of an electron-donating substituent.[15,16,19] Importantly, DA disassembly was not exclusively observed for the endo isomers of **4a** and **4b**. Whereas a negligible DA disassembly was noted for **4a$_{exo}$** at all temperatures investigated, as one would expect for an exo furan-maleimide DA adduct, a significant DA disassembly was noted for **4b$_{exo}$**. This finding emphasizes the highly tunable nature of this type of linker.

As physiological pH (7.4) is known to enhance the rDA reactions between furan and maleimides (faster hydrolysis of the released maleimide group),[5] and that the released maleimide might readily react with the plethora of thiols or amines present in biological environments (also contributing to shifting the equilibrium towards the rDA products), we have been interested to perform a few *in vitro* preliminary experiments involving human cell lines, to assess if a difference in antiproliferative activity could be noted between DA endo and exo isomers. For this study, **4a$_{endo}$** and **4a$_{exo}$** were selected given their high lipophilic character (Table S3). The antiproliferative activity of both isomers was assessed against two human breast cancer cell lines (MCF-7 and T47D) using the SRB assay. IC_{50} results are presented in Table 2.

Complex **4a** displayed a markedly enhanced antiproliferative activity against both cancer cell lines in comparison with the furan precursor **3**, which could be attributed to the higher lipophilicity of the DA complex. What was unexpected from the

results obtained is the lack of significant difference between the activity of the exo and endo forms of complex **4a**, suggesting that both isomers did not undergo any DA disassembly (or only underwent neglectable disassembly). The partial or full DA disassembly of both isomers (to the same extent) could not be ruled out, but are unlikely due to the different rDA profiles noted previously, and given the considerable antiproliferative activity of *N*-octyl maleimide (IC_{50} = 26.1 ± 5.1 and 24.4 ± 6.1 for MCF-7 and T47D cell lines, respectively).

Table 2. IC_{50} values determined for ruthenium complexes against human breast cancer MCF-7 and T47D cell lines.

	Endo:exo	IC_{50} (μM)[a]	
		MCF-7	T47D
3		>300	>300
4a	Endo	59.5 ± 1.9	70.1 ± 3.5
	Exo	57.2 ± 3.0	72.8 ± 4.9
5a	Endo	51.3 ± 3.0	78.0 ± 1.2
	Exo	54.7 ± 8.1	73.5 ± 4.5

[a]Inhibitory activity was determined by exposure of cell lines to solutions of each complex for 48 h and expressed as the concentration required to inhibit cell viability by 50 % (IC_{50}). Errors correspond. to the standard deviation of two to three independent experiments. IC_{50} of *N*-octyl maleimide = 26.1 ± 5.1 and 24.4 ± 6.1 for MCF-7 and T47D cell lines, respectively.

To shed light on whether the disassembly of **4a** might be taking place in the above-described *in vitro* biological environment, and with the assumption that reducing the double bond involved in the rDA reaction would result in a complex with a similar cytotoxicity than that of intact **4a** by preventing any DA disassembly to occur, we synthesized a thermostable version of complex **4a** (Scheme 3). Thermostable complex **5a** was obtained in quantitative yield via the direct hydrogenation of a **4a** mixture of endo and exo isomers. Complex **5a** was characterized by NMR, HR-MS and elemental analysis. Notably, in its ^{1}H NMR spectrum, we observed the absence of the two signals at 5.23 and 5.12 ppm, which were respectively attributed to the endo and exo alkenyl protons (see Figure 1, $H_{a'}$) of the ruthenium adduct **4a** (Figure S7). When tested against the same two human breast cancer cell lines, **5a** displayed a IC_{50} which was not significantly different than that of both isomers of **4a**, after 48h (Table 2). This result supports the hypothesis that the DA disassembly of this specific system might not be taking place in the biological setting studied.

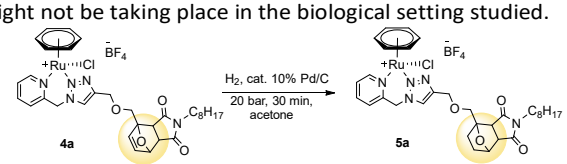

Scheme 3. Hydrogenation of the DA linkage double bond in **4a**.

Diels-Alder reactions between a furan-containing ruthenium complex and two maleimides of a different electronic nature were achieved. Although performing the DA reaction on the ligand prior to its complexation was found advantageous in the specific example shown here, performing the DA reaction on the complex remains a suitable strategy for complexation reactions that require heat. It was shown that the choice of maleimide substituent has a drastic effect on the disassembly, and can even allow the rDA of the exo adduct to occur at biologically-relevant temperatures. Results reported here will pave the way to the development/design of improved drug conjugates or delivery systems involving ruthenium- or other metal-based drug/drug candidates.

This work was supported by the Natural Sciences and Engineering Research Council of Canada (NSERC), the Fonds de Recherche du Québec Santé (FRQS), the Institut national de la recherche scientifique (INRS), and the Canada Foundation for Innovation (CFI). We are grateful to colleagues from INRS for providing human cancer cell lines and access to some of the instruments used in this study.

Conflicts of interest

There are no conflicts to declare.

Notes and references

1. O. Diels and K. Alder, *Justus Liebigs Ann. Chem.*, 1928, **460**, 98-122.
2. S. Kotha and S. Banerjee, *RSC Adv.*, 2013, **3**, 7642-7666.
3. J. Canadell, H. Fischer, G. De With and R. A. T. M. van Benthem, *J. Polym. Sci. A Polym. Chem.*, 2010, **48**, 3456-3467.
4. A. Castonguay, E. Wilson, N. Al-Hajaj, L. Petitjean, J. Paoletti, D. Maysinger and A. Kakkar, *Chem. Commun.*, 2011, **47**, 12146-12148; Z. Wei, J. H. Yang, X. J. Du, F. Xu, M. Zrinyi, Y. Osada, F. Li and Y. M. Chen, *Macromol. Rapid Commun.* 2013, **34**, 1464-1470; A. Oluwasanmi, W. Al-Shakarchi, A. Manzur, M. H. Aldebasi, R. S. Elsini, M. K. Albusair, K. J. Haxton, A. D. M. Curtis and C. Hoskins, *J. Control. Release*, 2017, **266**, 355-364.
5. S. Kirchhof, A. Strasser, H.-J. Wittmann, V. Messmann, N. Hammer, A. M. Goepferich and F. P. Brandl, *J. Mater. Chem. B*, 2015, **3**, 449-457.
6. M. Gregoritza and F. P. Brandl, *Eur. J. Pharm. Biopharm.*, 2015, **97**, 438-453.
7. A. F. A. Peacock and P. J. Sadler, *Chem. Asian J.*, 2008, **3**, 1890-1899.
8. L. Zeng, P. Gupta, Y. Chen, E. Wang, L. Ji, H. Chao and Z.-S. Chen, *Chem. Soc. Rev.*, 2017, **46**, 5771-5804; A. Bergamo and G. Sava, *Dalton Trans.*, 2011, **40**, 7817-7823.
9. M. R. Gill and J. A. Thomas, *Chem. Soc. Rev.*, 2012, **41**, 3179-3192.
10. H. Komatsu, K. Yoshihara, H. Yamada, Y. Kimura, A. Son, S.-i. Nishimoto and K. Tanabe, *Chem. Eur. J*, 2013, **19**, 1971-1977; S. Mehanna, N. Mansour, H. Audi, K. Bodman-Smith, M. A. Mroueh, R. I. Taleb, C. F. Daher and R. S. Khnayzer, *RSC Adv.*, 2019, **9**, 17254-17265; S. W. Chang, A. R. Lewis, K. E. Prosser, J. R. Thompson, M. Gladkikh, M. B. Bally, J. J. Warren and C. J. Walsby, *Inorg. Chem.*, 2016, **55**, 4850-4863.
11. C. Chen, C. Xu, T. Li, S. Lu, F. Luo and H. Wang, *Eur. J. Med. Chem.*, 2020, **203**, 112605.
12. M. Haghdoost, G. Golbaghi, M. Létourneau, S. A. Patten and A. Castonguay, *Eur. J. Med. Chem.*, 2017, **132**, 282-293.
13. D. Urankar, M. Steinbücher, J. Kosjek and J. Košmrlj, *Tetrahedron*, 2010, **66**, 2602-2613.
14. R. J. Brea and N. K. Devaraj, *Chemoselective and Bioorthogonal Ligation Reactions: Concepts and Applications*, 2017, **1**, 67-95.
15. V. Froidevaux, M. Borne, E. Laborbe, R. Auvergne, A. Gandini and B. Boutevin, *RSC Adv.*, 2015, **5**, 37742-37754.
16. B. M. deRonde, A. Birke and G. N. Tew, *Chemistry (Weinheim an der Bergstrasse, Germany)*, 2015, **21**, 3013.
17. J. Sauer, *Angew. Chem. Int. Ed. Engl.* , 1967, **6**, 16-33.
18. D. Urankar, B. Pinter, A. Pevec, F. De Proft, I. Turel and J. Košmrlj, *Inorg. Chem.*, 2010, **49**, 4820-4829.
19. M. Gregoritza, V. Messmann, A. M. Goepferich and F. P. Brandl, *J. Mater. Chem. B*, 2016, **4**, 3398-3408.

4. CONCLUSIONS

In the course of this thesis, we have developed synthetic pathways to functionalize a ruthenium-based drug candidate with two maleimides of a different electronic nature via furan/maleimide DA linkages. Indeed, the Ru DA complex could be prepared by either heating the Ru furan complex with maleimides in organic solvents or performing the complexation on the DA ligand adduct at room temperature. Ru DA complexes were purified by chromatographic methods or precipitation and characterized by NMR spectroscopy, mass spectrometry, and single crystal X-Ray diffraction analysis.

The formation of Ru DA complexes through the first synthetic pathway could be accelerated by using a microwave reactor at a moderate temperature, 40°C. However, Ru DA complexes prepared by this method were obtained in very low yields due to product loss during the chromatography purification process. In addition, the latter method did not allow the separation of the endo and exo forms of the complexes.

By contrast, improved isolated yields were obtained when Ru DA complexes were prepared by performing the complexation on DA ligand adducts. This method also allowed the independent preparation of the endo or exo forms of the Ru DA complexes by performing the complexation with endo or exo ligand adducts that were previously separated by semi-preparative reverse phase HPLC. However, because DA ligand adducts could undergo rDA reactions under heat, the preparation of Ru DA complexes by complexation was carried out at room temperature, requiring longer reaction times.

It is worthy to note that each synthetic method reported in this thesis has its unique advantages. For example, performing the DA reaction on the complex could be useful in cases requiring heat.

The stability and solubility of the complexes were studied by ^{1}H-NMR spectroscopy and UV-Vis techniques before assessing their biological activity, and the results obtained showed that all complexes had no solubility and stability issues under biologically-relevant solutions at room temperature. Furthermore, the behavior of Ru DA complexes was also examined under biologically-relevant conditions. As expected, we found that the presence of an electron-withdrawing substituent on maleimide leads to an enhancement of the DA disassembly of Ru DA complexes compared to the presence of an electron-donating substituent. Interestingly, our results showed that not only endo

adducts, but exo adducts could also undergo a rDA reaction at biologically-relevant temperatures. This finding is promising for the modulation of different stimuli-responsive drug delivery strategies.

In addition, we also demonstrated that functionalizing the furan precursor with the most lipophilic of both maleimides resulted in a complex that displayed an improved antiproliferative activity against two human breast cancer cell lines, MCF-7 and T47D. This result confirmed our hypothesis that the functionalization of Ru-based drug candidates with furan/maleimide DA reaction can modulate their biological activity.

The research findings reported in this thesis provide important information that will pave the way to the development/design of improved drug conjugates or delivery systems involving ruthenium- or other metal-based drugs/drug candidates.

5. PERSPECTIVES

In this thesis, we have achieved our main goal: to develop synthetic pathways to Ru DA complexes and study their reactivity/ stability under biologically-relevant conditions. The next step would be to design a DA thermo-sensitive system with a more relevant cell-targeting agent within its structure for the selective delivery of ruthenium drug candidates to cancer cells (Figure 8). Furthermore, that thermosensitive system could also be attached to the surface of AuNPs or iron oxide NPs, which would allow a controlled release via laser irradiation or magnetic field exposure after the drug candidate has reached its target. Introducing an -CF_3 group in such a construct would also allow the efficient *in vitro* and *in vivo* tracking of the drug candidate release by ^{19}F-NMR.[20]

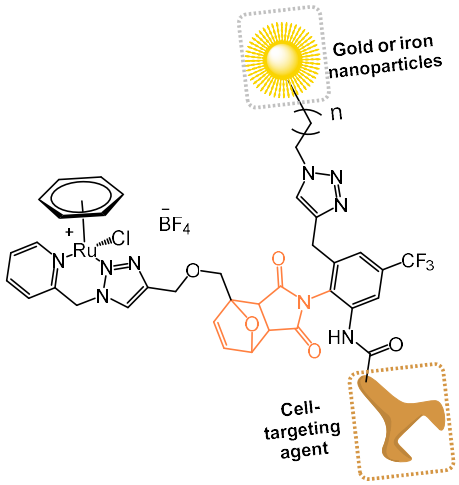

Figure 8. Example of an envisaged targeted stimuli-responsive drug delivery system.

For instance, such a system (Scheme 4) could be prepared from 4-(trifluoromethyl)benzene-1,2-diamine, an inexpensive commercial compound, followed by the halogenation of the arene ring and the Hiyama-catalyzed coupling reaction to produce a modified aniline **8**. Afterward, the corresponding maleimide **10** could be obtained by condensing the modified aniline with maleic anhydride, catalyzed by an excess of glacial acid acetic, followed by deprotection of the Boc group using concentrated HCl. The maleimide **10** could then undergo a DA reaction with furan-

containing ligand **1** to afford multi-functionalized ligand DA **11**, which could be used to synthesize the DA-thermo-sensitive platform:

- The cell-targeting agent could be attached to the system through an amidification on -NH_2 substituents.
- The complexation with $[Ru(\eta^6\text{-}C_6H_6)Cl_2]_2$ and NH_4BF_4 could be performed at room temperature. It is important to note that performing complexation at room temperature is advantageous since the high refluxing temperature can affect the stability/activity of cell-targeting agents.
- Finally, the ligand DA adducts attachment to metallic NPs could be performed via a CuAAC cycloaddition (CuAAC).

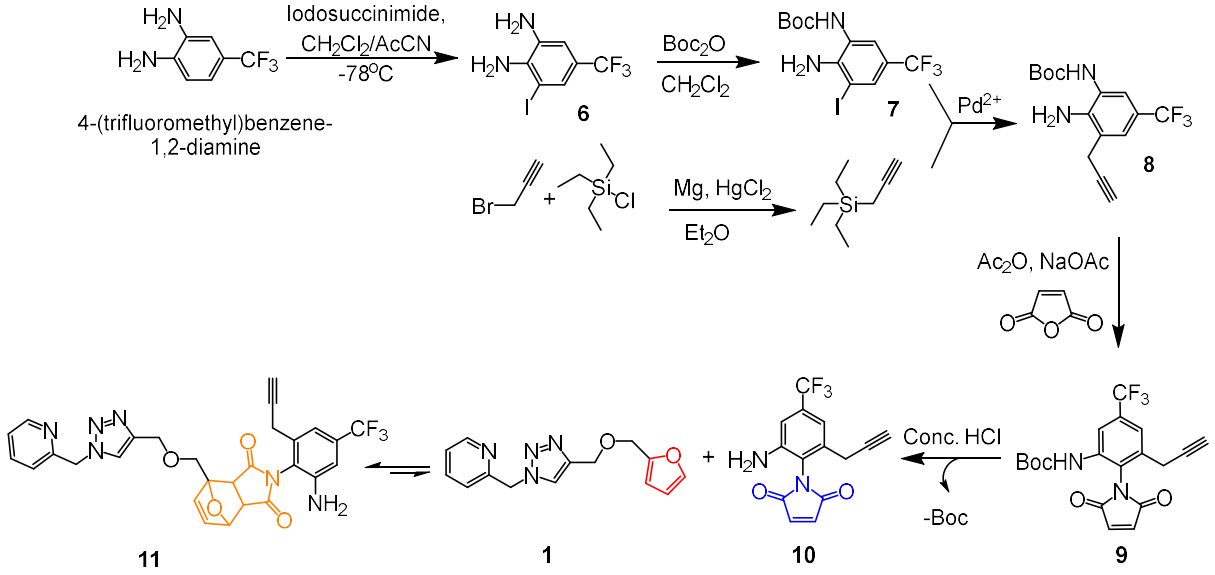

Scheme 4. Example of a synthetic route that could potentially be employed for the obtention of multi-functionalized ligand DA **11**.

6. REFERENCES

[1] R. A. Alderden, M. D. Hall, T. W. Hambley, *Journal of chemical education* **2006**, *83*, 728.

[2] R. J. Browning, P. J. T. Reardon, M. Parhizkar, R. B. Pedley, M. Edirisinghe, J. C. Knowles, E. Stride, *ACS nano* **2017**, *11*, 8560-8578.

[3] P. C. Bruijnincx, P. J. Sadler, *Current opinion in chemical biology* **2008**, *12*, 197-206.

[4] C. G. Hartinger, N. Metzler-Nolte, P. J. Dyson, *Organometallics* **2012**, *31*, 5677-5685.

[5] S. Page, R. Wheeler, *Education in Chemistry* **2012**, *49*, 26.

[6] a) X. Meng, M. L. Leyva, M. Jenny, I. Gross, S. Benosman, B. Fricker, S. Harlepp, P. Hébraud, A. Boos, P. Wlosik, *Cancer research* **2009**, *69*, 5458-5466; b) I. Bratsos, S. Jedner, T. Gianferrara, E. Alessio, *CHIMIA International Journal for Chemistry* **2007**, *61*, 692-697.

[7] V. Brabec, O. Nováková, *Drug Resistance Updates* **2006**, *9*, 111-122.

[8] A. F. Peacock, P. J. Sadler, *Chemistry–An Asian Journal* **2008**, *3*, 1890-1899.

[9] W. Guo, W. Zheng, Q. Luo, X. Li, Y. Zhao, S. Xiong, F. Wang, *Inorganic chemistry* **2013**, *52*, 5328-5338.

[10] Y. Zhang, A. Ho, J. Yue, L. Kong, Z. Zhou, X. Wu, F. Yang, H. Liang, *European journal of medicinal chemistry* **2014**, *86*, 449-455.

[11] S. Kapitza, M. Pongratz, M. Jakupec, P. Heffeter, W. Berger, L. Lackinger, B. Keppler, B. Marian, *Journal of cancer research and clinical oncology* **2005**, *131*, 101-110.

[12] E. S. Antonarakis, A. Emadi, *Cancer chemotherapy and pharmacology* **2010**, *66*, 1-9.

[13] A. Bergamo, G. Sava, *Dalton Transactions* **2011**, *40*, 7817-7823.

[14] R. E. Aird, J. Cummings, A. A. Ritchie, M. Muir, R. E. Morris, H. Chen, P. J. Sadler, D. I. Jodrell, *British Journal Of Cancer* **2002**, *86*, 1652.

[15] A. L. Noffke, A. Habtemariam, A. M. Pizarro, P. J. Sadler, *Chemical Communications* **2012**, *48*, 5219-5246.

[16] M. Haghdoost, G. Golbaghi, M. Létourneau, S. A. Patten, A. Castonguay, *European Journal of Medicinal Chemistry* **2017**, *132*, 282-293.

[17] a) K. Cho, X. Wang, S. Nie, D. M. Shin, *Clinical cancer research* **2008**, *14*, 1310-1316; b) B. Wang, L. Hu, T. J. Siahaan, *Drug delivery: principles and applications*, John Wiley & Sons, **2016**.

[18] a) B. Rudolf, M. Palusiak, J. Zakrzewski, *Journal of Organometallic Chemistry* **2009**, *694*, 1354-1358; b) A. Kubicka, E. Parfieniuk, E. Fornal, M. Palusiak, D. Lizińska, A. Gumieniczek, B. Rudolf, *Journal of Photochemistry and Photobiology A: Chemistry* **2018**, *351*, 115-123; c) A. Tosik, M. Bukowska-Strzyżewska, B. Rudolf, J. Zakrzewski, *Journal of organometallic chemistry* **1997**, *531*, 41-46.

[19] E. Gabano, E. Perin, D. Bonzani, M. Ravera, *Inorganica Chimica Acta* **2019**, *488*, 195-200.

[20] N. Kitamura, K. Tanaka, Y. Chujo, *Bioorganic & medicinal chemistry letters* **2013**, *23*, 281-286.

7. APPENDIX (EXPERIMENTAL SECTION OF PUBLICATIONS 2)

SUPPLEMENTARY INFORMATION

Exploiting exo and endo furan-maleimide Diels-Alder linkages for the functionalization of organoruthenium complexes

Hoang-Van Tran,[a] Mohammad Mehdi Haghdoost,[a] Sylvain Poulet,[a] Paul Tcherkawsky[a] and Annie Castonguay[*a]

[a]INRS-Centre Armand-Frappier Santé Biotechnologie, Université du Québec, Laval, QC, H7V 1B7, Canada

*Email: annie.castonguay@inrs.ca

TABLE OF CONTENTS

Table S1. Optimization of the DA reaction between **3** and each maleimide by ^{1}H NMR spectroscopy.

Ent.	Maleimide	Eq.	Solvent	Time (day)	T (ºC)	Conv. (%)[a]	Endo/Exo[a]
1	*N*-Octyl	30 eq	Chloroform	1 d	40	15	7/3
2			MeOH	1 d	40	25	5/2
3			DMSO	1 d	40	n.d[b]	n.d[b]
4			Acetonitrile	1 d	40	37	5/2
5			Acetonitrile-MW[c]	1 d	40	70	2/1
6			Acetone	1 d	40	42	7/3
7			Acetone	1 d	RT	17	3/1
8			Acetone	3 d	RT	40	7/3
9			Acetone	1 d	65	75	4/5
10			Acetone	3 d	40	70	2.1/1
11			Acetone	5 d	40	83	1.7/1
12		5 eq	Acetone	1 d	40	8	2/1
13			Acetone	3 d	40	22	5/3
14	*N*-*p*-nitrophenyl	30 eq	Chloroform	1 d	40	17	1/1
15			MeOH	1 d	40	29	3/2
16			Acetonitrile	1 d	40	56	3/2
17			Acetonitrile-MW[c]	1 d	40	86	1/2
18			Acetone	1 d	40	40	3/2
19			Acetone	1 d	RT	15	5/1
20			Acetone	1 d	65	70	1/3
21			Acetone	3 d	40	69	3/5
22			Acetone	5 d	40	83	1/3.8
23		5 eq	Acetone	1 d	40	20	5/3
24			Acetone	3 d	40	32	5/7

[a] Determined by ^{1}H NMR. Briefly, 5 mg of **3** was dissolved in 0.7 mL of acetone-d_6 with 2 µL of anhydrous DMF as a reference standard. In a 3 mm NMR tube with cap, the final solution of complex **3** was added to each maleimide. The sample was agitated for 5 min, and the NMR tube was sealed with parafilm. The NMR tube was heated in an oil bath at different temperatures. The ^{1}H NMR resonances corresponding to **4a$_{endo}$** and **4a$_{exo}$** adducts at 5.24 and 5.12 ppm, respectively and at 5.38 and 5.24 ppm for **4b$_{endo}$** and **4b$_{exo}$** adducts, respectively, were used to calculate the %conversion of DA reaction (and isomer ratio). These experiments were done in two to triplicate.

[b] Free benzene was detected in the ^{1}H NMR spectra.

[c] Reaction performed in a microwave (MW) reactor (0 psi, 6.5 W).

Table S2. Crystallographic data and structure refinement for complexes **3** and **4a$_{exo}$**. Complexes were structurally characterized by single-crystal X-ray analysis.[a]

	3	**4a$_{exo}$**
Empirical formula	$C_{20}H_{20}BClF_4N_4O_2Ru$	$C_{36}H_{46}BClF_4N_5O_6Ru$
Formula weight	571.73	868.11
Crystal size [mm^3]	0.38×0.22×0.2	0.2×0.18×0.04
Crystal colour	clear light orange	clear light colourless
Crystal shape	Block	Plate
Crystal system	Triclinic	Monoclinic
Space group (number)	$P\overline{1}$ (2)	$P2_1/c$ (14)
Unit cell dimensions	*a* [Å] = 9.0308(4)	*a* [Å] = 14.619(5)
	b [Å] = 9.5157(4)	*b* [Å] = 14.258(4)
	c [Å] = 14.3909(7)	*c* [Å] = 21.155(7)
	α [°] = 82.575(2)	α [°] = 90
	β [°] = 78.701(2)	β [°] = 106.214(12)
	γ [°] = 63.403(1)	γ [°] = 90
Volume [Å^3]	1083.16(9)	4234(2)
Z	2	4
ρ_{calc} [gcm^{-3}]	1.753	1.362
***F*(000)**	572	1788
μ [mm^{-1}]	5.079	2.770
Temperature [K]	150	150
Radiation	Ga K_α (λ=1.34139 Å)	Ga K_α (λ = 1.34139 Å)
Index ranges	-11 ≤ h ≤ 11	-17 ≤ h ≤ 16
	-11 ≤ k ≤ 12	-17 ≤ k ≤ 15
	-18 ≤ l ≤ 18	-25 ≤ l ≤ 20
2θ range [°]	5.45 to 121.30 (0.77 Å)	6.59 to 110.58 (0.82 Å)
Reflections collected	34010	16543
Independent reflections	4812	7760
	R_{int} = 0.0349	R_{int} = 0.0583
	R_{sigma} = 0.0232	R_{sigma} = 0.0574
Data/parameters/restraints	4812/64/335	7760/300/444
Goodness-of-fit on F^2	1.100	1.051
Final R indices	R_1 = 0.0246	R_1 = 0.0960
[$I \geq 2\sigma(I)$][b,c]	wR_2 = 0.0643	wR_2 = 0.2704
Final R indices	R_1 = 0.0247	R_1 = 0.1390
[all data]	wR_2 = 0.0643	wR_2 = 0.3197
Largest diff. peak and hole [eÅ^{-3}]	0.88/-0.56	0.61/-0.49
CCDC deposition no.	2100514	2100515

[a] Single crystals were obtained by slow evaporation of the solutions of complexes **3** and **4a$_{exo}$** in dichloromethane and ethyl acetate, respectively. Structures were solved by direct methods using *XT* and refined by full-matrix least-squares methods against F^2 by *XL*.[1, 2]

[b] $R_1 = \Sigma||F_o| - |F_c|| / \Sigma|F_o|$.

[c] $wR_2 = \{\Sigma[w(F_o^2 - F_c^2)^2] / \Sigma[w(F_o^2)^2]\}^{1/2}$

Table S3. Estimated lipophilicity (LogP) for some of the compounds reported in this study.

Compounds	LogP (estimated)[a]
N-octyl maleimide	3.18
N-*p*-nitrophenyl maleimide	0.89
3[b]	1.90
4a[b]	3.26
4b[b]	1.79
5a[b]	3.26

[a]The ALOGSP 2.1[3, 4] software was used to estimate the LogP values presented in this table.

[b]This value represents the estimated LogP of the N,N-donor ligand corresponding to this complex.[5]

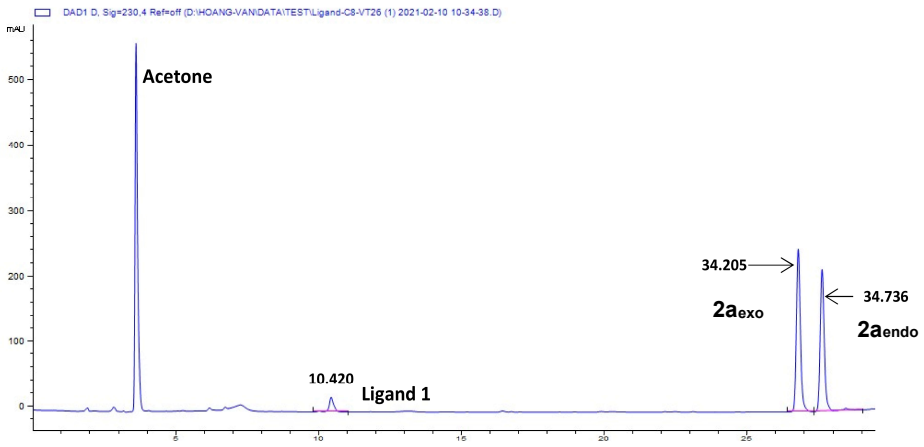

Figure S1. RP-HPLC chromatogram (semi-preparative C18 column, H_2O/acetonitrile) of a mixture of **2a**$_{endo}$ and **2a**$_{exo}$ (prior to separation).

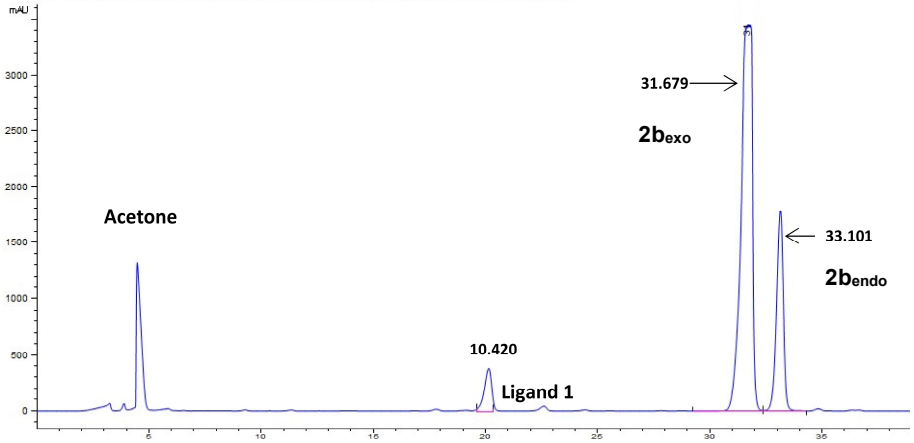

Figure S2. RP-HPLC chromatogram (semi-preparative C18 column, H_2O/acetonitrile) of a mixture of **2b**$_{endo}$ and **2b**$_{exo}$ (prior to separation).

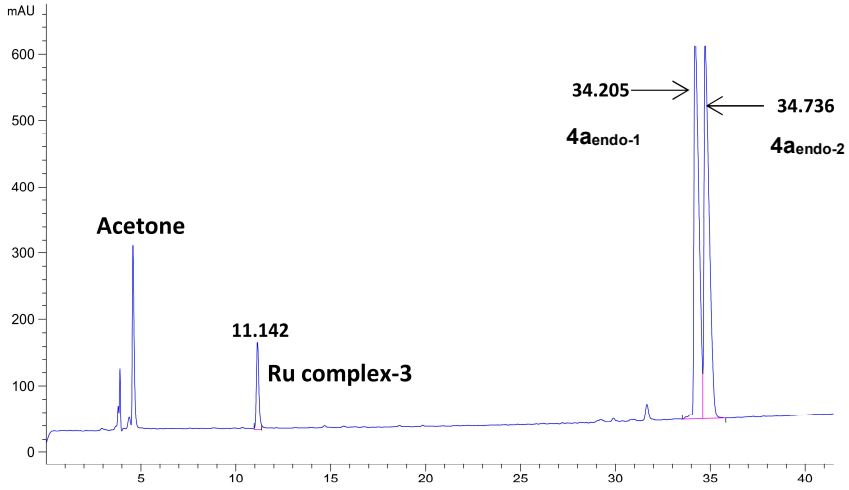

Figure S3. RP-HPLC chromatogram (semi-preparative C18 column, H_2O/acetonitrile/0.1% TFA) of **4a**$_{endo}$ (prior to separation).

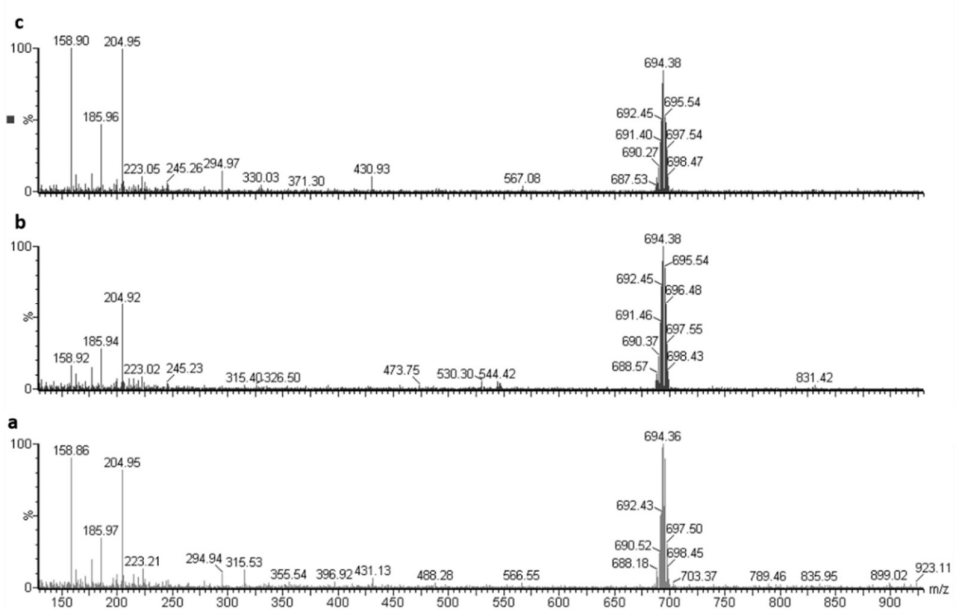

Figure S4. ESI-MS spectra of **4a**$_{\textbf{endo-1}}$ (a), **4a**$_{\textbf{endo-2}}$ (b) and **4a**$_{\textbf{exo}}$ (c) (positive mode, H_2O/acetonitrile/0.1% acetic acid).

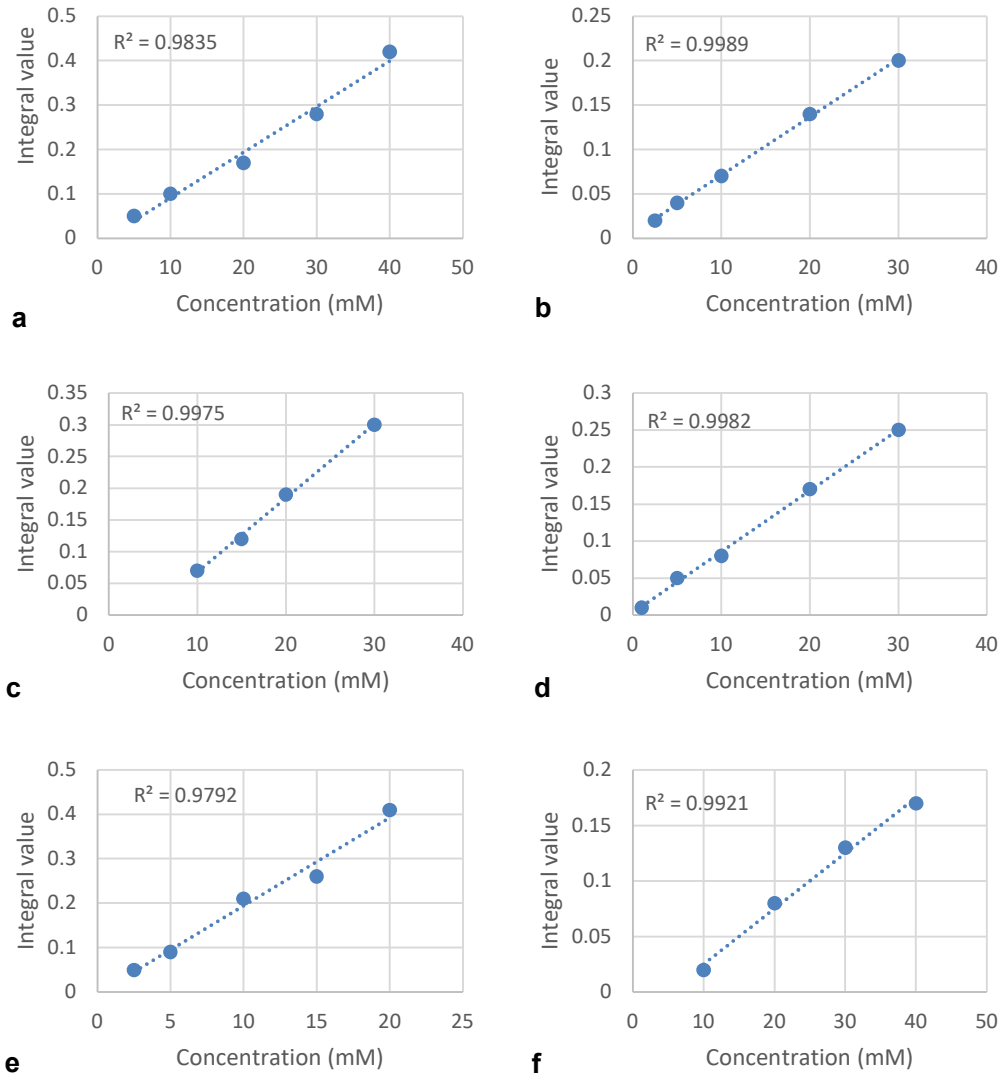

Figure S5. Solubility assessment of complexes **3** (a), **4a** (b), **4b** (c), **5a** (d), *N*-octyl maleimide (e) and *N*-*p*-nitrophenyl maleimide (f) in DMSO-d_6 using ^{1}H NMR spectroscopy at various concentrations. DMSO stock solutions were filtered (0.22 µm) prior to the analysis. The linearity between concentration and the signal intensity of one of the protons resonances for each compound was considered as an indication of the solubility of that compound at the desired concentration.

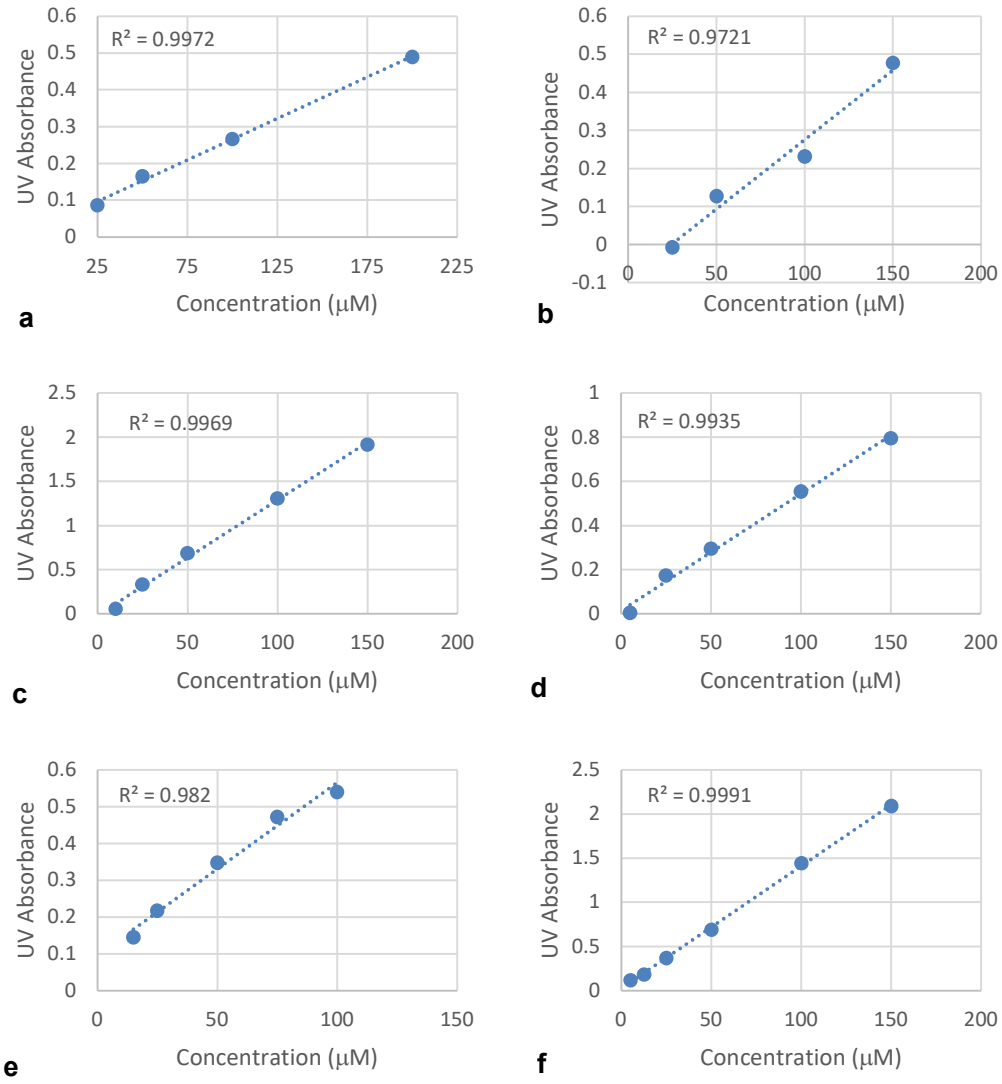

Figure S6. Solubility assessment of complexes **3** (a), **4a** (b), **4b** (c), **5a** (d), *N*-octyl maleimide (e) and *N*-*p*-nitrophenyl maleimide (f) in H_2O/0.5% DMSO using absorbance at 274-278 nm at various concentrations. Stock solutions in DMSO were diluted in miliQ water to reach the concentrations that were used for the *in vitro* cell viability assay (final DMSO concentration = 0.5%). Solutions were filtered (0.22 μm) prior to the analysis. The concentration of saturation of the compounds in this media was assessed by determining the concentration at which the maximum absorbance intensity was observed.

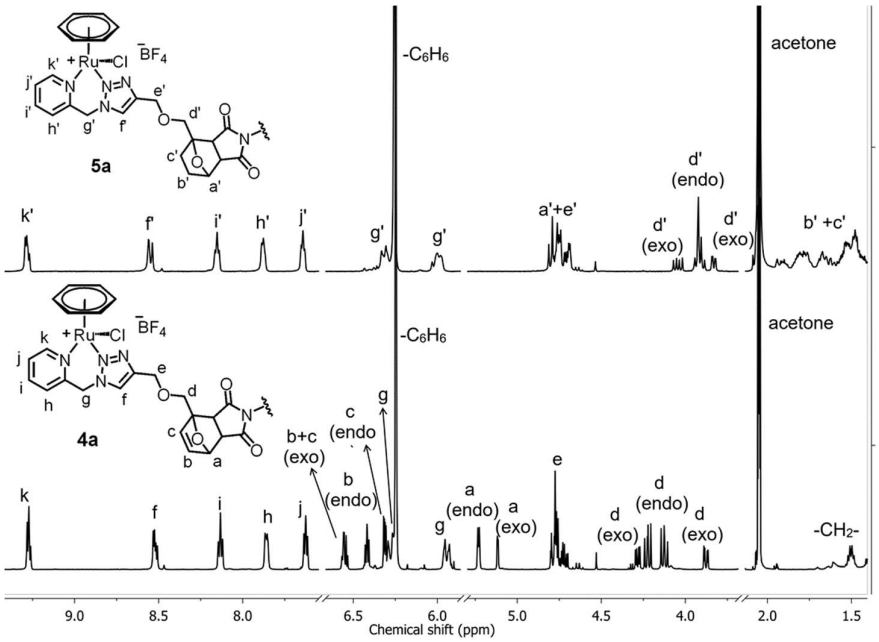

Figure S7. ^{1}H NMR spectra of complex **4a** (bottom) (**4a**$_{endo}$/**4a**$_{exo}$: 2/1) and its hydrogenation product **5a** (top) (**5a**$_{endo}$/**5a**$_{exo}$: 2/1) in acetone-d_6.

Experimental section

General remarks

All chemicals were purchased from commercial suppliers and used without further purification. Ru(η^6-C_6H_6)Cl_2]$_2$,[6] *N*-octylmaleimide,[7] *N*-*p*-nitrophenylmaleimide,[8] 2-((prop-2-ynyloxy)methyl)furan,[9] and 2-(azidomethyl)pyridine,[10] were synthesized according to literature procedures. All solvents were dried using a solvent purification system (Pure Process Technology). The absorbance of multi-well plates (510 nm) was measured using a Tecan Infinite M1000 PRO microplate reader. NMR spectra (^{1}H, ^{13}C{^{1}H}, COSY, HSQC and HMBC) were recorded on 400 MHz Varian and 600 MHz Bruker Avance III NMR spectrometers. Chemical shifts (δ) and coupling constants (J) are reported in parts per million (ppm) and Hertz (Hz), respectively. ^{1}H and ^{13}C{^{1}H} NMR spectra were referenced to solvent peaks as an internal standard, and spectral assignments were confirmed by 2D experiments. High-resolution and high accuracy mass spectra (HR-ESI-MS) were obtained using an Exactive Orbitrap spectrometer (Department of Chemistry, McGill University) or an LTQ Orbitrap (CQIB-INRS) from ThermoFisher Scientific. Column chromatography was performed using a Biotage Isolera One flash purification system with silica gel KP-Sil SNAP cartridges. Semi-preparative separation was performed using an Agilent 1260 Infinity II HPLC equipped with an Agilent Pursuit 5 C18 150 ×10.0 mm column. Diffraction measurements were performed on a Bruker Venture Metaljet k-geometry diffractometer with a Metal Jet using Helios MX Mirror Optics as monochromator and a Bruker CMOS Photon III detector (Department of Chemistry, Université de Montréal). Elemental analyses of Ru complexes were performed by ThermoFisher Flash 2000 analyzer with Mettler MT5 balance (ANALEST, Department of Chemistry, University of Toronto). All statistical analyses were done using the GraphPad Prism 6.01 software. ANOVA analysis was used for testing the significance of the difference between the means and a p-value <0.05 was considered statistically significant.

Synthesis of 1. Ligand **1** was prepared by reacting 2-((prop-2-ynyloxy)methyl)furan (265 mg, 1.95 mmol) with 2-(azidomethyl)pyridine (313 mg, 2.33 mmol) in a mixture of water/THF (1:1) (2 mL). The reaction was catalyzed by adding drop by drop an aqueous solution of $CuSO_4.5H_2O$ (0.389 mL, 0.5 M) and then an aqueous solution of sodium ascorbate in water (0.778 mL, 0.5 M). The solution mixture was stirred vigorously for 2-4h at room temperature and the completion of reaction was confirmed by GC-MS. The solvent was evaporated, and the crude product was purified by flash chromatography (R_f = 0.24, hexane/ethyl acetate, 50:50). The most intensive band was collected, the solvent was then evaporated under vacuum to give ligand **1** (420 mg, 80%) as a yellowish oil. **^{1}H NMR (600 MHz, $CDCl_3$):** δ_H = 8.56 (ddd, J = 4.9, 1.9, 0.9 Hz, 1H, H10), 7.68 (s, 1H, H20), 7.65 (td, J = 7.7, 1.8 Hz, 1H, H9), 7.36 (dd, J = 1.9, 0.9 Hz, 1H, H6), 7.23 (ddd, J = 7.7, 4.9, 1.1 Hz, 1H, H8), 7.16 (dt, J = 7.8, 1.1 Hz, 1H, H1), 6.31 (dd, J = 3.3, 0.9 Hz, 1H, H4), 6.30 (dd, J = 3.3, 1.9 Hz, 1H, H5), 5.62 (s, 2H, H13), 4.65 (s, 2H, H18), 4.51 (s, 2H, H2) ppm. **^{13}C{^{1}H} NMR (150 MHz, $CDCl_3$):** δ_C = 155.4 (C12), 152.3 (C19), 150.7 (C10), 146.2 (C3), 143.9 (C6), 138.3 (C9), 124.4 (C20), 124.4 (C8), 123.4 (C1), 111.3 (C5), 110.8 (C4), 65.1 (C2), 64.3 (C18), 56.5 (C13) ppm. **HR-ESI-MS *m/z* (+):** $[M + Na]^+$ calc. for $C_{14}H_{14}N_4NaO_2^+$ 293.1009, found: 293.1008.

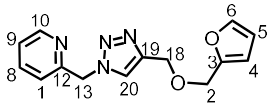

1

General procedure for the synthesis of 2a and 2b. In a 35 mL pressure vessel sealed with a silicone cap (CEM), acetonitrile (25 mL) was added to ligand furan **1** (1.0 eq) and maleimides (15 eq). The reaction was carried out with a CEM Discover S microwave reactor (T = 40°C, power: 6.5 W, P: 0 psi, hold time: 24h) and was followed by TLC (hexane/ethyl acetate, 1:9). After 24h, the completion of the reaction was confirmed by ^{1}H-NMR (acetone-d_6), then the solvent was evaporated. The crude product was dissolved in minimum amount of dichloromethane and loaded on 50 g KP-Sil column (Biotage SNAP) and eluted with hexane/ethyl acetate to afford the ligand DA **2a** or **2b**.

Synthesis of 2a. Ligand **1** (218 mg, 0.81 mmol) was reacted with *N*-octyl maleimide (2.6 g, 12.42 mmol). After purification by flash chromatography (R_f = 0.19, hexane:ethyl acetate, 15:85), ligand **2a** was obtained (**2a$_{endo}$**/**2a$_{exo}$**: 1.5/1) (358 mg, 93%) as a colorless oil. **2a$_{endo}$** and **2a$_{exo}$** were separated by further purification with 1260 Infinity II LC system (Agilent) using a semi-preparative RP column (Pursuit C18 150×10.0 mm, 5 µm) using a CH_3CN/H_2O gradient (H_2O/acetonitrile, 80:20 to 40:60 in 25 min, flow: 3.0 mL min^{-1}). **2a$_{endo}$. ^{1}H NMR (600 MHz, acetone-d_6):** δ_H = 8.56 (dt, *J* = 4.9, 1.3 Hz, 1H, H9), 8.05 (s, 1H, H12), 7.80 (td, *J* = 7.7, 1.8 Hz, 1H, H7), 7.32 (dd, *J* = 7.6, 4.9 Hz, 1H, H8), 7.26 (d, *J* = 7.8 Hz, 1H, H6), 6.41 (dd, *J* = 5.8, 1.7 Hz, 1H, H20), 6.32 (d, *J* = 5.8 Hz, 1H, H21), 5.72 (s, 2H, H14), 5.22 (dd, *J* = 5.5, 1.7 Hz, 1H, H19), 4.72 (s, 2H, H15), 4.18 and 4.09 (d, *J* = 12.1 Hz, 2H, H17), 3.61 (dd, *J* = 7.7, 5.5 Hz, 1H, H18), 3.45 (d, *J* = 7.7 Hz, 1H, H22), 3.23 (t, *J* = 7.3 Hz, 2H, H30), 1.39 (p, *J* = 7.3 Hz, 2H, H31), 1.32 – 1.19 (m, 10H, -CH_2-), 0.87 (t, *J* = 7.0 Hz, 3H, H37) ppm. **^{13}C{^{1}H} NMR (150 MHz, acetone-d_6):** δ_C = 175.7 and 175.5 (C25/26), 156.3 (C5), 150.4 (C9), 145.5 (C11), 138.0 (C7), 135.9 (C21), 135.9 (C20), 124.9 (C12), 124.0 (C8), 122.9 (C6), 92.1 (C23), 80.1 (C19), 68.9 (C17), 65.5 (C15), 55.8 (C14), 48.5 (C18), 46.6 (C22), 38.8 (C30), 32.5 (-CH_2-), 29.9 (2C, -CH_2-), 28.1 (C31), 27.5 (-CH_2-), 23.2 (-CH_2-), 14.3 (C37) ppm. **2a$_{exo}$. ^{1}H NMR (600 MHz, acetone-d_6):** δ_H = 8.56 (dt, *J* = 4.8, 1.4 Hz, 1H, H9), 8.03 (s, 1H, H12), 7.79 (td, *J* = 7.7, 1.8 Hz, 1H, H7), 7.33 (dd, *J* = 7.6, 4.9 Hz, 1H, H8), 7.26 (d, *J* = 7.8 Hz, 1H, H6), 6.55 (dd, *J* = 5.7, 1.7 Hz, 1H, H20), 6.52 (d, *J* = 5.7 Hz, 1H, H21), 5.71 (s, 2H, H14), 5.10 (d, *J* = 1.7 Hz, 1H, H19), 4.73 and 4.68 (d, *J* = 12.1 Hz, 2H, H15), 4.24 and 3.85 (d, *J* = 11.5 Hz, 2H, H17), 3.40 (td, *J* = 7.0, 1.6 Hz, 2H, H30), 3.02 (d, *J* = 6.4 Hz, H18), 2.93 (d, *J* = 6.4 Hz, 1H, H22), 1.50 (p, *J* = 7.1 Hz, 3H), 1.33 – 1.20 (m, 10H, -CH_2-), 0.87 (t, *J* = 6.9 Hz, 3H, H37) ppm. **^{13}C{^{1}H} NMR (150 MHz, acetone-d_6):** δ_C = 176.8 and 175.5 (C25/26), 156.3 (C5), 150.4 (C9), 145.6 (C11), 138.7 (C21), 138.0 (C7), 137.3 (C20), 124.9 (C12), 124.0 (C8), 122.9 (C6), 91.4 (C23), 81.8 (C19), 68.6 (C17), 65.6 (C15), 55.7 (C14), 50.7 (C18), 49.1 (C22), 38.9 (C30), 32.5 (-CH_2-), 29.5 (2C, -CH_2-), 28.2 (C31), 27.2 (-CH_2-), 23.3 (-CH_2-), 14.3 (-CH_3, C37) ppm. **HR-ESI-MS *m/z* (+):** $[M + H]^+$ calc. for $C_{26}H_{34}N_5O_4^+$ 480.2605, found: 480.2599; $[M + Na]^+$ calc. for $C_{26}H_{33}N_5NaO_4^+$ 502.2425, found: 502.2415; $[2M+Na]^+$ calc. for $C_{52}H_{66}N_{10}NaO_8^+$ 981.4957, found: 981.4950.

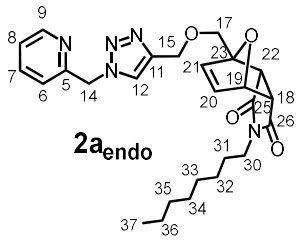

2a$_{endo}$

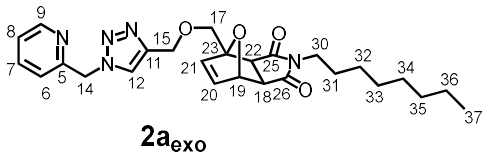

2a$_{exo}$

Synthesis of 2b. Ligand furan **1** (100 mg, 0.37 mmol) was reacted with *N*-*p*-nitrophenylmaleimide (1.21 g, 5.56 mmol). After purification by flask chromatography (R_f = 0.40, hexane/ethyl acetate, 15:85), ligand **2b** was obtained (**2b$_{endo}$**/**2b$_{exo}$**: 1/4) (115 mg, 80%) as a colorless foam. **2b$_{endo}$** and **2b$_{exo}$** were separated by further purification with 1260 Infinity II LC system (Agilent) using a semi-preparative RP column (Pursuit C18 150×10.0 mm, 5 µm) using a H_2O/acetonitrile gradient (H_2O/acetonitrile, 85:15 to 40:60, flow: 3.0 mL min^{-1}). **2b$_{endo}$**. **^{1}H NMR (600 MHz, acetone-*d*$_6$):** δ_H = 8.55 (dt, *J* = 4.8, 1.8 Hz, 1H, H9), 8.32 (d, *J* = 9.1 Hz, 2H, H32 and H34), 8.07 (s, 1H, H12), 7.78 (td, *J* = 7.7, 1.8 Hz, 1H, H7), 7.53 (d, *J* = 9.1 Hz, 2H, H31 and H35), 7.31 (ddd, *J* = 7.6, 4.8, 1.1 Hz, 1H, H8), 7.27 (d, *J* = 8.0 Hz, 1H, H6), 6.65 (dd, *J* = 5.8, 1.6 Hz, H20), 6.56 (d, *J* = 5.8 Hz, 1H, H21), 5.72 (s, 2H, H14), 5.38 (dd, *J* = 5.5, 1.6 Hz, 1H, H19), 4.75 (s, 2H, H15), 4.24 and 4.17 (d, *J* = 12.1 Hz, 2H, H17), 3.87 (dd, *J* = 7.8, 5.5 Hz, 1H, H18), 3.72 (d, *J* = 7.8 Hz, 1H, H22) ppm. **^{13}C{^{1}H} NMR (150 MHz, acetone-*d*$_6$):** δ_C = 174.3 and 174.1 (2C, C25/26), 156.3 (2C, C30/33), 105.5 (C9), 147.9 (C5), 145.4 (C11), 138.7 (C7), 138.0 (C20), 136.3 (C21), 128.4 (2C, C31/C35), 125.0 (2C, C32/34), 124.9 (C12), 124.0 (C8), 122.9 (C6), 92.6 (C23), 80.6 (C19), 68.7 (C17), 65.4 (C15), 55.8 (C14), 48.8 (C18), 46.9 (C22) ppm. **2b$_{exo}$**. **^{1}H NMR (600 MHz, acetone-*d*$_6$):** δ_H = 8.53 (ddd, *J* = 4.9, 1.9, 1.0 Hz, 1H, H9), 8.33 (d, *J* = 9.0 Hz, 2H, H32 and H34), 8.04 (s, 1H, H12), 7.75 (td, *J* = 7.7, 1.8 Hz, 1H, H7), 7.63 (d, *J* = 9.1 Hz, 2H, H31 and H35), 7.29 (ddd, *J* = 7.7, 4.8, 1.1 Hz, 1H, H6), 7.25 (dd, *J* = 7.9, 1.1 Hz, 1H, H8), 6.62 (dd, *J* = 5.7, 1.7 Hz, 1H, H20), 6.59 (d, *J* = 5.7 Hz, 1H, H21), 5.70 (s, 2H, H14), 5.28 (d, *J* = 1.8 Hz, 1H, H19), 4.72 (q, *J* = 7.0 Hz, 2H, H15), 4.31 and 3.99 (d, *J* = 11.5 Hz, 2H, H17), 3.31 (d, *J* = 6.5 Hz, 1H, H18), 3.18 (d, *J* = 6.5 Hz, 1H, H22) ppm. **^{13}C{^{1}H} NMR (150 MHz, acetone-*d*$_6$):** δ_C = 175.6 and 174.3 (2C, C25/26), 156.2 (2C, C30/33), 150.4 (C9), 147.8 (C5), 145.4 (C11), 139.0 (C7), 138.9 (C20), 137.6 (C21), 128.3 (2C, C31/C35), 125.0 (C12), 124.8 (2C, C32/34), 123.9 (C8), 122.9 (C6), 92.0 (C23), 82.3 (C19), 68.3 (C17), 65.5 (C15), 55.7 (C14), 51.3 (C18), 49.6 (C22) ppm. **HR-ESI-MS *m/z* (+):** $[M + H]^+$ calc. for $C_{24}H_{21}N_6O_6^+$ 489.1517, found: 489.1510; $[M + Na]^+$ calc. for $C_{24}H_{20}N_6NaO_6^+$ 511.1337, found: 511.1328; $[2M+Na]^+$ calc. for $C_{48}H_{40}N_{12}NaO_{12}^+$ 999.2781, found: 999.2774.

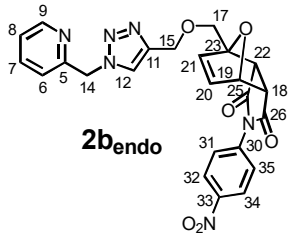

2b$_{endo}$

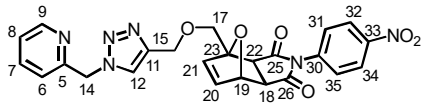

2b$_{exo}$

Synthesis of 3. Under N_2 atmosphere, 10 mL of dry ethanol was added to $Ru(\eta^6\text{-}C_6H_6)Cl_2]_2$ (50 mg, 0.1 mmol) and ligand **1** (60 mg, 0.22 mmol) in the presence of 52 mg of NH_4BF_4 (0.497 mmol) in a Schlenk flask. The reaction mixture was refluxed and stirred for 3h. The mixture was cooled down to room temperature and the precipitate was filtered and washed with ethanol/diethyl ether and dried in air to afford the final complex **3** (54 mg, 95%) as a light brown solid. **^{1}H NMR (600 MHz, acetone-*d*$_6$):** δ_H = 9.27 (dd, *J* = 5.8, 1.5 Hz, 1H, H8), 8.48 (s, 1H, H13), 8.13 (td, *J* = 7.7, 1.5 Hz, 1H, H6), 7.86 (dt, *J* = 7.9, 1.1 Hz, 1H, H5), 7.62 (ddd, *J* = 7.3, 5.7, 1.3 Hz, 1H, H7), 7.54 (dd, *J* = 1.9, 0.8 Hz, 1H, H20), 6.43 (dd, *J* = 3.2, 0.8 Hz, 1H, H18), 6.37 (dd, *J* = 3.2, 1.8 Hz, 1H, H19), 6.29 and 5.94 (d, *J* = 15.7 Hz, 2H, H3), 6.24 (s, 6H, C_6H_6), 4.62 (m, 2H, H14), 4.53 (s, 2H, H16) ppm. **^{13}C{^{1}H} NMR (150 MHz, acetone-*d*$_6$):** δ_C = 159.8 (C8), 154.5 (C4), 152.4 (C12), 148.7 (C17), 143.9 (C20), 141.4 (C6), 130.1 (C13), 127.0 (C5), 126.6 (C7), 111.2 (C19), 110.8 (C18), 87.9 (6C, C_6H_6), 64.6 (C16), 63.1 (C14), 55.4 (C3) ppm. **^{19}F{^{1}H} NMR (565 MHz, acetone-*d*$_6$)** δ_F = −151.22 (s, 4F, $^{10}BF_4$), −151.27 (s, 4F, $^{11}BF_4$). Found (%): C, 40.88; H, 3.53; N, 9.69. $C_{20}H_{20}BClF_4N_4O_2Ru_1 \cdot H_2O$ requires C, 40.73; H, 3.76; N, 9.50. **HR-ESI-MS *m/z* (+):** $[M]^+$ calc. for $C_{20}H_{20}ClN_4O_2Ru^+$ 485.0313, found: 485.0318; $[2M+BF_4]^+$ calc. for $C_{40}H_{40}BCl_2F_4N_8O_4Ru_2^+$ 1057.0660, found: 1057.0703; **HR-ESI-MS *m/z* (−):** $[M]^-$ calc. for BF_4^- 87.0035; found 87.0020.

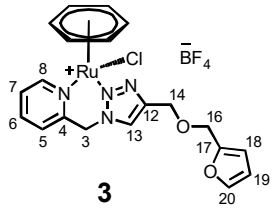

3

General procedures for the synthesis of **4a** and **4b**. *Method 1:* in a 35 mL pressure vessel sealed with a silicone cap (CEM), acetonitrile (25.0 mL) was added to the mixture of **3** (1.0 eq) and maleimides (30 eq). The Diels-Alder reaction was carried out with a CEM Discover S microwave reactor (T = 40°C, power: 6.5 W, P: 0 PSI, hold time: 24h). After 24h, the completion of the reaction was confirmed by ^{1}H-NMR (acetone-*d*$_6$), then the solvent was evaporated with rotary evaporator. The crude product was dissolved in minimum amount of dichloromethane and loaded on 50 g KP-Sil column (Biotage SNAP) and eluted with CH_2Cl_2/MeOH to afford Ru complex DA **4a** and **4b** correspondent (two consecutively purifications were needed). *Method 2:* in a 15 mL Pyrex® tube, 5 mL of ethanol anhydrous was added to the mixture of ligand DA **2a** or **2b** (1.5 eq), $[Ru(\eta^6\text{-}C_6H_6)Cl_2]_2$ (1.0 eq) and NH_4BF_4 (3.5 eq). The tube was sealed carefully with parafilm to prevent the evaporation of solvent. The reaction was carried out at room temperature for 48h. The completion of the reaction was confirmed by ^{1}H-NMR (acetone-*d*$_6$). The solvent was evaporated then the crude product was re-dissolved in 1-2 mL of dichloromethane and the solution was filtered on a Celite pad. Complexes **4a** and **4b** were obtained by adding 2 mL of Et_2O, scratching the flask with a spatula and then drying the precipitate under vacuum.

Synthesis of 4a. *Method 1:* **3** (100 mg, 0.175 mol) was reacted with *N*-octyl maleimide (1.050 g, 5.02 mmol). After two consecutive purifications by flask chromatography, **4a** was obtained (**4a$_{endo}$**/**4a$_{exo}$**: 1.7/1) (29 mg, 21%) as a yellowish solid. *Method 2:* Ligand **2a** (**2a$_{endo}$**/**2a$_{exo}$**: 2) (27 mg, 0.0346 mmol) was reacted with $[Ru(\eta^6\text{-}C_6H_6)Cl_2]_2$ (19 mg) in the presence of NH_4BF_4 (14 mg, 0.103 mmol) in EtOH anhydrous (5 mL). After purification, **4a** was obtained (**4a$_{endo}$**/**4a$_{exo}$**: 1.5/1) as a yellowish solid (40 mg, 90%). **4a$_{endo}$. ^{1}H NMR (600 MHz, acetone-*d*$_6$):** δ_H = 9.29 (t, *J* = 6.3 Hz, 1H, H9), 8.53 (s, 1H, H12), 8.15 (t, *J* = 7.5 Hz, 1H, H7), 7.88 (d, *J* = 7.4 Hz, 1H, H6), 7.64 (t, *J* = 6.7 Hz, 1H, H8), 6.42 (dd, *J* = 5.7, 1.6 Hz, 1H, H20), 6.31 (dd, *J* = 5.8, 3.0 Hz, 1H, H21), 6.28 and 5.97 (d, *J* = 15.6 Hz, 2H, H14), 6.26 (m, 6H, C_6H_6), 5.23 (d, *J* = 5.2 Hz, 1H, H19), 4.78 (m, 2H, H15), 4.24 (dd, *J* = 12.2, 9.7 Hz, 1H, H17), 4.14 (dd, *J* = 12.2, 10.7 Hz, 1H, H17), 3.60 (dt, *J* = 13.4, 6.6 Hz, 1H, H18), 3.47 (d, *J* = 7.6 Hz, 1H, H22$_{endo\text{-}2}$), 3.42 (d, *J* = 7.6 Hz, 1H, H22$_{endo\text{-}1}$), 3.23 (t, *J* = 7.3 Hz, 1H, H30$_{endo\text{-}2}$), 3.18 and 3.14 (dt, *J* = 13.2, 7.3 Hz, 1H,

H30$_{endo-1}$), 1.38 (m, 2H, H31), 1.33-1.11 (m, 10H, -CH$_2$-), 0.86 (t, *J* = 7.0 Hz, 3H, H37) ppm. **^{13}C{^{1}H} NMR (150 MHz, acetone-*d*$_6$):** δ_C = 175.9 and 175.5 (2C, C25 and C26), 159.9 (C9), 154.5 (C5), 148.5 (C11), 141.4 (C7), 136.1 (C20), 135.8 (C21), 131.0 (C12), 127.4 (C6), 126.7 (C8), 91.9 (C23), 88.2 (6C, C_6H_6), 80.2 (C19), 69.2 (C17$_{endo-2}$) and 68.8 (C17$_{endo-1}$), 64.9 (C15$_{endo-2}$) and 64.8 (C15$_{endo-1}$), 56.2 (C14), 48.6 (C18), 46.7 (C22$_{endo-2}$) and 46.5 (C22$_{endo-1}$), 38.8 (C30), 27.5 (C31), 32.5, 29.8, 28.1, 27.5, 23.2 (5C, -CH$_2$-), 14.3 (-CH$_3$, C37) ppm. **^{19}F{^{1}H} NMR (565 MHz, acetone-*d*$_6$)** δ_F = −150.69 (s, 4F, $^{10}BF_4$), −150.75 (s, 4F, $^{11}BF_4$). **4a$_{exo}$. ^{1}H NMR (600 MHz, acetone-*d*$_6$):** δ_H = 9.28 (d, *J* = 5.7 Hz, 1H, H9), 8.51 (d, *J* = 5.7 Hz, 1H, H12), 8.14 (t, *J* = 7.5 Hz, 1H, H7), 7.86 (d, *J* = 7.7 Hz, 1H, H6), 7.63 (t, *J* = 6.6 Hz, 1H, H8), 6.56 (m, 1H, H20), 6.54 (t, *J* = 5.9 Hz, 1H, H21), 6.28 and 5.95 (d, *J* = 15.6 Hz, 2H, H14), 6.25 (s, 6H, C_6H_6), 5.12 (t, *J* = 1.9 Hz, 1H, H19), 4.81 and 4.74 (m, 2H, H15), 4.28 (dd, *J* = 11.4, 4.4 Hz, 1H, H17) and 3.88 (dd, *J* = 11.5, 3.3 Hz, 1H, H17), 3.39 (q, *J* = 6.7 Hz, 2H, H30), 3.03 (dd, *J* = 6.4, 3.8 Hz, 1H, H18), 2.97 (t, *J* = 6.6 Hz, 1H, H22), 1.50 (m, 2H, H31), 1.33-1.11 (m, 10H, -CH$_2$-), 0.86 (t, *J* = 7.0 Hz, 3H, H37) ppm**. ^{13}C{^{1}H} NMR (150 MHz, acetone-*d*$_6$):** δ_C = 176.8 and 175.6 (2C, C25 and C26), 159.8 (C9), 154.5 (C5), 148.8 (C11), 141.4 (C7), 138.6 (C20), 137.5 (C21), 130.2 (C12), 127.1 (C6), 126.6 (C8), 91.2 (C23), 88.0 (6C, C_6H_6), 81.9 (C19), 69.0 (C17), 65.1 (C15), 55.7 (C14), 50.7 (C18), 49.1 (C22), 39.0 (C30), 27.3 (C31), 32.5, 29.9, 29.8, 28.3, 23.3 (5C, -CH$_2$-), 14.4 (-CH$_3$, C37) ppm. **^{19}F{^{1}H} NMR (565 MHz, acetone-*d*$_6$):** δ_F = −151.06 (s, 4F, $^{10}BF_4$), −151.11 (s, 4F, $^{11}BF_4$). Found (%): C, 46.70; H, 4.84; N, 8.47. $C_{32}H_{39}BClF_4N_5O_4Ru_1 \cdot ½CHCl_3$ requires C, 46.43; H, 4.74; N, 8.33. **HR-ESI-MS *m/z* (+):** $[M]^+$ calc. for $C_{32}H_{39}ClN_5O_4Ru^+$ 694.1729, found: 694.1738; $[2M+BF_4]^+$ calc. for $C_{64}H_{78}BCl_2F_4N_{10}O_8Ru_2^+$ 1475.3492, found: 1475.3521; **HR-ESI-MS *m/z* (−):** $[M]^-$ calc. for BF_4^- 87.0035; found 87.0020.

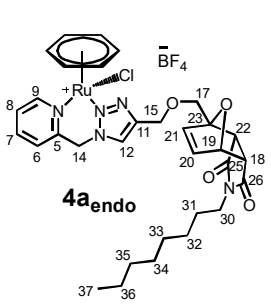

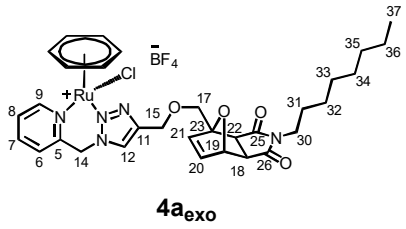

NOTE: After purification of **4a$_{endo}$** by HPLC (H_2O/acetonitrile/0.1% TFA), two different isomers (for which the counterion was replaced by trifluoroacetate during the analysis) were separated. HPLC method: A: H_2O + 0.1% trifluoroacetic acid (TFA), B: acetonitrile + 0.1% TFA; 0-2 min 15% B, 2-40 min 60% B, 40-43 100% B, 43-47 min 100% B, 47-50 min, 15% B, flow: 3.0 mL min^{-1}. **4a$_{endo-1}$. ^{1}H NMR (600 MHz, acetone-*d*$_6$):** δ_H = 9.27 (d, *J* = 5.7 Hz, 1H, H9), 8.65 (s, 1H, H12), 8.13 (t, *J* = 7.4 Hz, 1H, H7), 7.90 (d, *J* = 7.5 Hz, 1H, H6), 7.63 (t, *J* = 6.6 Hz, 1H, H8), 6.41 (td, *J* = 6.3, 1.6 Hz, 1H, H20), 6.31 (d, *J* = 5.7 Hz, 1H, H21), 6.46 and 6.00 (d, *J* = 15.4 Hz, 1H, 2H, H14), 6.27 (s, 6H, C_6H_6), 5.23 (dd, *J* = 5.5, 1.6 Hz, 1H, H19), 4.77 (m, 2H, H15), 4.21 and 4.13 (d, *J* = 12.1 Hz, 2H, H17), 3.59 (dd, *J* = 7.6, 5.5 Hz, 1H, H18), 3.42 (d, *J* = 7.5 Hz, 1H, H22), 3.20 and 3.13 (dt, *J* = 13.6, 7.3 Hz, 2H, H30), 1.36 (p, *J* = 7.3 Hz, 2H, H31), 1.33-1.11 (m, 10H, -CH$_2$-), 0.86 (t, *J* = 6.9 Hz, 3H, H37) ppm. **^{13}C{^{1}H} NMR (150 MHz, acetone-*d*$_6$):** δ_C = 175.9 and 175.5 (2C, C25 and C26), 159.8 (C9), 154.7 (C5), 148.6 (C11), 141.3 (C7), 136.1 (C20), 135.8 (C21), 130.6 (C12), 127.1 (C6), 126.6 (C8), 91.9 (C23), 88.1 (6C, C_6H_6), 80.2 (C19), 68.8 (C17), 64.7 (C15), 55.8 (C14), 48.5 (C18), 46.5 (C22), 38.8 (C30), 27.6 (C31), 32.5, 29.6, 28.1, 28.1, 23.3 (5C, -CH$_2$-), 14.3 (C37) ppm. **^{19}F{^{1}H} NMR (565 MHz, acetone-d$_6$):** δ_F = −75.75 (s, 3F, CF_3COO^-). **HR-ESI-MS *m/z* (+):** $[M]^+$ calc. for $C_{32}H_{39}ClN_5O_4Ru^+$ 694.1729, found: 694.1722; **HR-ESI-MS *m/z* (−):** $[M]^-$ calc. for CF_3COO^- 112.9856, found 112.9857. **4a$_{endo-2}$. ^{1}H NMR (600 MHz, acetone-*d*$_6$):** δ_H = 9.28 (d, *J* = 5.7 Hz, 1H, H9), 8.65 (s, 1H, H12), 8.14 (t, *J* = 7.6 Hz, 1H, H7), 7.90 (d, *J* = 7.5 Hz, 1H, H6), 7.63 (t, *J* = 6.6 Hz, 1H, H8), 6.43 (td, *J* = 6.3, 1.6 Hz, 1H, H20), 6.31 (d, *J* = 5.7 Hz, 1H, H21), 6.46 and 6.02 (d, *J* = 15.4 Hz, 2H, H14), 6.26 (s, 6H, C_6H_6), 5.23 (dd, *J* = 5.6, 1.7

Hz, 1H, H19), 4.78 (m, 2H, H15), 4.23 and 4.11 (d, *J* = 12.1 Hz, 2H, H17), 3.62 (dd, *J* = 7.6, 5.5 Hz, 1H, H18), 3.47 (d, *J* = 7.6 Hz, 1H, H22), 3.23 (t, *J* = 7.3 Hz, 2H, H30), 1.39 (p, *J* = 7.4 Hz, 2H, H31), 1.33-1.11 (m, 10H, -CH_2-), 0.86 (t, *J* = 7.0 Hz, 3H, H37) ppm. **^{13}C{^{1}H} NMR (150 MHz, acetone-*d*$_6$):** δ_C = 175.9 and 175.5 (2C, C25 and C26), 159.9 (C9), 154.6(C5), 148.6 (C11), 141.4 (C7), 136.1 (C20), 135.8 (C21), 130.4 (C12), 127.1 (C6), 126.6 (C8), 92.0 (C23), 88.0 (6C, C_6H_6), 80.2 (C19), 69.2 (C17), 64.8 (C15), 55.6 (C14), 48.5 (C18), 46.7 (C22), 38.8 (C30), 28.2 (C31), 32.4, 29.8, 28.0, 27.6, 23.2 (5C, -CH_2-), 14.3 (C37) ppm. **^{19}F{^{1}H} NMR (565 MHz, acetone-*d*$_6$):** δ_F = −75.87 (s, 3F, CF_3COO^-). **HR-ESI-MS *m/z* (+):** $[M]^+$ calc. for $C_{32}H_{39}ClN_5O_4Ru^+$ 694.1729, found: 694.1721; **HR-ESI-MS *m/z* (−):** $[M]^-$ calc. for CF_3COO^- 112.9856, found 112.9857.

Synthesis of 4b. *Method 1:* **3** (80 mg, 0.14 mol) was reacted with *N*-*p*-nitrophenylmaleimide (920 mg, 4.22 mmol). After two consecutive purifications by flask chromatography, **4b** was obtained (**4b$_{endo}$/4b$_{exo}$** : 1/3.8) (27 mg, 25%) as a yellowish solid. *Method 2:* **2b** (**2b$_{endo}$/2b$_{exo}$**: 1/2) (50 mg, 0.102 mmol) was reacted with $[Ru(\eta^6\text{-}C_6H_6)Cl_2]_2$ (34 mg) in the presence of NH_4BF_4 (25 mg, 0.238 mmol) in EtOH anhydrous (5 mL). After purification, **4b** was obtained (**4b$_{endo}$/4b$_{exo}$**: 1/4) as a yellowish solid (68 mg, 87%). **4b$_{endo}$. ^{1}H NMR (600 MHz, DMSO-*d*$_6$):** δ_H = 9.13 and 9.09 (d, *J* = 5.6 Hz, 1H, H9), 8.64 (d, *J* = 5.6 Hz, 1H, H12), 8.31 (t, *J* = 8.3 Hz, 2H, H32/34), 8.14 (t, *J* = 7.6 Hz, 1H, H7), 7.78 (m, 1H, H6), 7.64 (t, *J* = 6.8 Hz, 1H, H8), 7.47 and 7.41 (d, *J* = 9.0 Hz, 2H, H31/35), 6.65 and 6.62 (dd, *J* = 5.8, 1.6 Hz, 1H, H20), 6.55 (m, 1H, H21), 6.24 and 5.73 (d, *J* = 15.6 Hz, 2H, H14), 6.14 (m, 6H, C_6H_6), 5.38 (td, *J* = 6.3, 5.5, 1.5 Hz, 1H, H19), 4.74 (m, 2H, H15), 4.19 and 4.11 (m, 2H, H17), 3.84 (ddd, *J* = 13.6, 7.7, 5.5 Hz, 1H, H18), 3.61 and 3.57 (d, *J* = 7.6 Hz, 1H, H22) ppm. **^{13}C{^{1}H} NMR (150 MHz, DMSO-*d*$_6$):** δ_C = 173.5 and 173.4 (2C, C25/26), 158.7 (C9), 153.3 (C5), 146.7 (C11), 143.3 (2C, C30/33), 140.5 (C7), 135.6 (C20), 135.1 (C21), 129.6 (C12), 127.8 and 127.7 (2C, C31/35), 126.0 (C6), 125.6 (C8), 124.3 (2C, C32/34), 91.1 (C23), 86.7 (6C, C_6H_6), 79.2 (C19), 67.7 (C17), 63.5 (C15), 54.1 (C14), 47.7 (C18), 46.1 (C22) ppm. **^{19}F{^{1}H} NMR (565 MHz, acetone-*d*$_6$):** δ_F = −150.91 (s, 4F, $^{10}BF_4$), −150.96 (s, 4F, $^{11}BF_4$). **4b$_{exo}$. ^{1}H NMR (600 MHz, DMSO-*d*$_6$):** δ_H = 9.13 (d, *J* = 6.1 Hz, 1H, H9), 8.59 (s, 1H, H12), 8.35 (m, 2H, H32/34), 8.13 (tdd, *J* = 7.7, 2.6, 1.6 Hz, 1H, H7), 7.78 (t, *J* = 7.4 Hz, 1H, H6), 7.64 (t, *J* = 6.7 Hz, 1H, H8), 7.58 (m, 2H, H31/35), 6.61 (t, *J* = 6.7 Hz, 1H, H20), 6.54 (m, 1H, H21), 6.19 and 5.70 (m, 2H, H14), 6.13 (s, 6H, C_6H_6), 5.24 (dd, *J* = 3.9, 1.6 Hz, 1H, H19), 4.71 (m, 2H, H15), 4.28 and 3.93 (d, *J* = 12.3 Hz, 2H, H17), 3.27 (d, *J* = 6.6 Hz, 1H, H18), 3.13 (dd, *J* = 6.5, 4.9 Hz, 1H, H22) ppm. **^{13}C{^{1}H} NMR (150 MHz, DMSO-*d*$_6$):** δ_C = 175.0 and 173.5 (C25/26), 158.7 (C9), 153.3 (C5), 147.0 (C11), 146.6 (C30/33), 140.5 (C7), 137.5 (C21), 136.9 (C20), 129.4 (C12), 127.7 (2C, C32/34), 126.0 (C6), 125.6 (C8), 124.3 (2C, C31/35), 90.6 (C23), 86.7 (6C, C_6H_6), 80.9 (C19), 67.7 (C17), 63.7 (C15), 54.0 (C14), 50.3 (C18), 48.7 (C22) ppm. **^{19}F{^{1}H} NMR (565 MHz, acetone-*d*$_6$):** δ_F = −151.28 (s, 4F, $^{10}BF_4$), −151.33 (s, 4F, $^{11}BF_4$). Found (%): C, 44.05; H, 3.59; N, 9.40. $C_{30}H_{26}BClF_4N_6O_6Ru_1 \cdot ½CH_2Cl_2$ requires C, 44.01; H, 3.27; N, 9.74. **HR-ESI-MS *m/z* (+):** $[M]^+$ calc. for $C_{30}H_{26}ClN_6O_6Ru^+$ 703.0640, found: 703.0644; **HR-ESI-MS *m/z* (−):** $[M]^-$ calc. for BF4$^-$ 87.0035; found 87.0018.

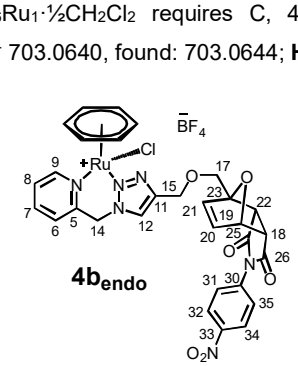

4b$_{endo}$

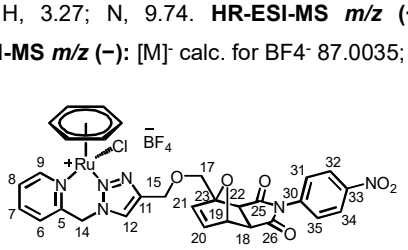

4b$_{exo}$

Synthesis of 5a. The hydrogenation of **4a** (50 mg, 0.064 mmol) was carried out with a H-Cube® reactor (ThalesNano) in 30 min using a catalyst cartridge 10% Pd/C in acetone (20 bar, flow rate: 1.0 mL/min, 23°C). After reaction completion, the solvent was evaporated and **5a** was obtained as a yellowish solid (48 mg, 95%) by adding Et_2O and scratching the vessel with a spatula. **5a$_{endo}$. ^{1}H NMR (600 MHz, DMSO-*d*$_6$):** δ_H = 9.12 (d, *J* = 6.1 Hz, 1H,

H9), 8.63 (d, *J* = 2.5 Hz, 1H, H12), 8.14 (td, *J* = 7.7, 1.5 Hz, 1H, H7), 7.79 (t, *J* = 7.1 Hz, 1H, H6), 7.65 (t, *J* = 6.7 Hz, 1H, H8), 6.21 (d, *J* = 15.6 Hz, 1H, H14) and 5.74 (d, *J* = 15.4 Hz, 1H, H14), 6.14 (s, 6H, C_6H_6), 4.77 (q, *J* = 6.2 Hz, 1H, H19), 4.71 (m, 2H, H15), 3.85 (m, 2H, H17), 3.48 (m, 1H, H18), 3.34 and 3.28 (m, 1H, H22), 3.32 (m, 2H, H30), 1.74 (m, 2H, H21), 1.61 (m, 2H, H20), 1.45 and 1.40 (m, 2H, H31), 1.28 – 1.14 (m, 10H, -CH_2-), 0.84 (t, *J* = 7.0 Hz, 3H, H37) ppm. **$^{13}C\{^1H\}$ NMR (150 MHz, DMSO-*d*$_6$):** δ_C = 175.7 (2C, C_{25} and C_{26}), 158.7 (C9), 153.3 (C5), 146.8 (C11), 140.5 (C7), 129.5 (C12), 126.0 (C6), 125.6 (C8), 87.6 (C23), 86.7 (6C, C_6H_6), 77.0 (C19), 69.0 (C17), 63.5 (C15), 54.0 (C14), 51.6 (C18), 50.4 (C22), 37.9 (C30), 29.1 (C20), 28.9 (C21), 26.3 (C31), 31.1, 28.5, 28.4 22.0, 27.1 (5C, -CH_2-), 13.9 (-CH_3, C37) ppm. **$^{19}F\{^1H\}$ NMR (565 MHz, acetone-*d*$_6$):** δ_F = −148.22 (s, 4F, $^{10}BF_4$), −148.28 (s, 4F, $^{11}BF_4$). **5a$_{exo}$. ^{1}H NMR (600 MHz, DMSO-*d*$_6$):** δ_H = 9.13 (d, *J* = 5.7 Hz, 1H, H9), 8.60 (s, 1H, H12), 8.14 (t, *J* = 7.7, 1.5 Hz, 1H, H7), 7.78 (t, *J* = 7.6 Hz, 1H, H6), 7.64 (t, *J* = 6.7 Hz, 1H, H8), 6.21 and 5.73 (d, *J* = 15.5 Hz, 2H, H14), 6.14 (s, 6H, C_6H_6), 4.66 (m, 1H, H19), 4.65 (m, 2H, H15), 3.97 (dd, *J* = 19.1, 11.1 Hz, 1H, H17), 3.75 (d, *J* = 11.1 Hz, 1H, H17), 3.12 (d, *J* = 7.1 Hz, 1H, H22), 3.04 (dd, *J* = 6.9, 4.2 Hz, 1H, H18), 3.30 (m, 2H, H30), 1.41 (m, 2H, H31), 1.76 (m, 2H, H20), 1.62 (m, 2H, H21), 1.28 – 1.14 (m, 10H, -CH_2-), 0.83 (t, *J* = 7.2 Hz, 3H, H37) ppm. **$^{13}C\{^1H\}$ NMR (150 MHz, DMSO-*d*$_6$):** δ_C = 177.3 and 175.6 (2C, C25 and C26), 158.7 (C9), 153.3 (C5), 147.0 (C11), 140.5 (C7), 129.6 (C12), 125.9 (C6), 125.6 (C8), 87.6 (C23), 86.7 (6C, C_6H_6), 78.5 (C19), 68.7 (C17), 63.7 (C15), 54.1 (C14), 50.5 (C18), 50.3 (C22), 37.9 (C30), 28.9 (C31), 25.9 (C20), 26.9 (C21), 31.1, 28.5, 28.4, 22.0, 26.2 (5C, -CH_2-), 13.9 (C37) ppm. **$^{19}F\{^1H\}$ NMR (565 MHz, acetone-*d*$_6$):** δ_F = −148.56 (s, 4F, $^{10}BF_4$), −148.61 (s, 4F, $^{11}BF_4$). Found (%): C, 47.45; H, 5.33; N, 8.63. $C_{32}H_{41}BClF_4N_5O_4Ru_1 \cdot ½CH_2Cl_2$ requires C, 47.29; H, 5.13; N, 8.48. **HR-ESI-MS *m/z* (+):** $[M]^+$ calc. for $C_{32}H_{41}ClN_5O_4Ru^+$ 696.1885, found: 696.1860; **HR-ESI-MS *m/z* (−):** $[M]^-$ calc. for $BF4^-$ 87.0035; found 87.0036.

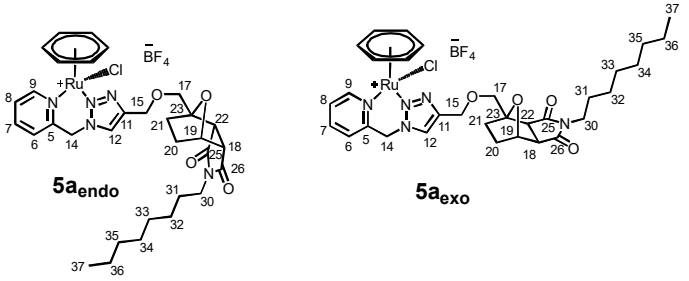

Cell culture. All protocols used for biological studies were approved by the Institutional Research Ethics Committee of INRS-Centre Armand-Frappier Santé Biotechnologie. The human breast cancer cell lines, MCF-7 and T47D were respectively provided by Prof. Chatenet and Prof. Plante (INRS). MCF-7 cells were grown routinely in RPMI-1640 containing fetal bovine serum (FBR, 10%). The growth medium for T47D cells was ATCC-formulated RPMI-1640 Medium supplemented with sodium pyruvate (0.11 g/L), HEPES (2.38 g/L), bovine insulin (10 µg/mL) and 10% fetal bovine serum. All cell growth media were supplemented with 1% penicillin/streptomycin. All cell culture products were purchased from Gibco, Invitrogen and Sigma-Aldrich. The growth of cells was carried out in a humidified atmosphere of 5% CO_2/95% air at 37°C. Passage of cells was performed at 70-80% confluency of cells (verified under microscope) by harvesting with trypsin:EDTA solution and seeding at a 1:4 to 1:10 ratio into 75 mL flasks. Cells were used up to 15 passages after thawing.

***In vitro* cell viability assay.** Cell viability was assessed by the SRB colorimetric assay described by Vichai and Kirtikara with some slightly modifications.[11] Briefly, cell culture treated 96-well plates (Sarstedt) were used to seed cells at a density of 1 × 104 cells/well for MCF-7 and T47D cancer cells and were pre-incubated in a humidified atmosphere at 37°C, 5% CO_2 for 24 h with drug-free complete growth medium. Stock solutions of test compounds were prepared in DMSO and the final concentration of DMSO was kept constant at 0.5% (non-cytotoxic concentration for cells). To achieve final concentration of 1, 4, 12.5, 25, 50, 75, 100 and 150 µM of drug solution, 200 µL of fresh and complete growth medium containing 0.5 µL of each stock solution was added to each well. Cancer cells were exposed also to drug-free complete growth medium, complete growth medium containing 0.5% DMSO as a negative control and complete growth medium containing 25% DMSO as a positive control. After incubation for 48h, 100 µL of cold trichloroacetic acid (TCA, 10% w/v) was added in each well to fix cells without removing the cell culture supernatant. After fixation at 4°C for 1 h, TCA was removed, and each well was washed three to four times with slow-running tap water then air-dried. Afterward, cells were exposed to a SRB solution (0.057% w/v) for 30 min at room temperature, then unbound SRB in each well were removed by washing three times with acetic acid solution (1% v/v) before drying cell-plate in air. To dissolve the protein-bound dye, 200 µL of 10 mM Tris bas solution (pH 10.5) was added to each well and cell-plate was stored in a dark-room for 30 min. Absorbance in each well was recorded with a microplate reader at 510 nm. Cell viability versus different concentration of each compound was reported. IC_{50} values, concentrations that respectively inhibit cell metabolic activity by 50% was also determined from concentration-effect curves by interpolation. This assay was carried out in three independent sets of experiments, each experiment with three or four replicates per concentration level.

NMR and HR-ESI-MS spectra

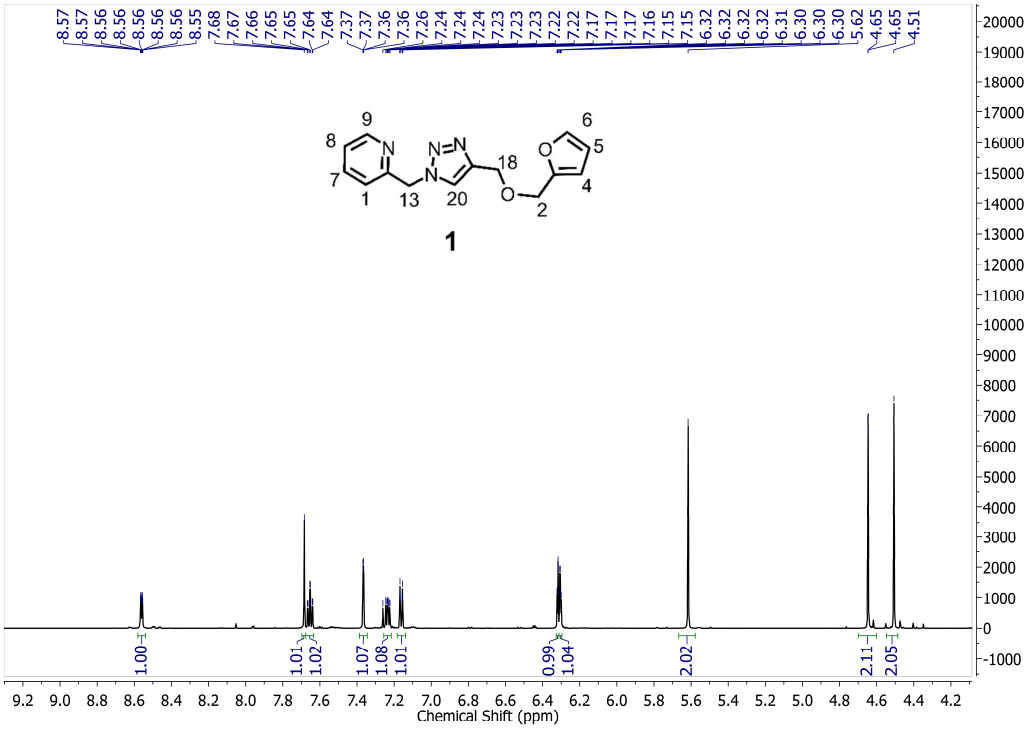

1

^{1}H NMR spectrum of **1** ($CDCl_3$).

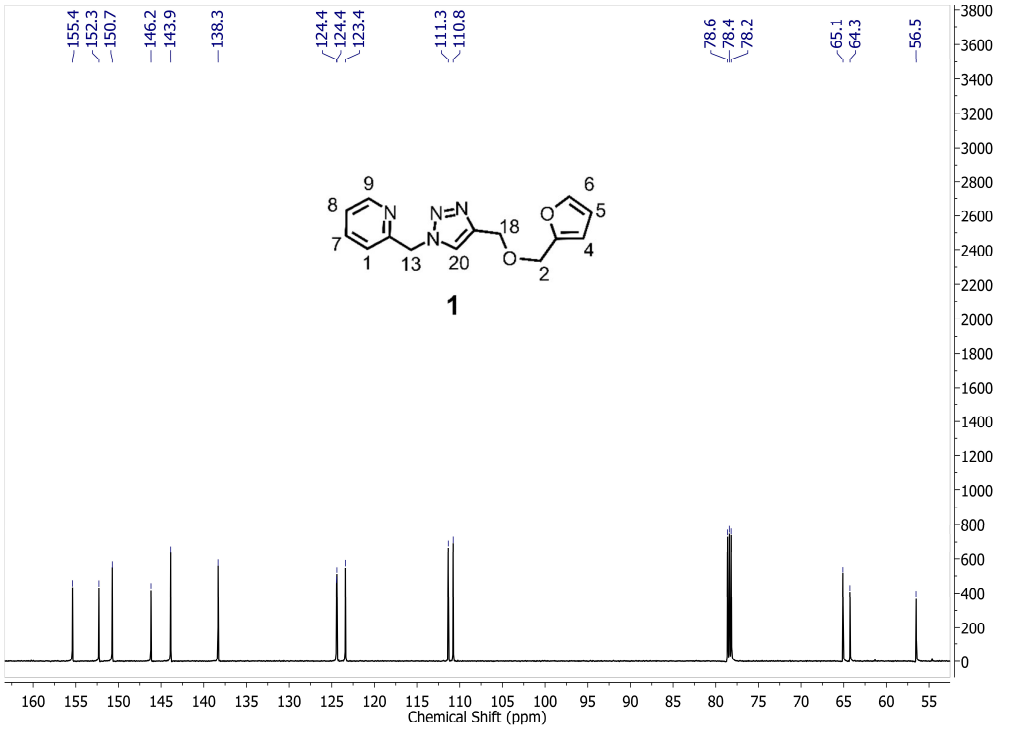

1

^{13}C{^{1}H} NMR spectrum of **1** ($CDCl_3$).

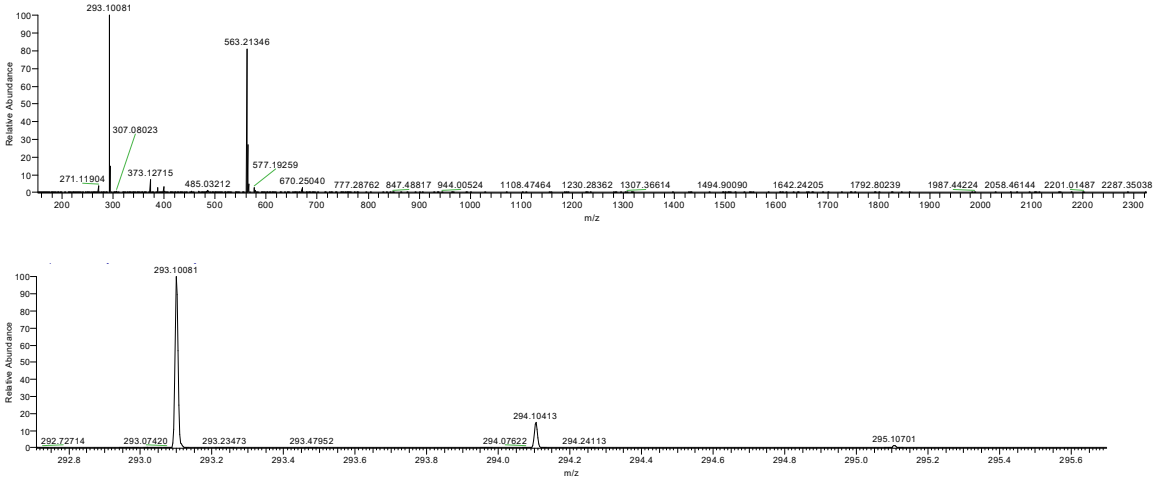

HR-ESI-MS spectrum of **1**, positive mode.

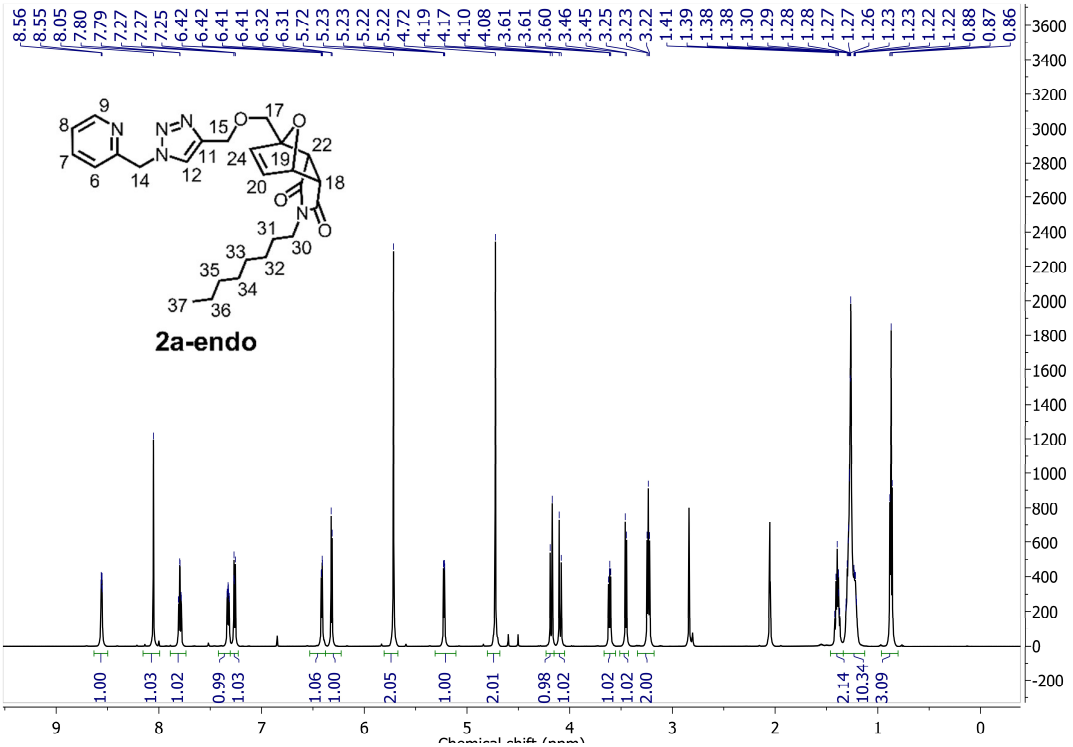

^{1}H NMR spectrum of **2a$_{endo}$** (acetone-d_6).

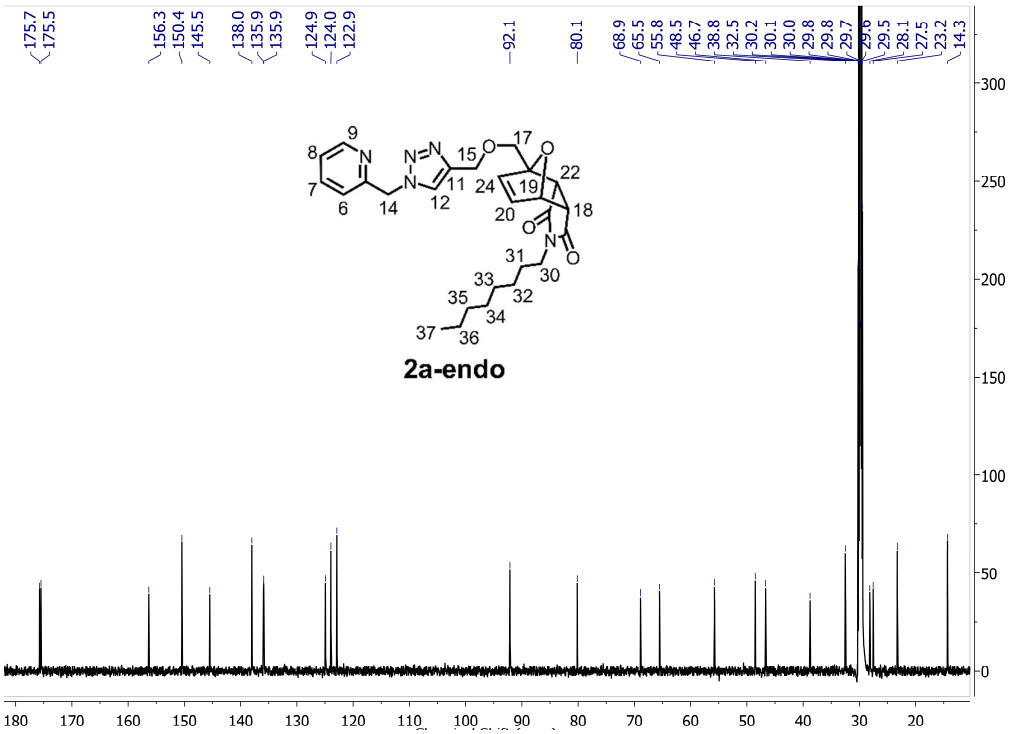

^{13}C{^{1}H} NMR spectrum of **2a$_{endo}$** (acetone-d_6).

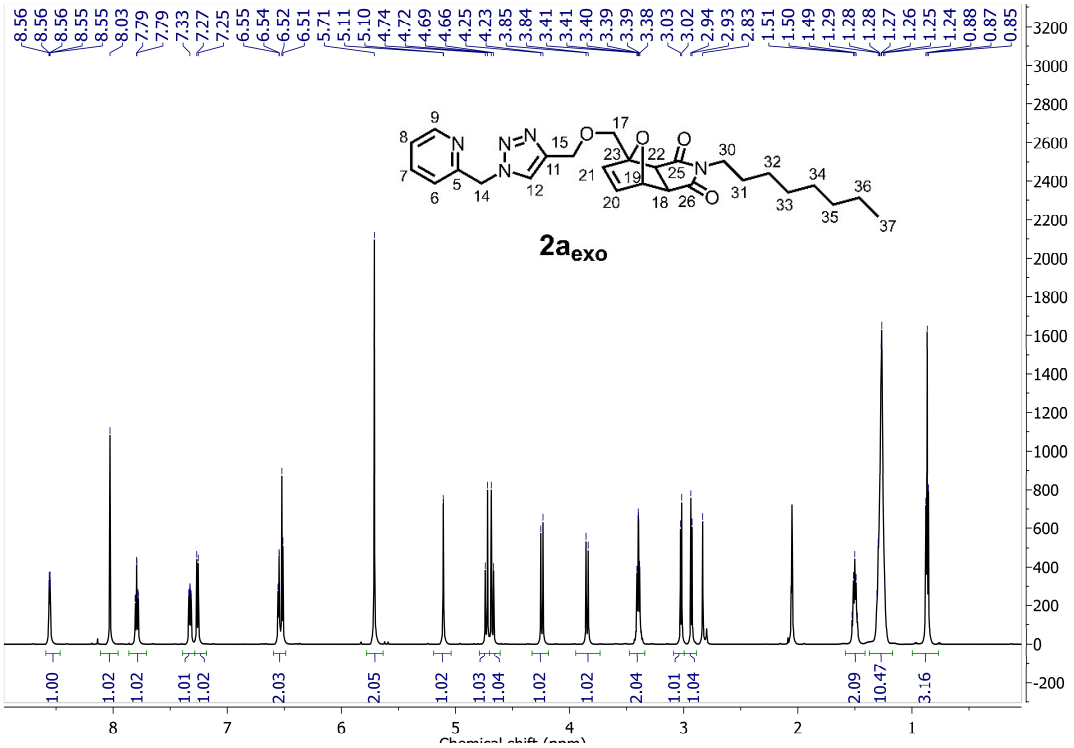

^{1}H NMR spectrum of **2a$_{exo}$** (acetone-d_6).

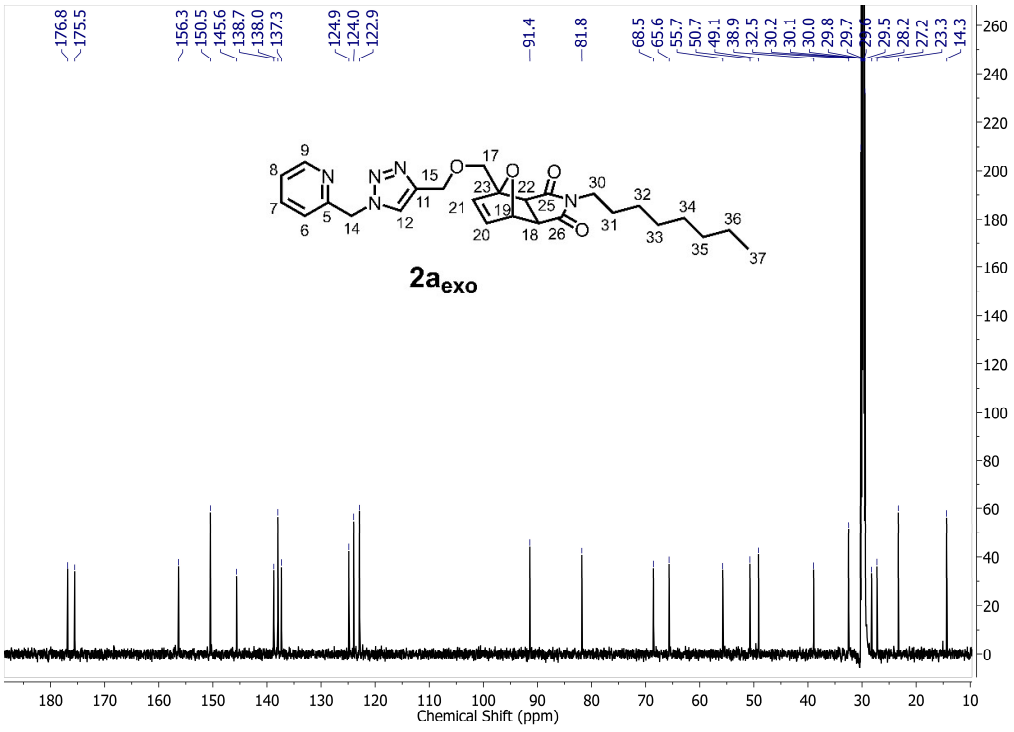

^{13}C{^{1}H} NMR spectrum of **2a$_{exo}$** (acetone-d_6).

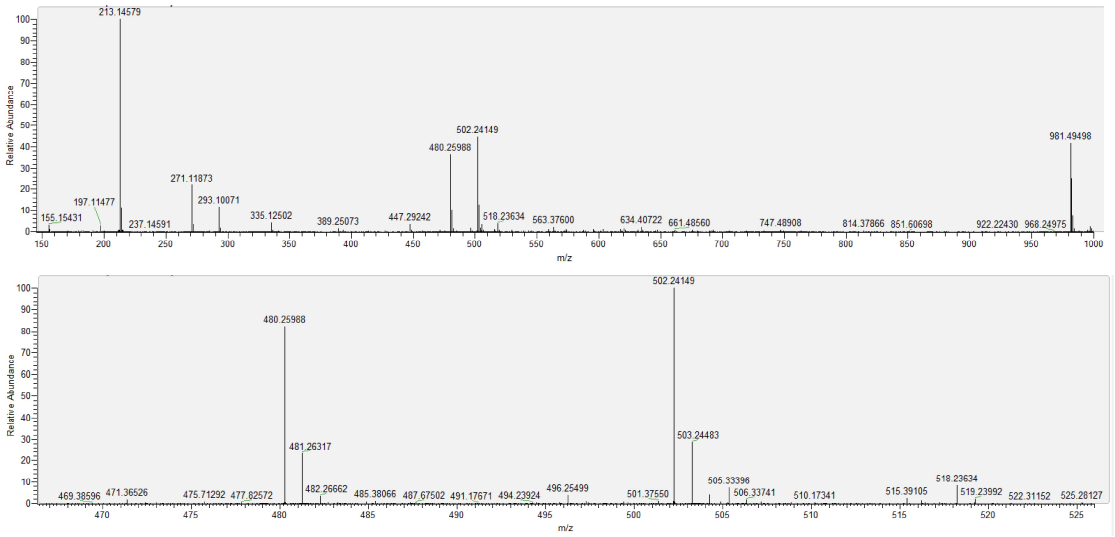

HR-ESI-MS spectrum of **2a** (**2a**$_{endo}$/**2a**$_{exo}$: 1.5/1), positive mode.

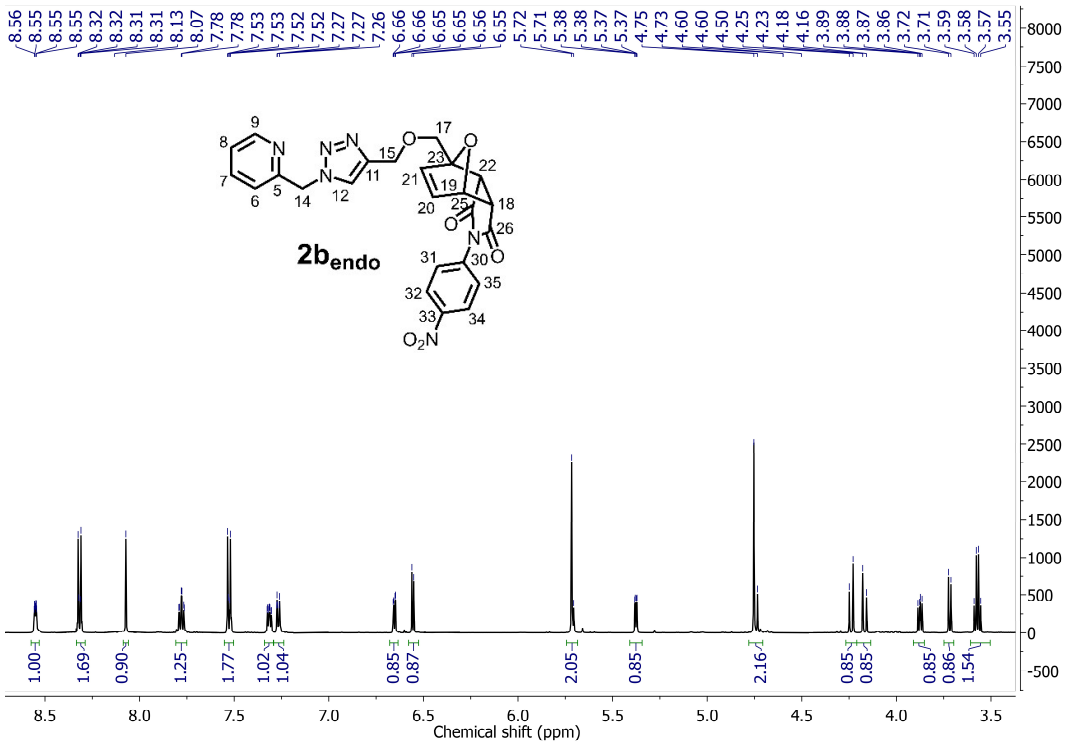

^{1}H NMR spectrum of **2b$_{endo}$** (acetone-d_6).

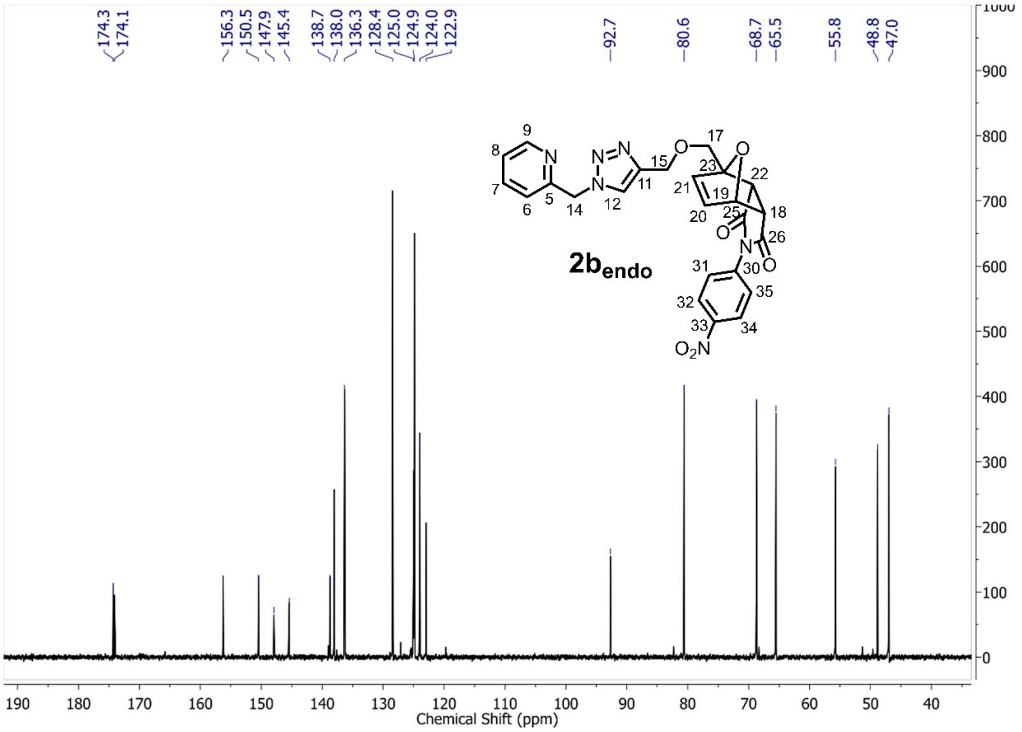

^{13}C{^{1}H} NMR spectrum of **2b$_{endo}$** (acetone-d_6).

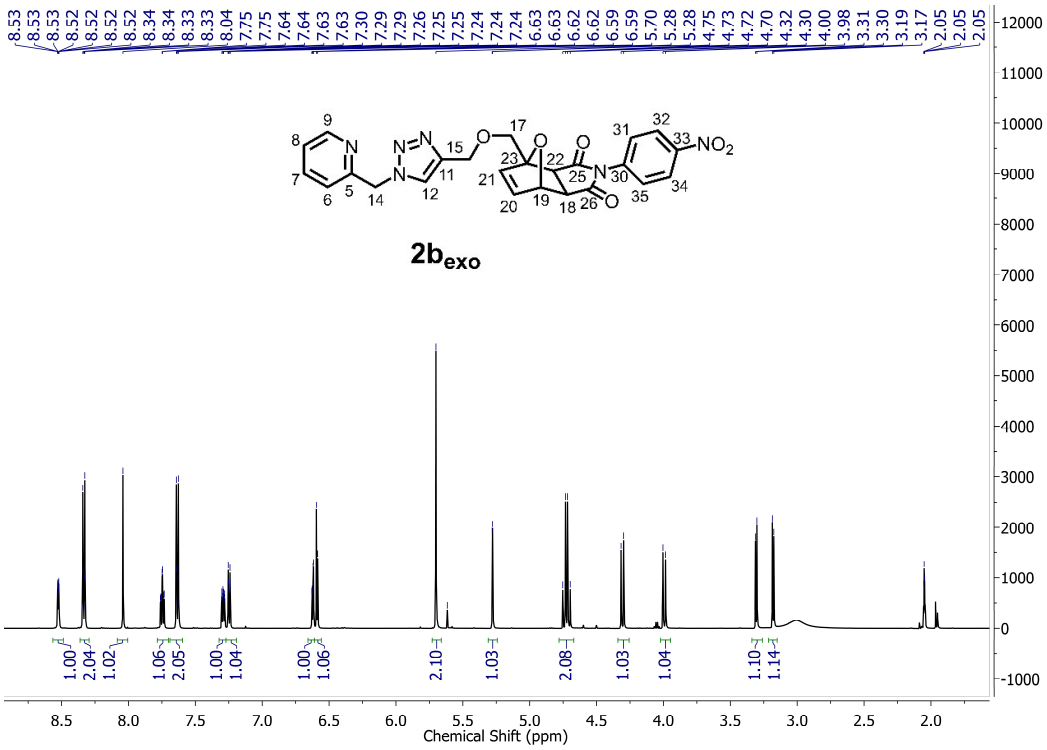

^{1}H NMR spectrum of **2b$_{exo}$** (acetone-d_6).

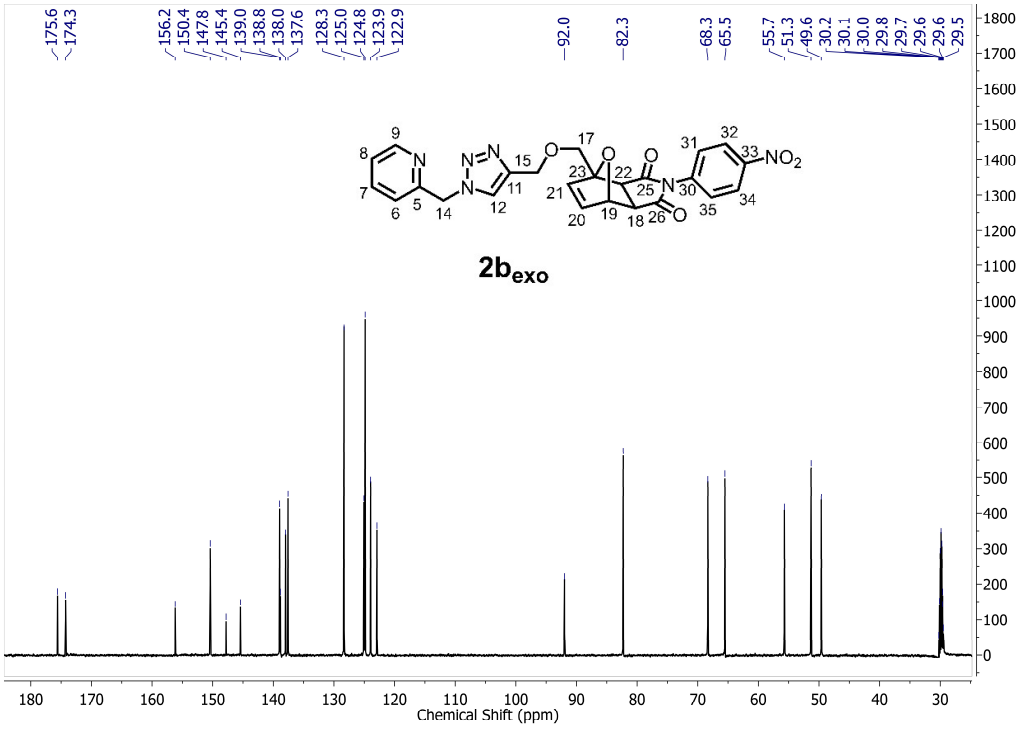

^{13}C{^{1}H} NMR spectrum of **2b$_{exo}$** (acetone-d_6).

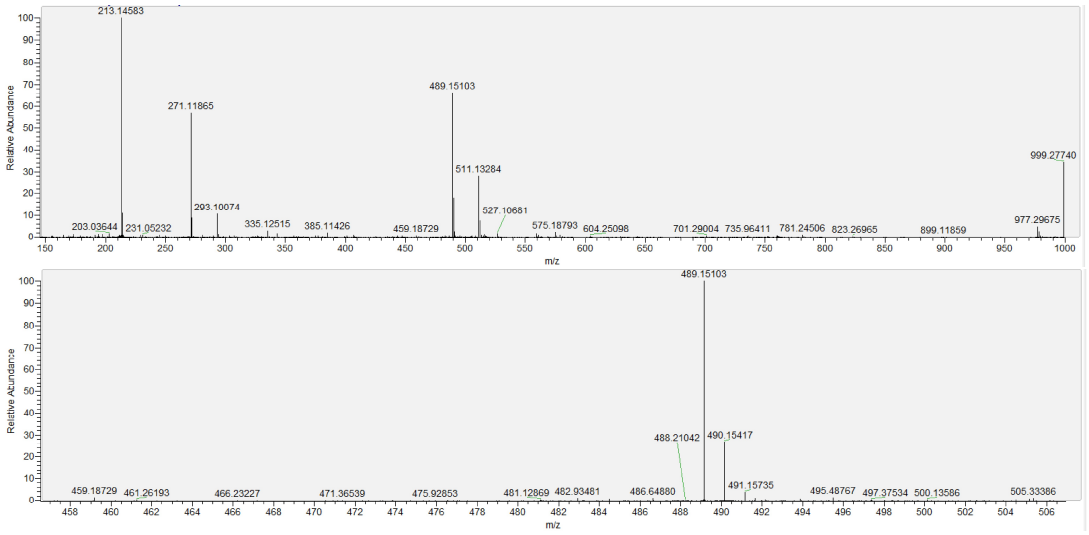

HR-ESI-MS spectrum of **2b** (**2b**$_{endo}$/**2b**$_{exo}$: 1/4), positive mode.

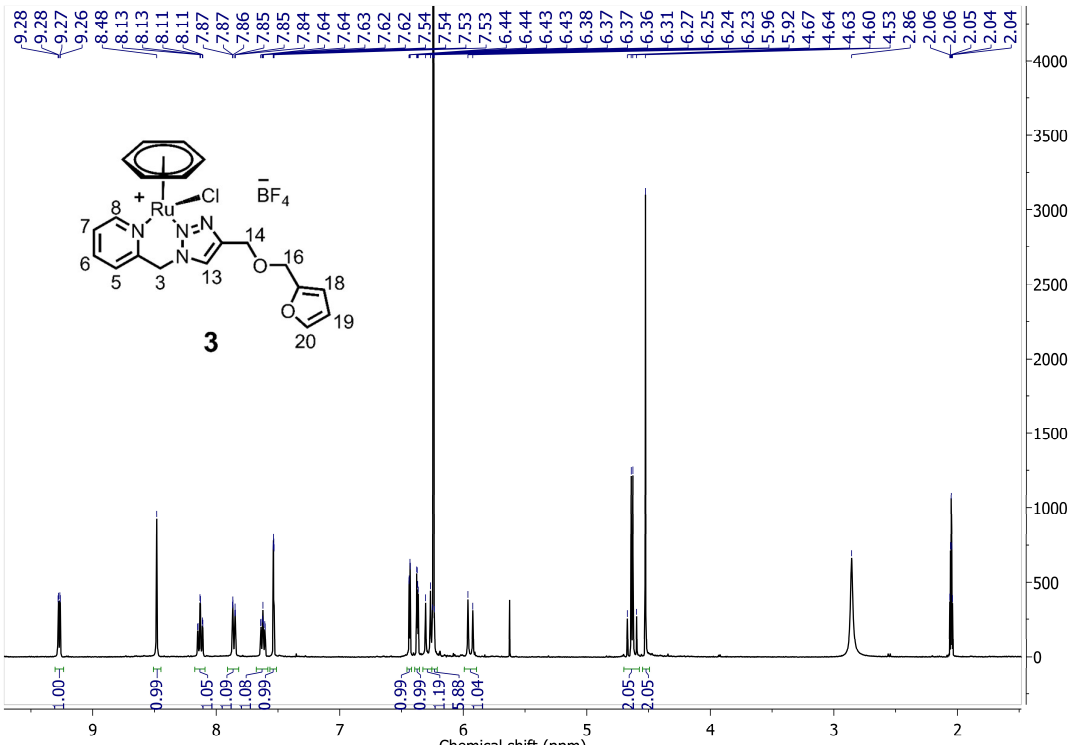

^{1}H NMR spectrum of **3** (acetone-d_6).

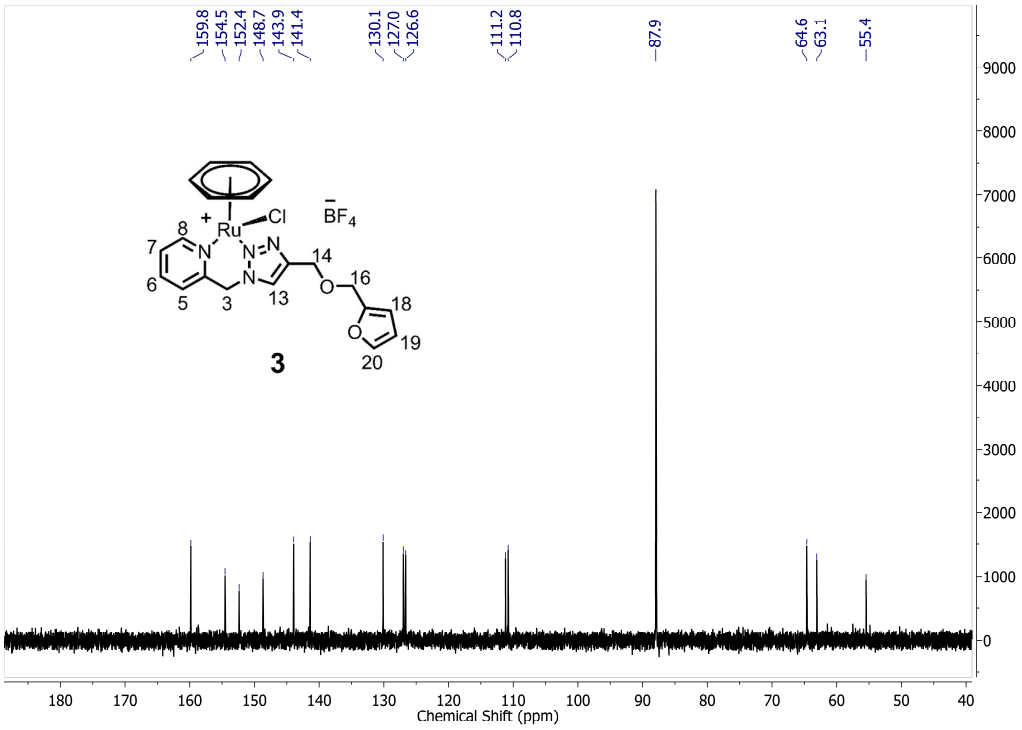

^{13}C{^{1}H} NMR spectrum of **3** (acetone-d_6).

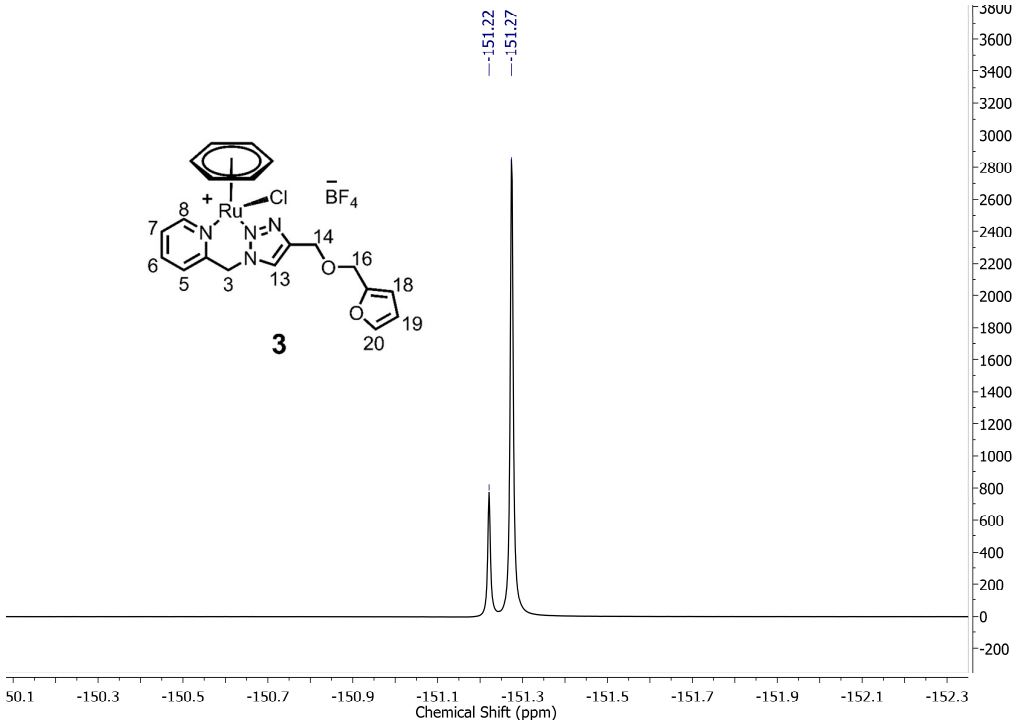

$^{19}F\{^{1}H\}$ NMR spectrum of **3** (acetone-d_6).

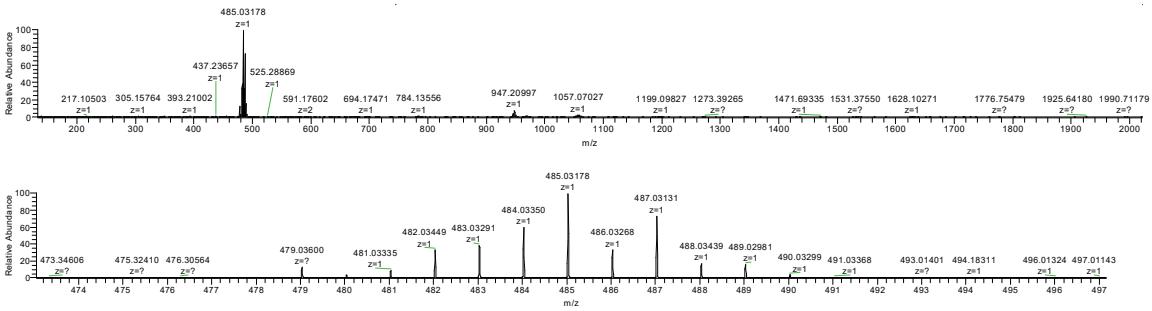

HR-ESI-MS spectrum of **3**, positive mode.

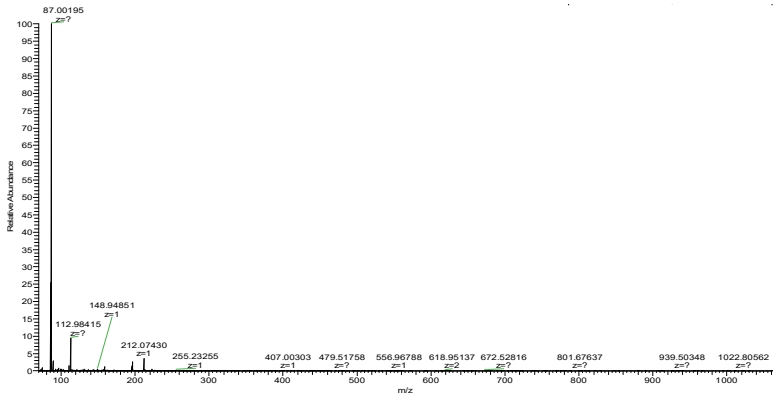

HR-ESI-MS spectrum of **3**, negative mode.

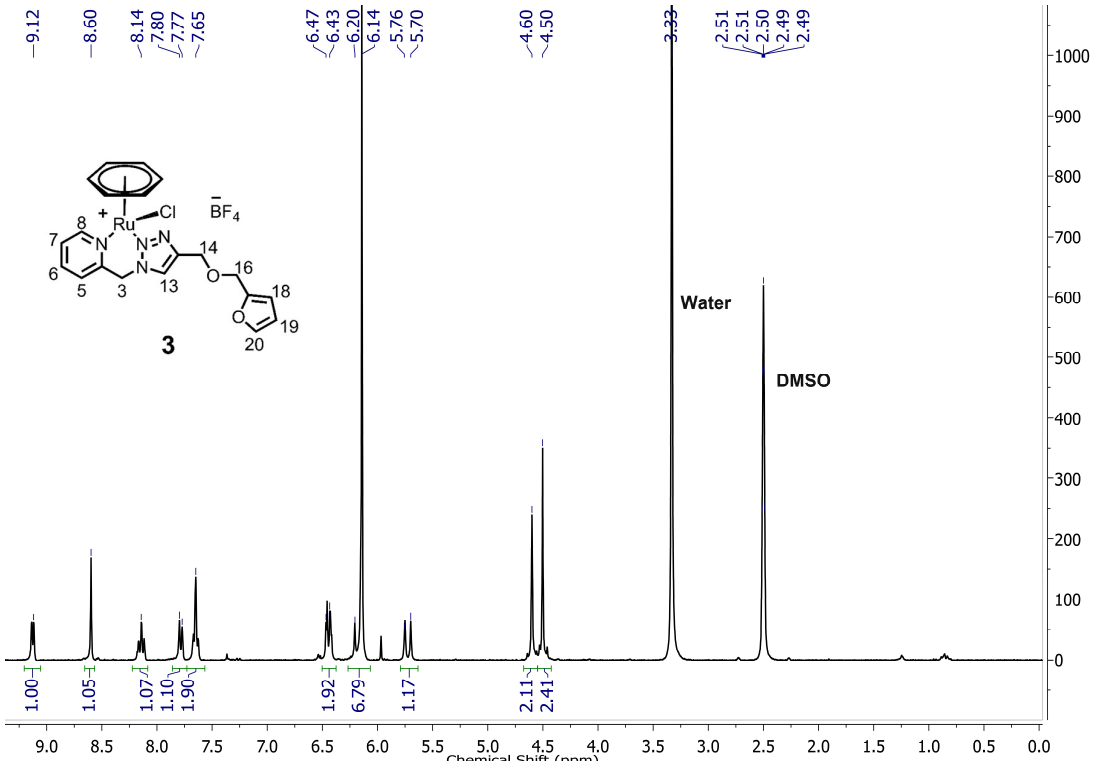

^{1}H NMR spectrum of **3** in DMSO-d_6 after 48h at room temperature.

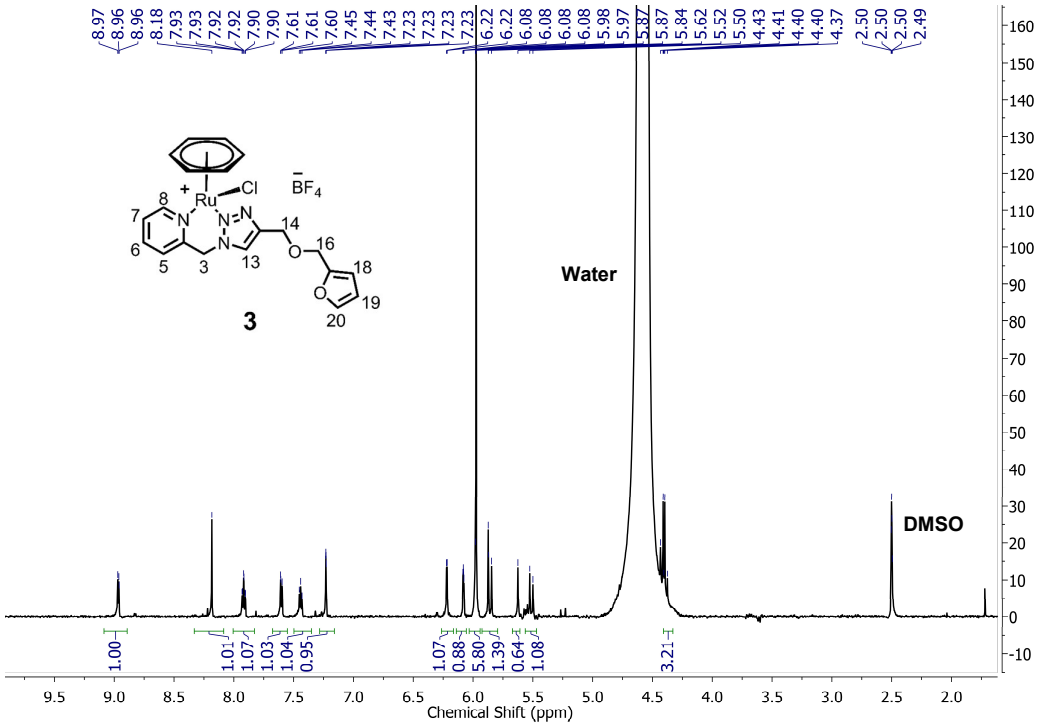

^{1}H NMR spectrum of **3** in D_2O containing 1% DMSO-d_6 (110 mM NaCl) after 2h at room temperature.

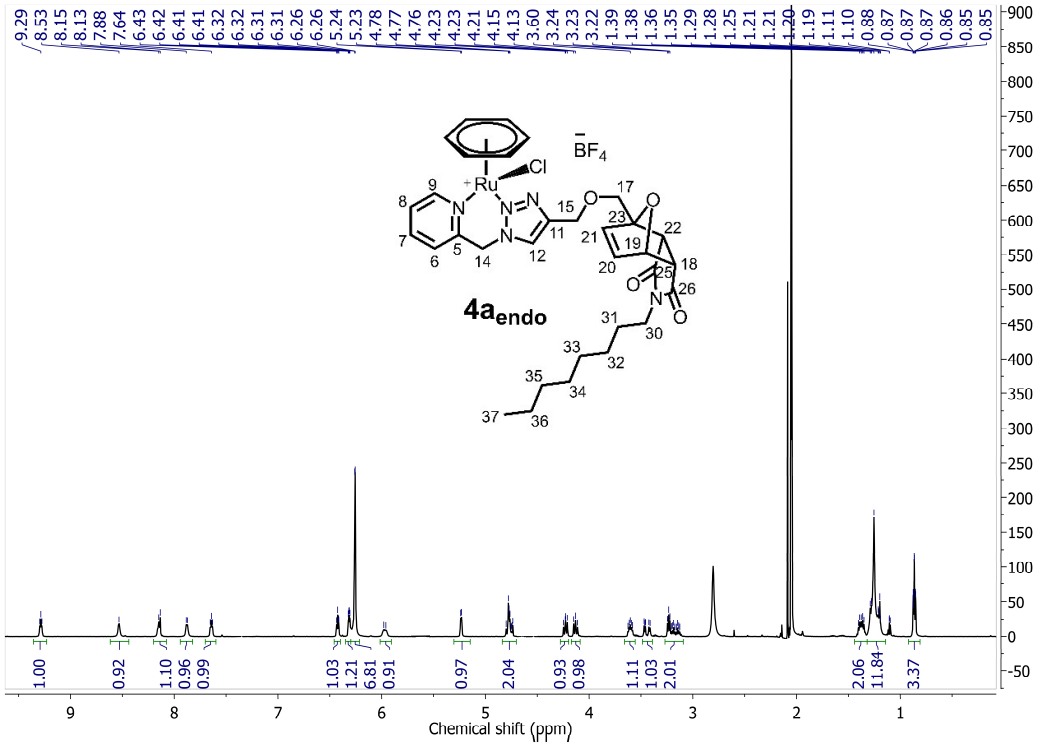

^{1}H NMR spectrum of **4a$_{endo}$** (acetone-d_6).

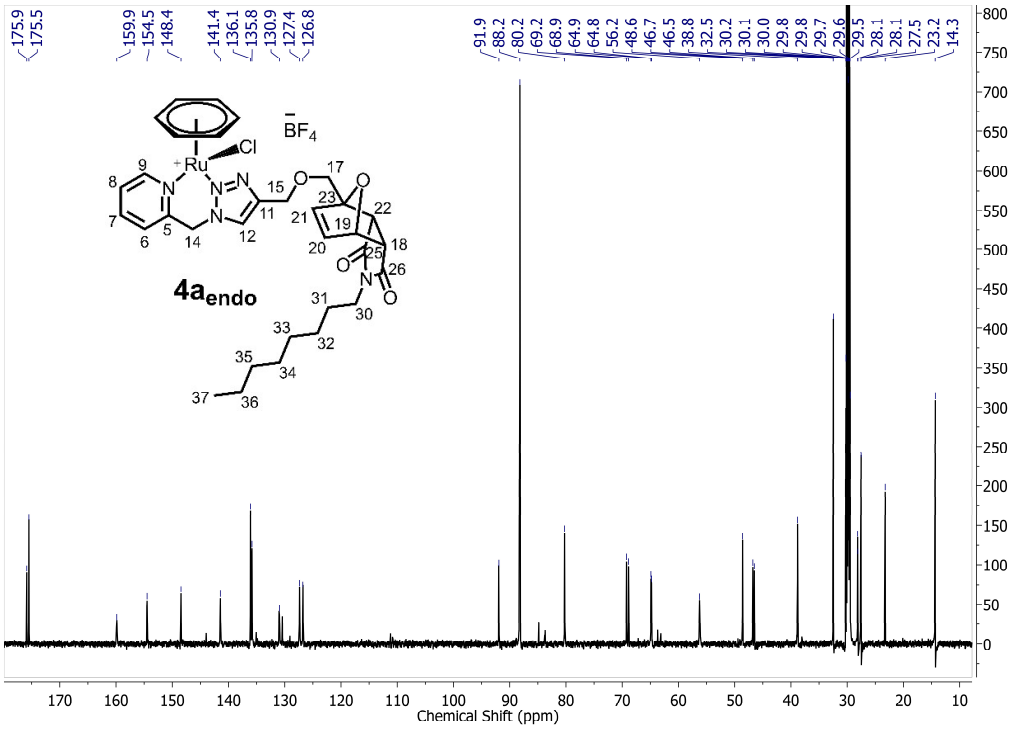

^{13}C{^{1}H} NMR spectrum of **4a$_{endo}$** (acetone-d_6).

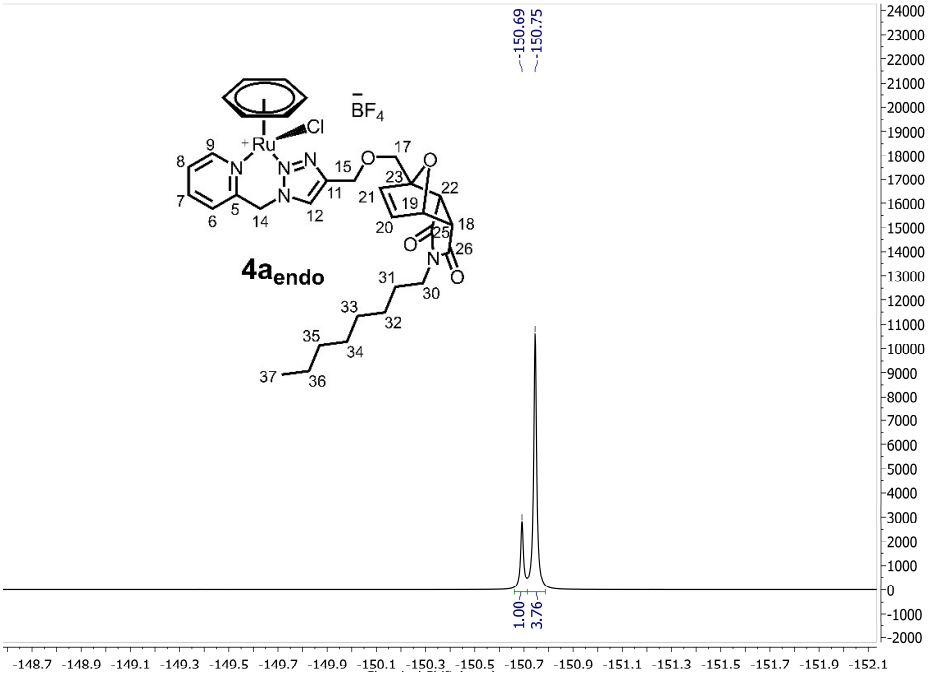

$^{19}F\{^{1}H\}$ NMR spectrum of **4a$_{endo}$** (acetone-d_6).

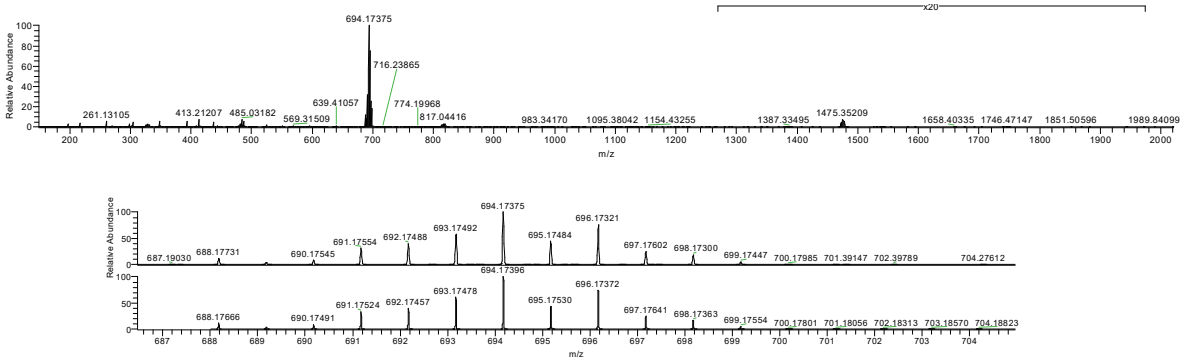

HR-ESI-MS spectrum of **4a** (**4a$_{endo}$**/**4a$_{exo}$** : 1.7/1), positive mode

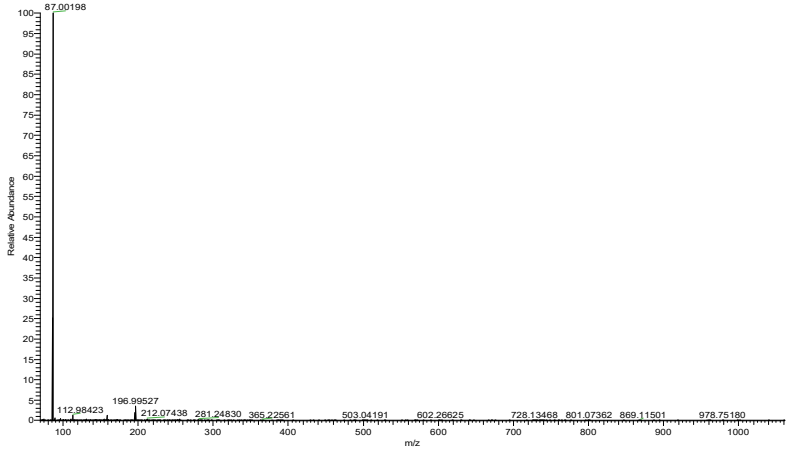

HR-ESI-MS spectrum of **4a** (**4a$_{endo}$**/**4a$_{exo}$** : 1.7/1), negative mode.

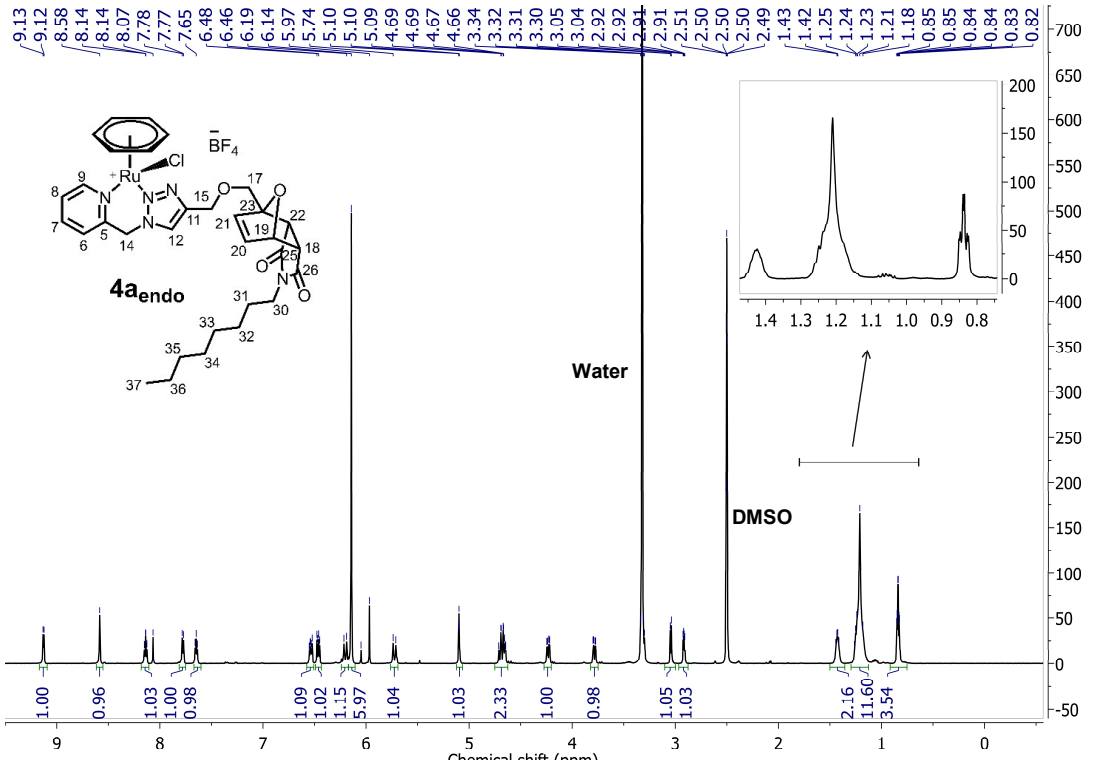

^{1}H NMR spectrum of **4a$_{endo}$** in DMSO-d_6 after 48h at room temperature.

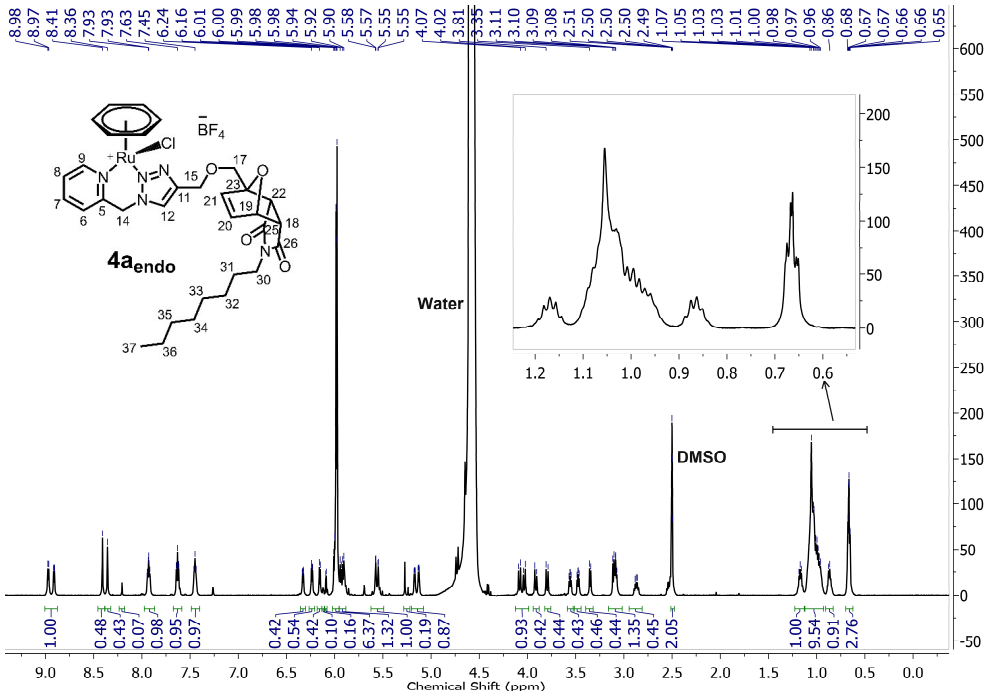

^{1}H NMR spectrum of **4a$_{endo}$** in D_2O containing 1% DMSO-d_6 (110 mM NaCl) after 2h at room temperature.

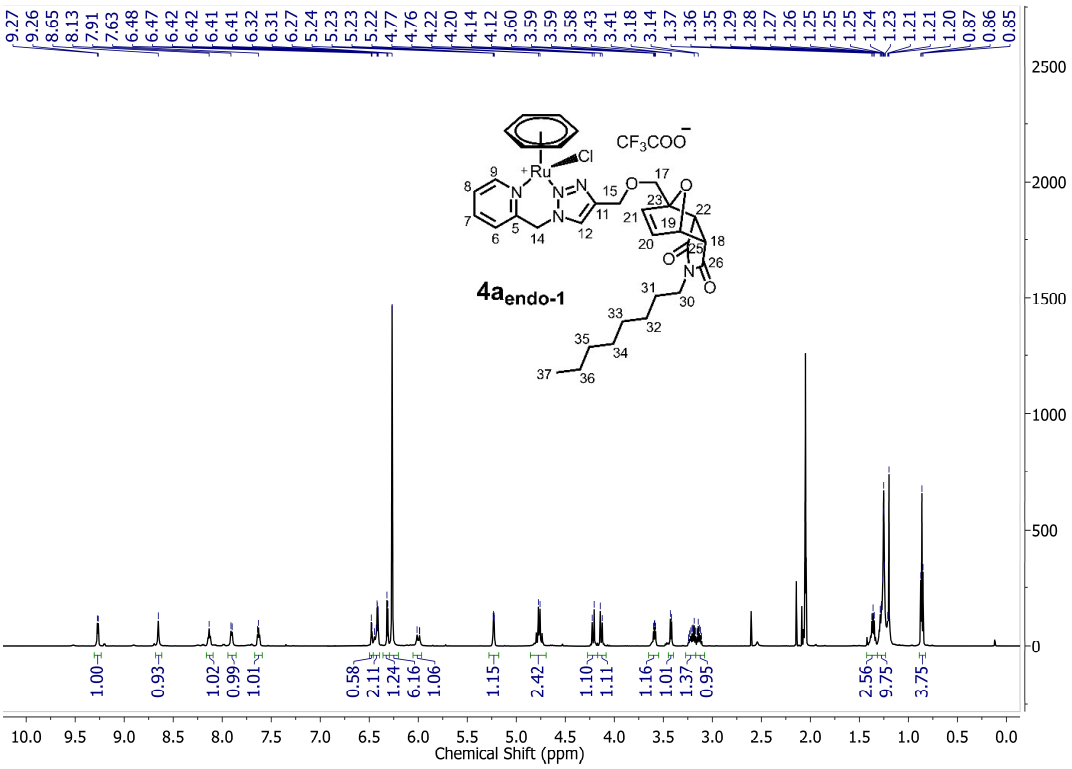

^{1}H NMR spectrum of **4a$_{endo-1}$** (acetone-d_6) (with trifluoroacetate counterion).

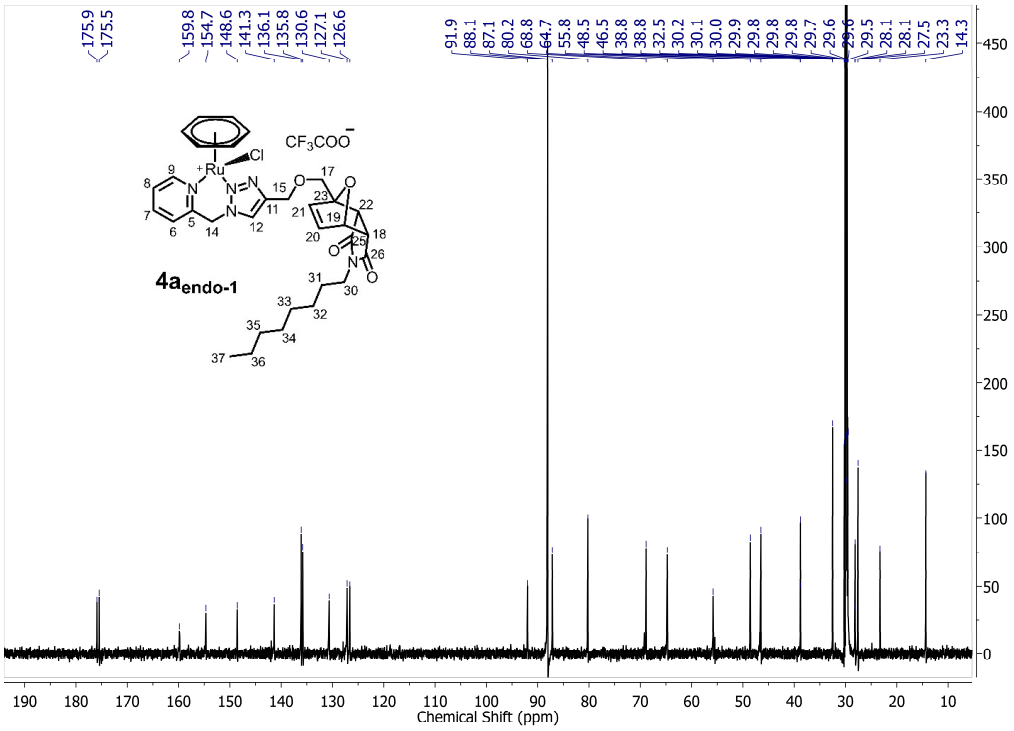

^{13}C{^{1}H} NMR spectrum of **4a$_{endo-1}$** (acetone-d_6) (with trifluoroacetate counterion).

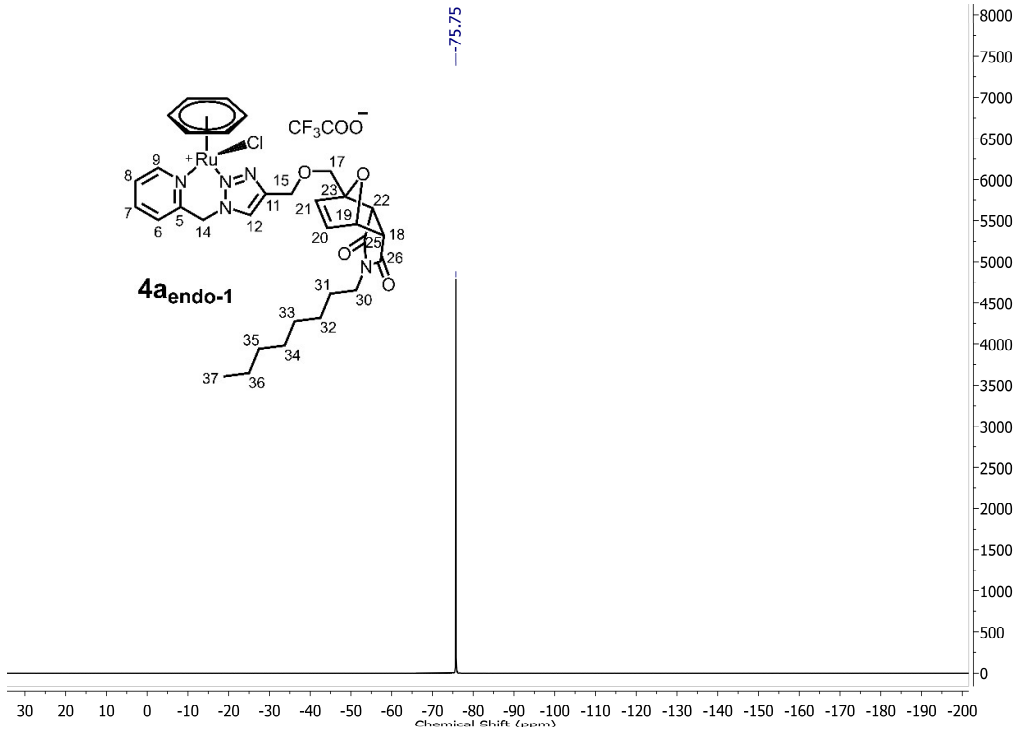

$^{19}F\{^{1}H\}$ NMR spectrum of **4a**$_{\textbf{endo-1}}$ (acetone-d_6) (with trifluoroacetate counterion).

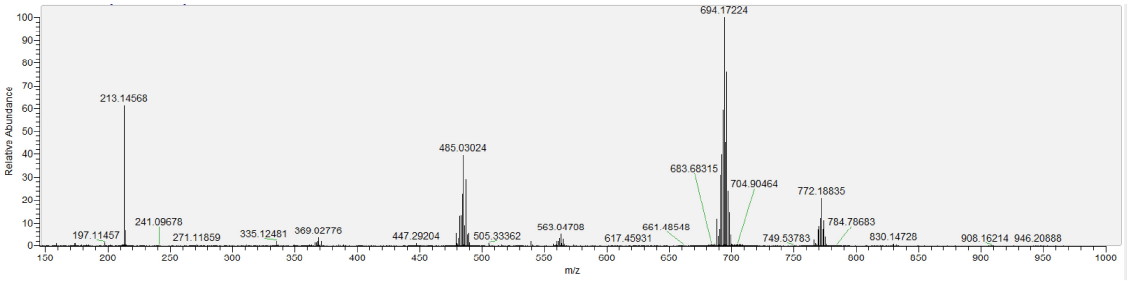

HR-ESI-MS spectrum of **4a**$_{\textbf{endo-1}}$, positive mode (with trifluoroacetate counterion).

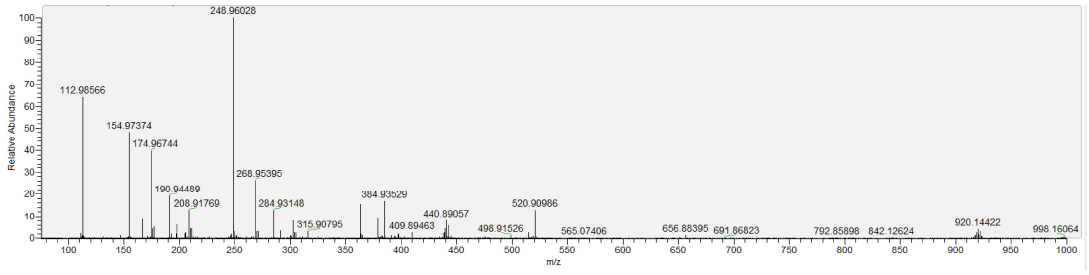

HR-ESI-MS spectrum of **4a**$_{\textbf{endo-1}}$, negative mode (with trifluoroacetate counterion).

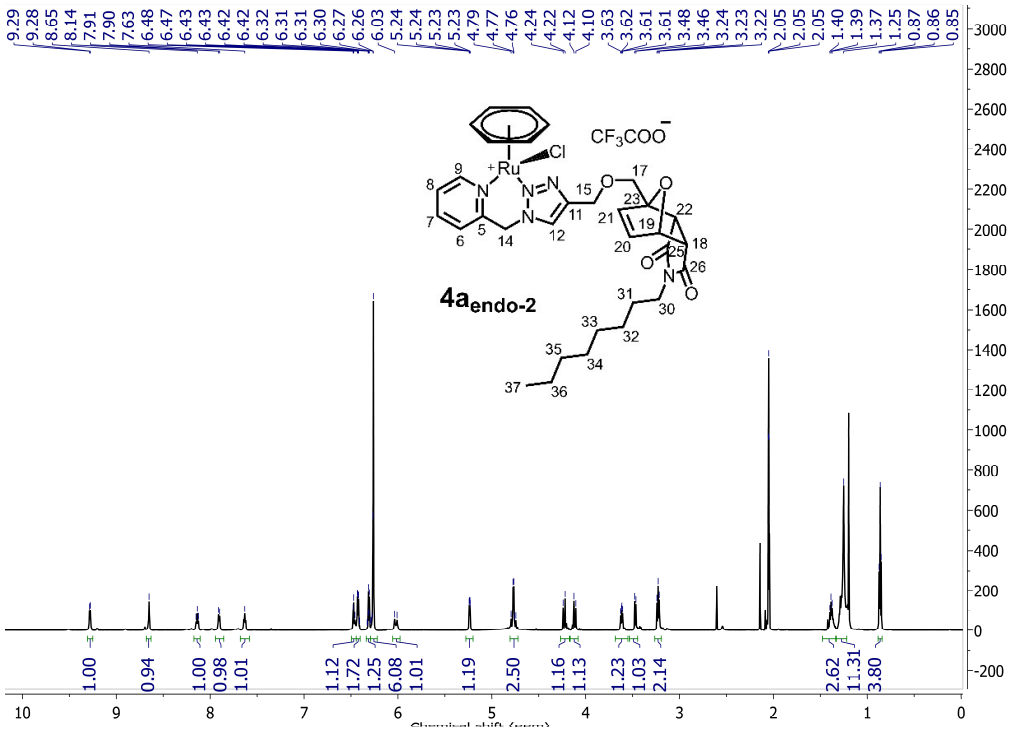

^{1}H NMR spectrum of **4a$_{endo-2}$** (acetone-d_6) (with trifluoroacetate counterion).

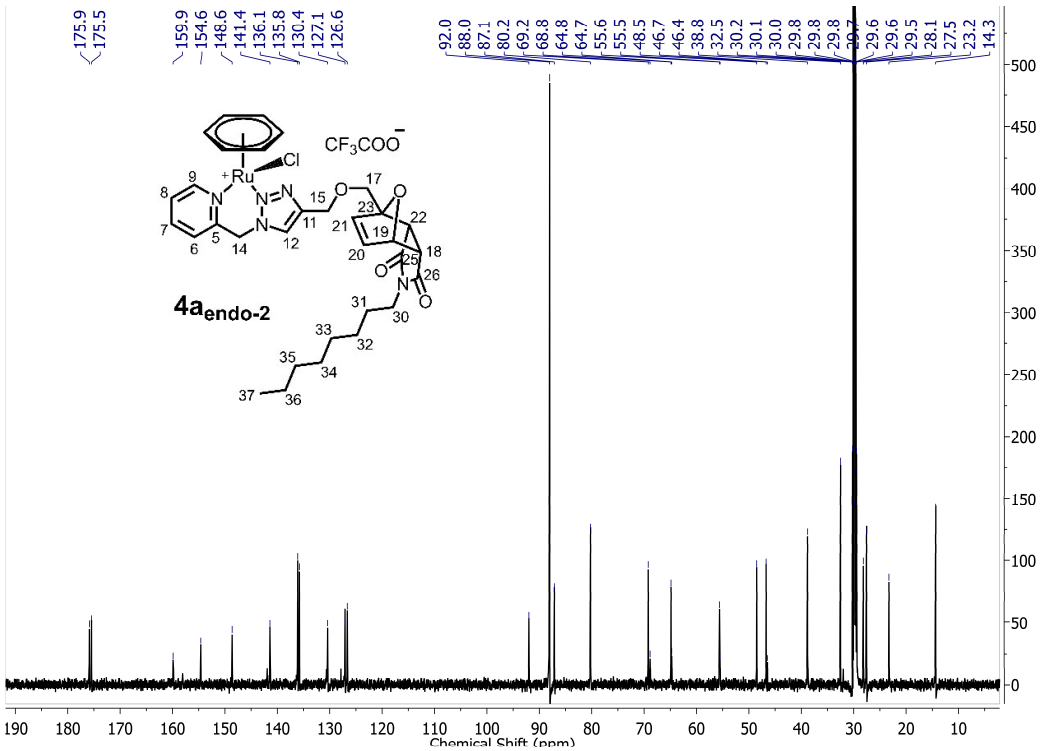

^{13}C{^{1}H} NMR spectrum of **4a$_{endo-2}$** (acetone-d_6) (with trifluoroacetate counterion).

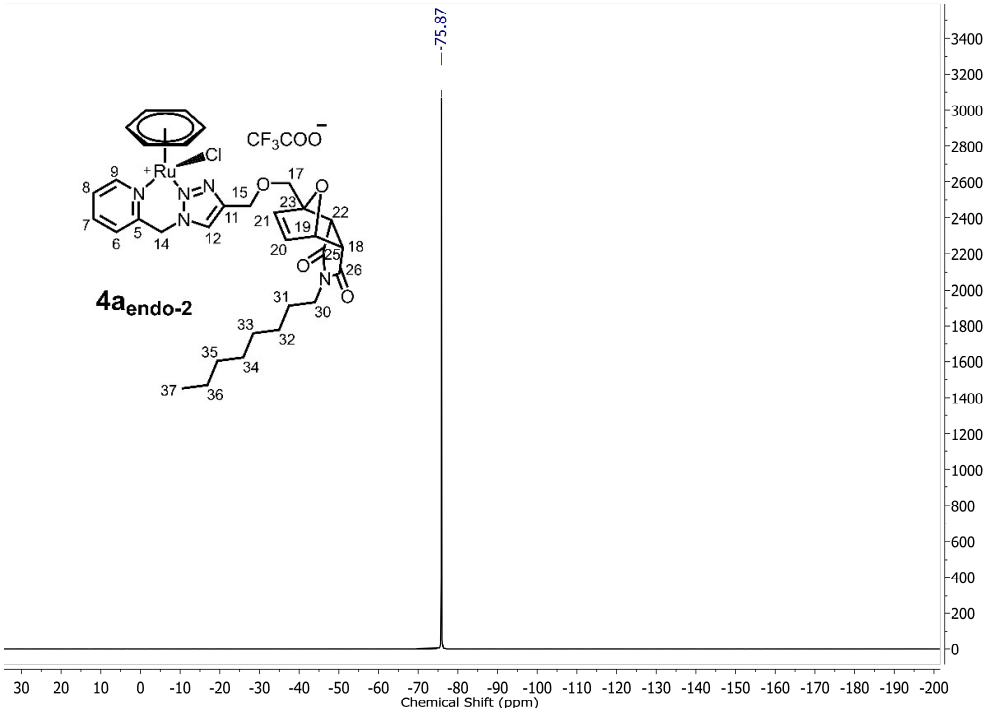

$^{19}F\{^{1}H\}$ NMR spectrum of **4a**$_{\textbf{endo-2}}$ (acetone-d_6) (with trifluoroacetate counterion).

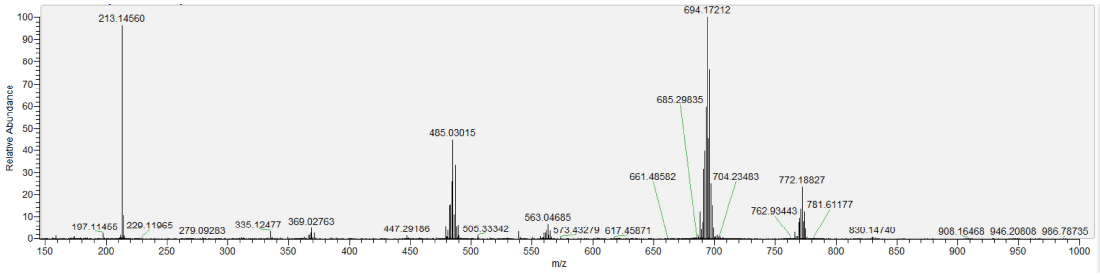

HR-ESI-MS spectrum of **4a**$_{\textbf{endo-2}}$, positive mode (with trifluoroacetate counterion).

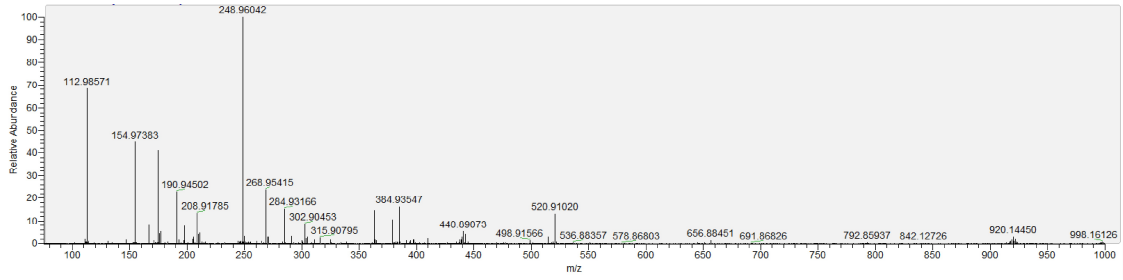

HR-ESI-MS spectrum of **4a**$_{\textbf{endo-2}}$, negative mode (with trifluoroacetate counterion).

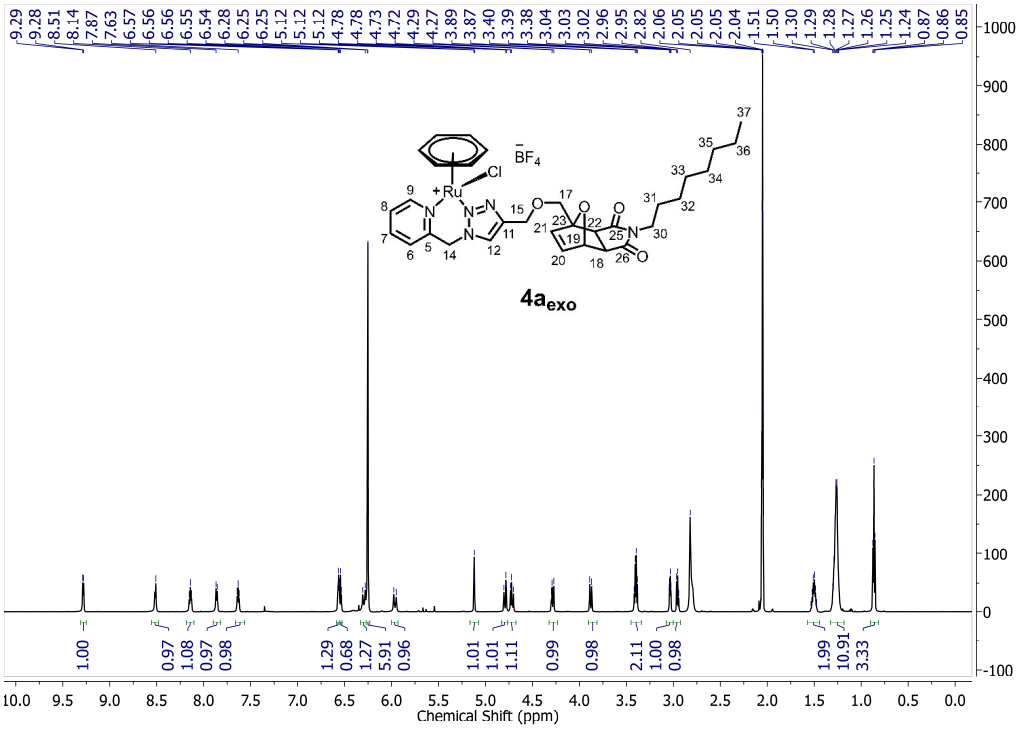

^{1}H NMR spectrum of **4a$_{exo}$** (acetone-d_6).

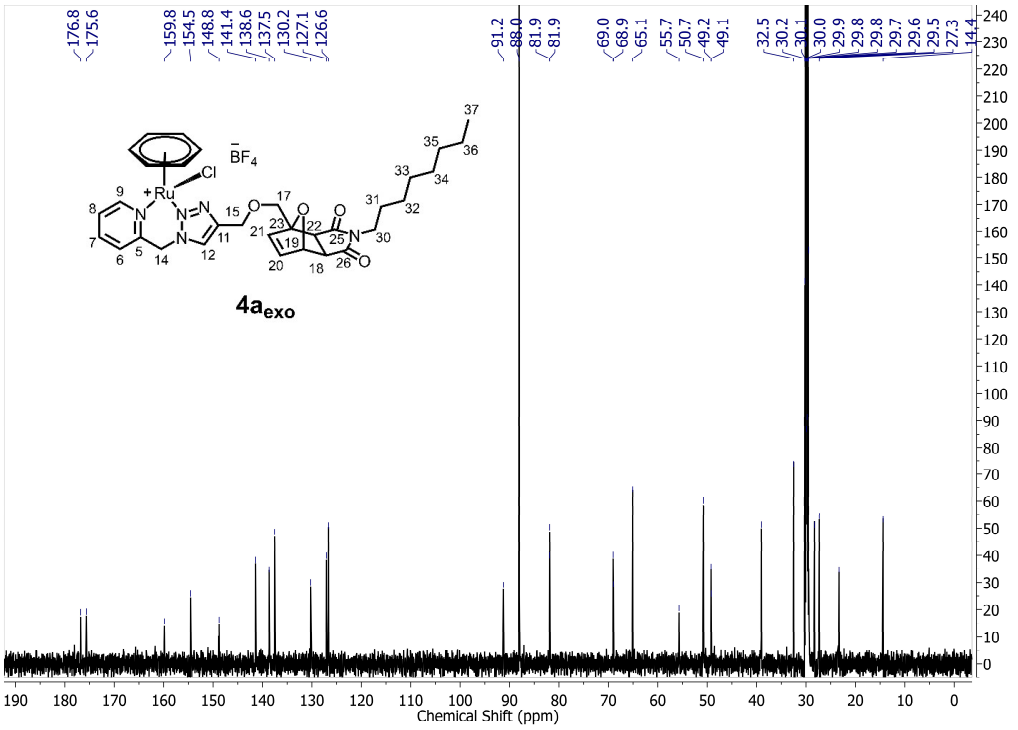

^{13}C{^{1}H} NMR spectrum of **4a$_{exo}$** (acetone-d_6).

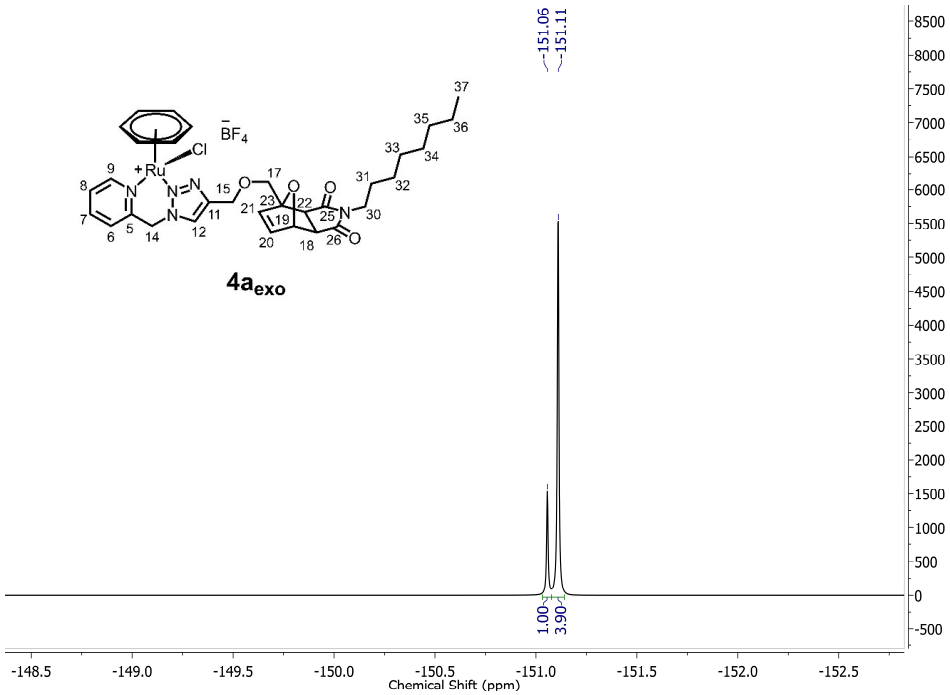

4a$_{exo}$

$^{19}F\{^{1}H\}$ NMR spectrum of **4a$_{exo}$** (acetone-d_6).

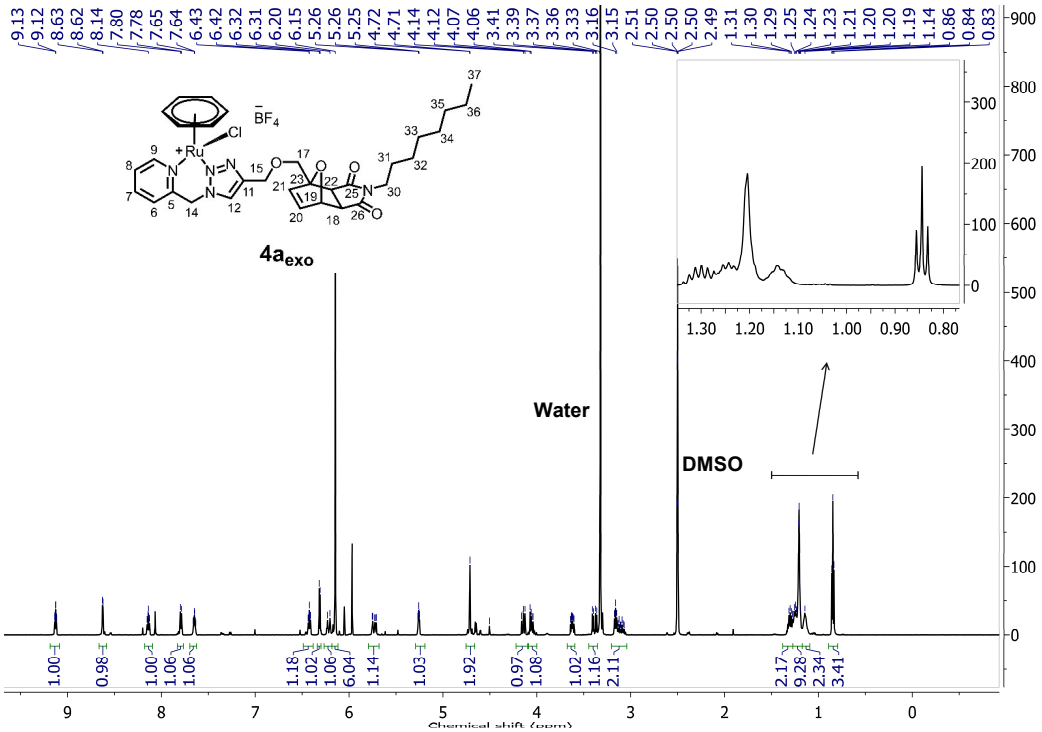

^{1}H-NMR spectrum of **4a$_{exo}$** in DMSO-d_6 after 48h at room temperature.

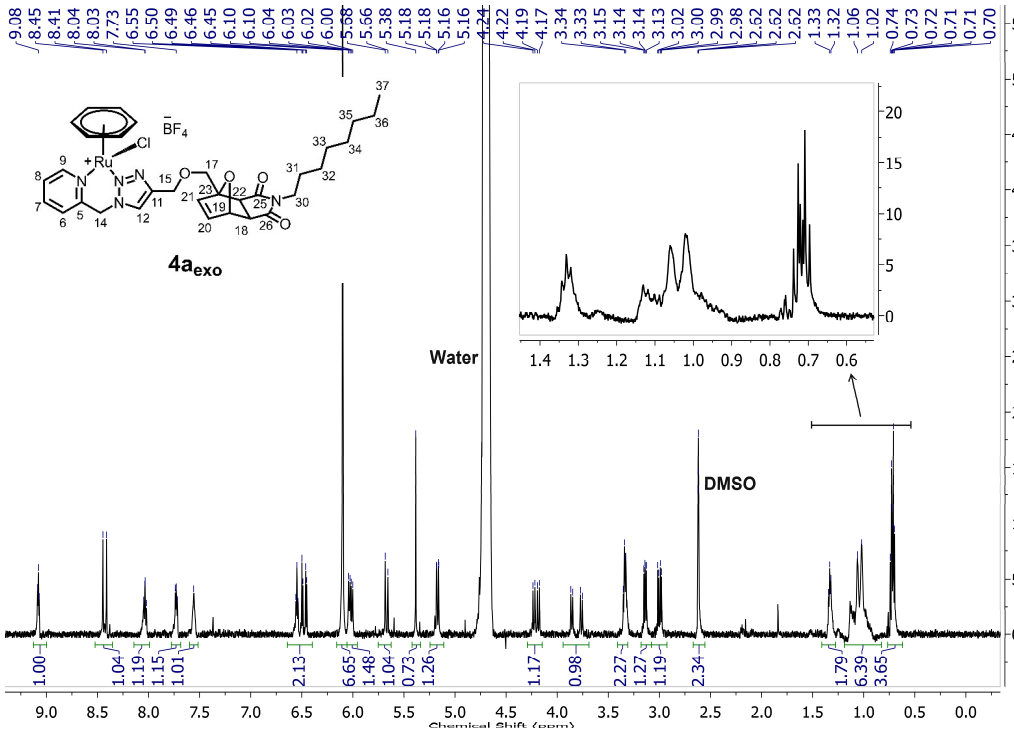

^{1}H-NMR spectrum of **4a$_{exo}$** in D_2O containing 1% DMSO-d_6 (110 mM NaCl) after 2h at room temperature.

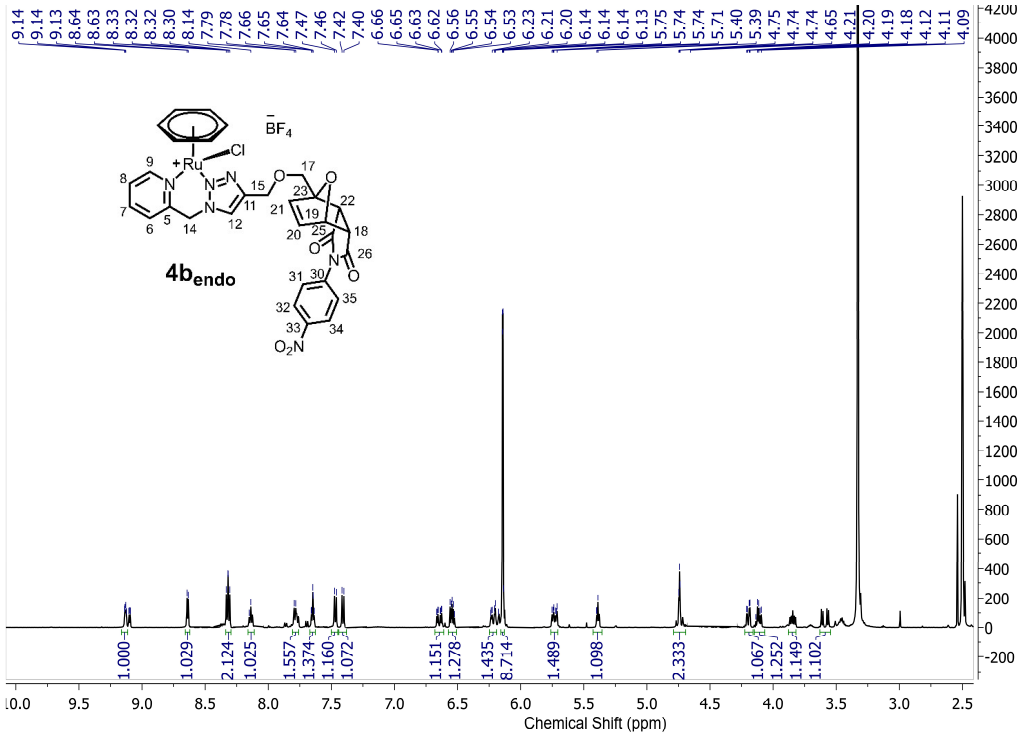

^{1}H NMR spectrum of **4b$_{endo}$** (DMSO-d_6).

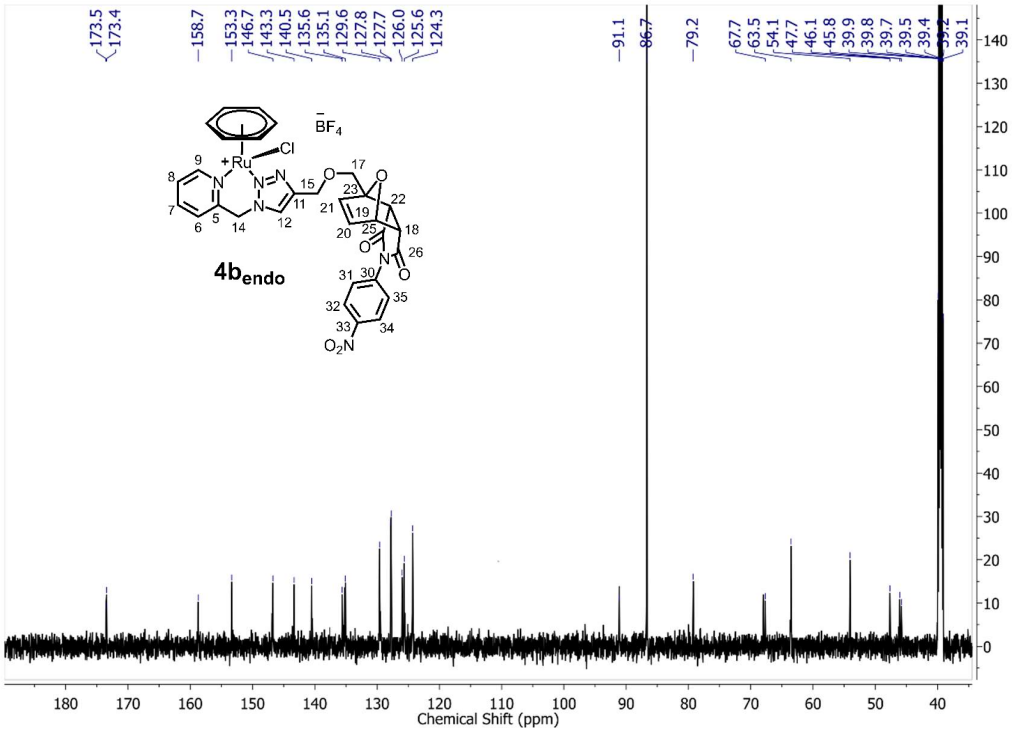

^{13}C{^{1}H} NMR spectrum of **4b$_{endo}$** (DMSO-d_6).

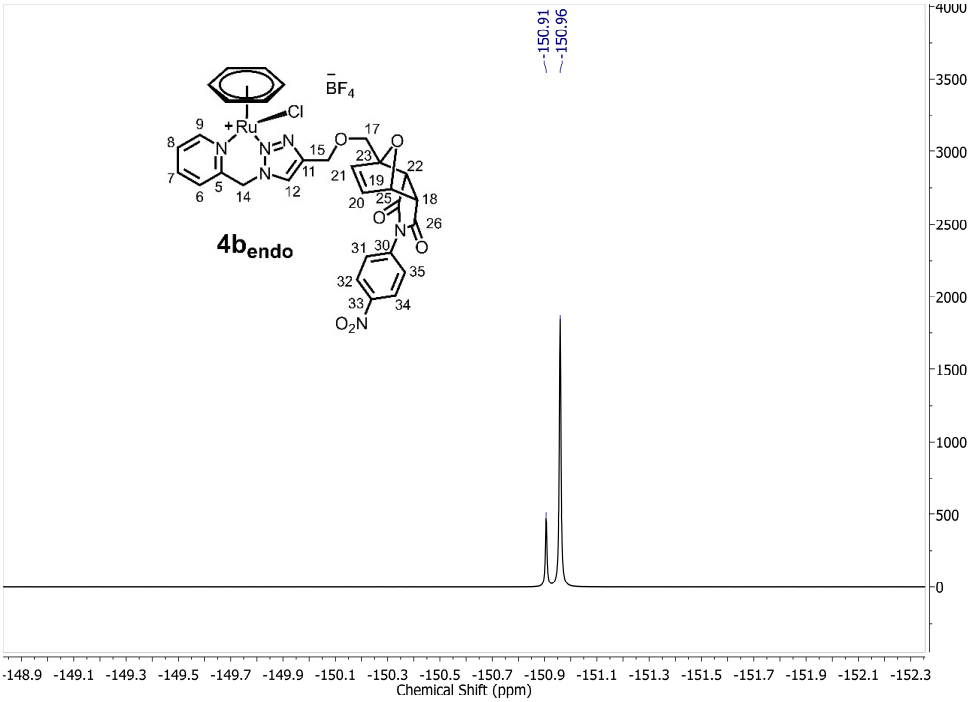

$^{19}F\{^{1}H\}$ NMR spectrum of **4b$_{endo}$** (acetone-d_6).

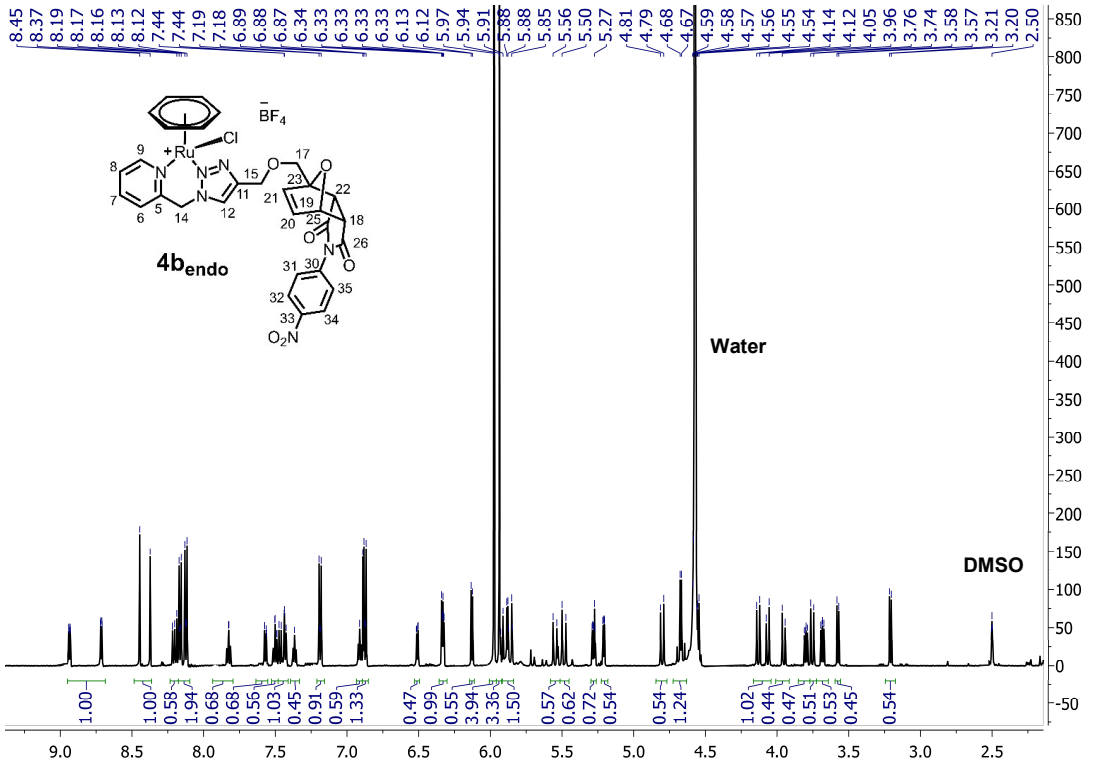

^{1}H-NMR spectrum of **4b$_{endo}$** in D_2O containing 1% DMSO-d_6 (110 mM NaCl) after 2h at room temperature.

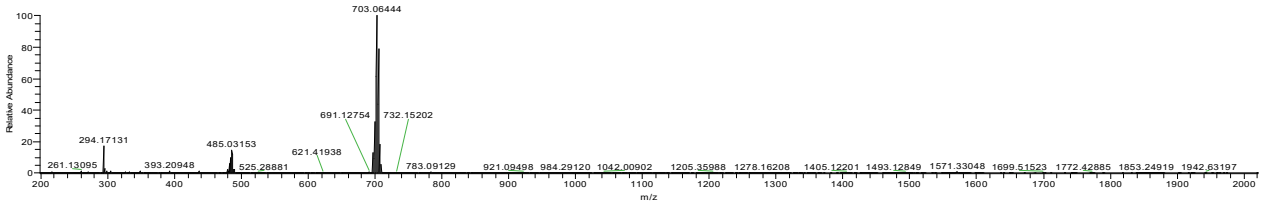

HR-ESI-MS of **4b** (**4b$_{endo}$**/**4b$_{exo}$** : 1/3.8), positive modes.

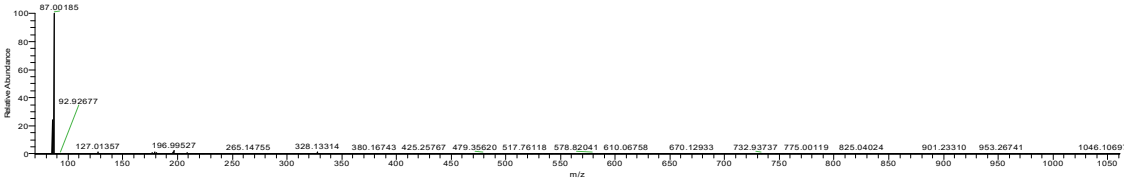

HR-ESI-MS of **4b** (**4b$_{endo}$**/**4b$_{exo}$** : 1/3.8), negative modes.

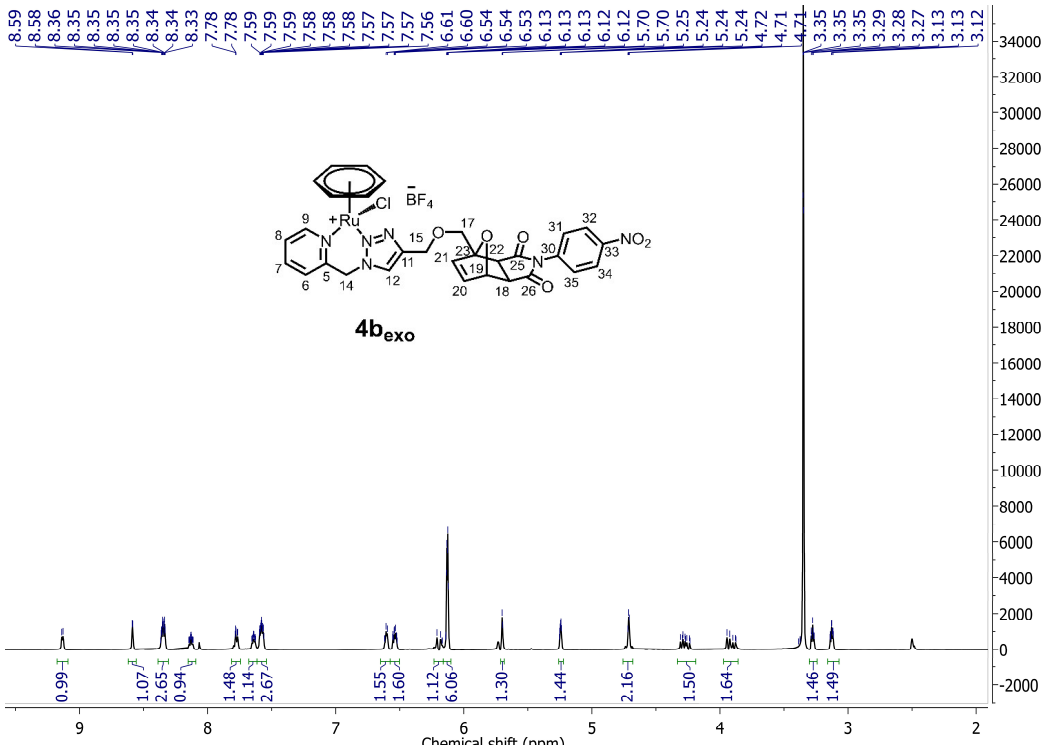

^{1}H NMR spectrum of **4b$_{exo}$** (DMSO-d_6).

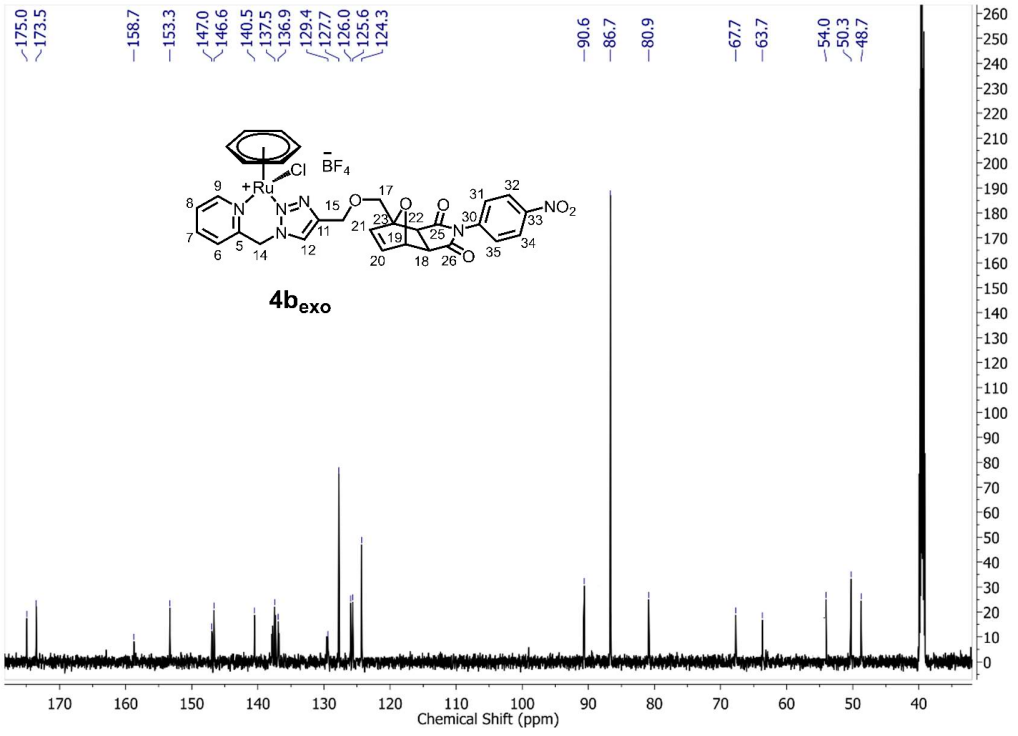

^{13}C{^{1}H} spectrum of **4b$_{exo}$** (DMSO-d_6).

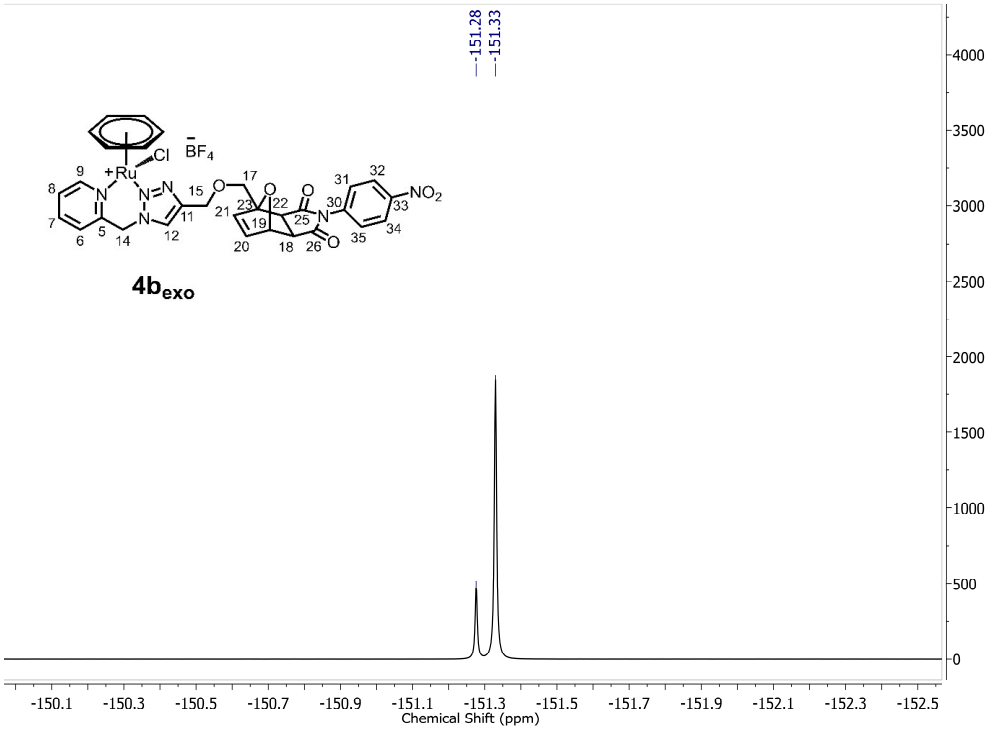

$^{19}F\{^{1}H\}$ NMR spectrum of **4b$_{exo}$** (acetone-d_6).

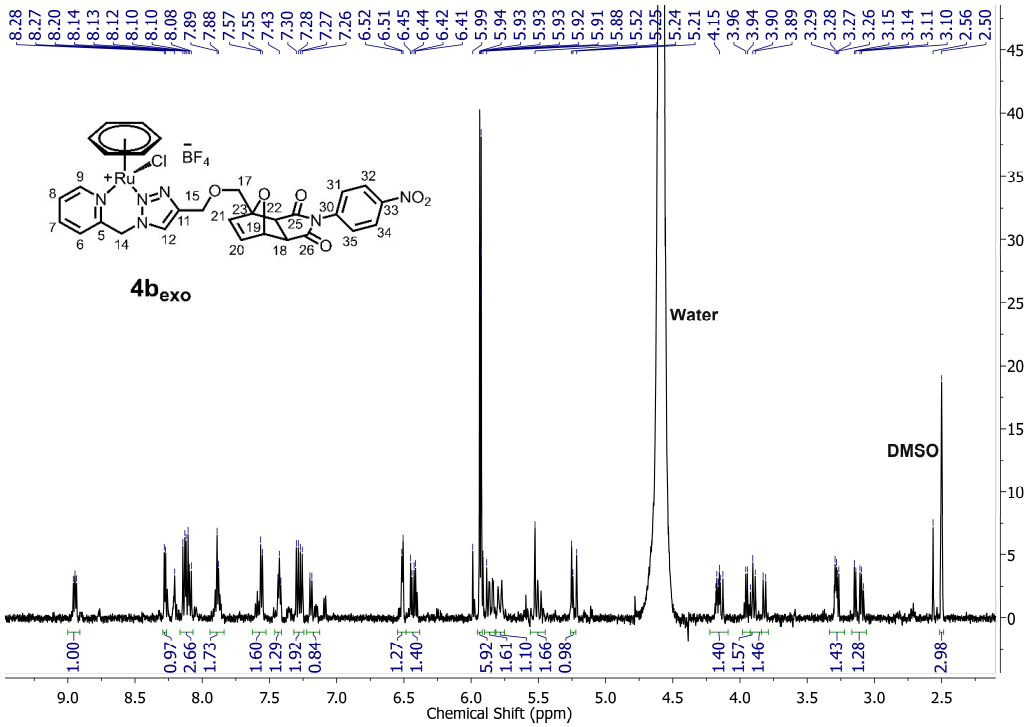

^{1}H-NMR spectrum of **4b$_{exo}$** in D_2O containing 1% DMSO-d_6 (110 mM NaCl) after 2h at room temperature.

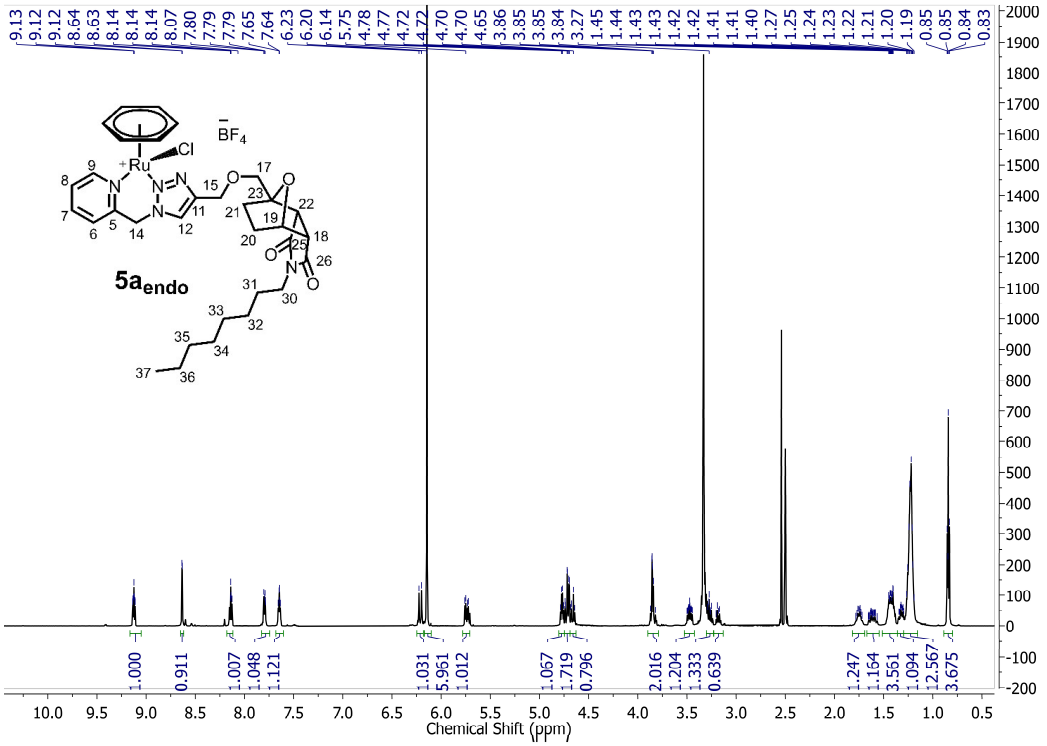

^{1}H NMR spectrum of **5a$_{endo}$** (DMSO-d_6).

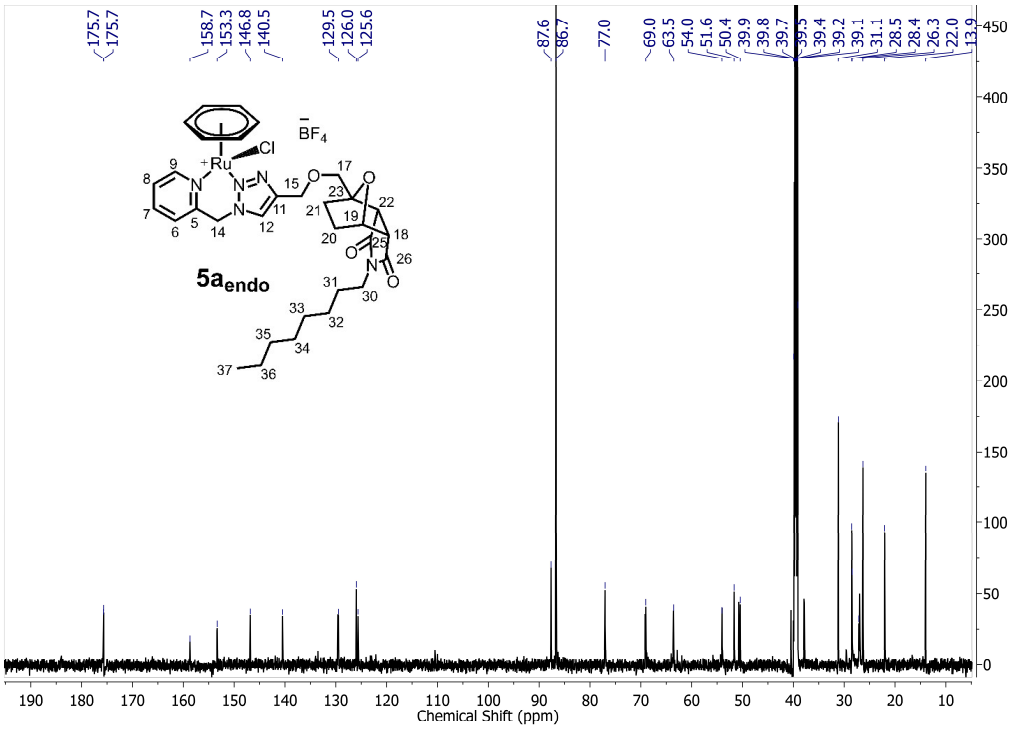

^{13}C{^{1}H} NMR spectrum of **5a$_{endo}$** (DMSO-d_6).

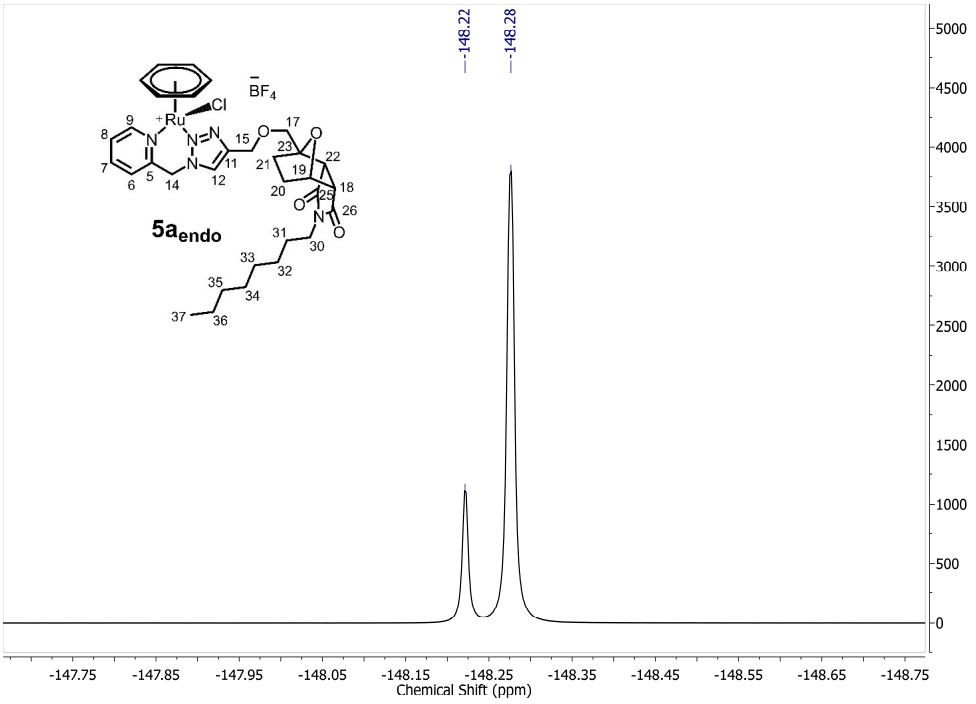

$^{19}F\{^{1}H\}$ NMR spectrum of **5a**$_{endo}$ (DMSO-d_6).

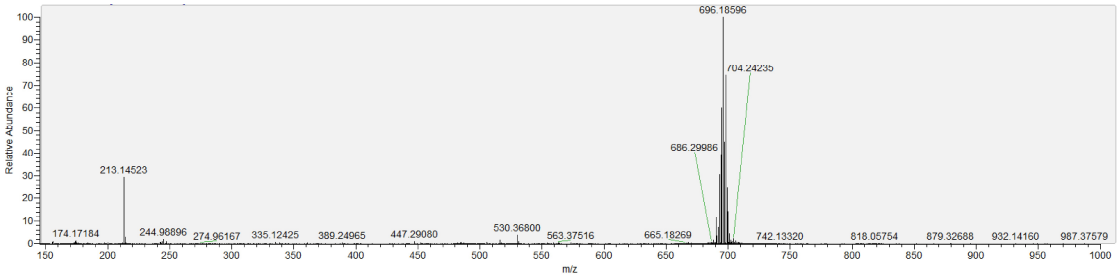

HR-ESI-MS of **5a** (**5a**$_{endo}$/**5a**$_{exo}$: 1.7/1), positive modes.

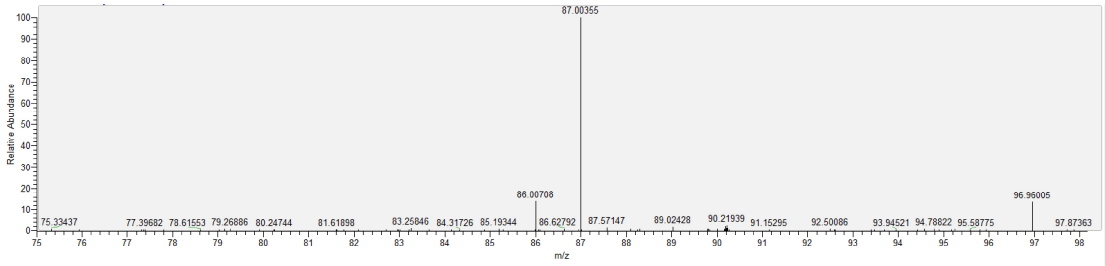

HR-ESI-MS of **5a** (**5a**$_{endo}$/**5a**$_{exo}$: 1.7/1), negative modes.

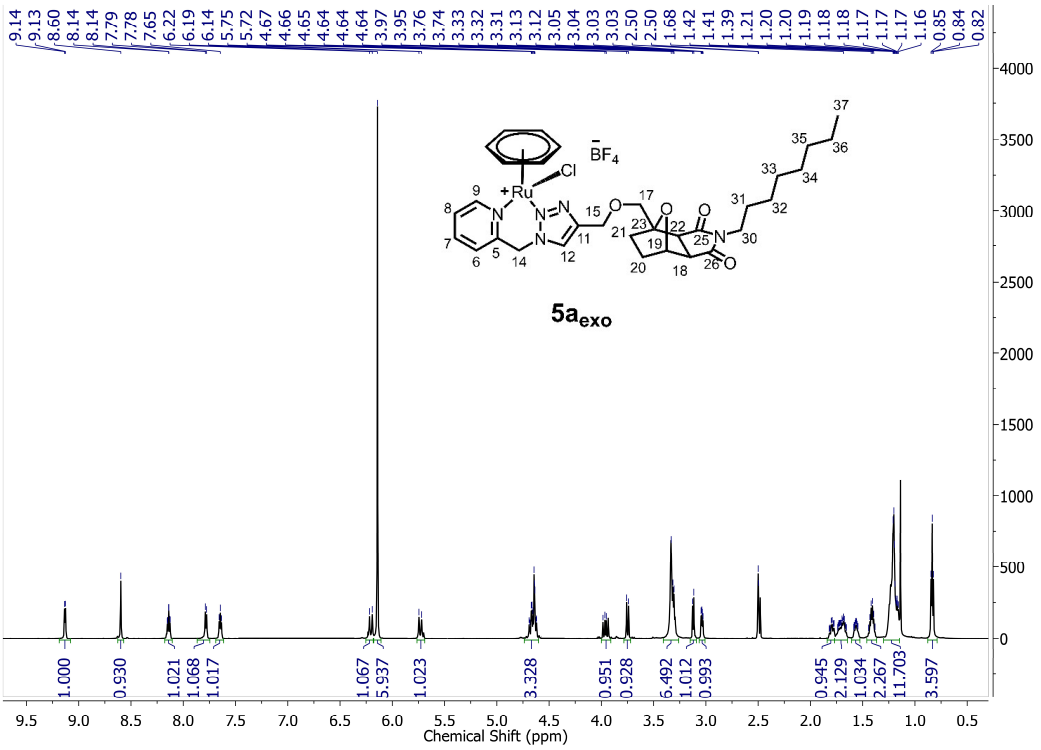

^{1}H NMR spectrum of **5a$_{exo}$** (DMSO-d_6).

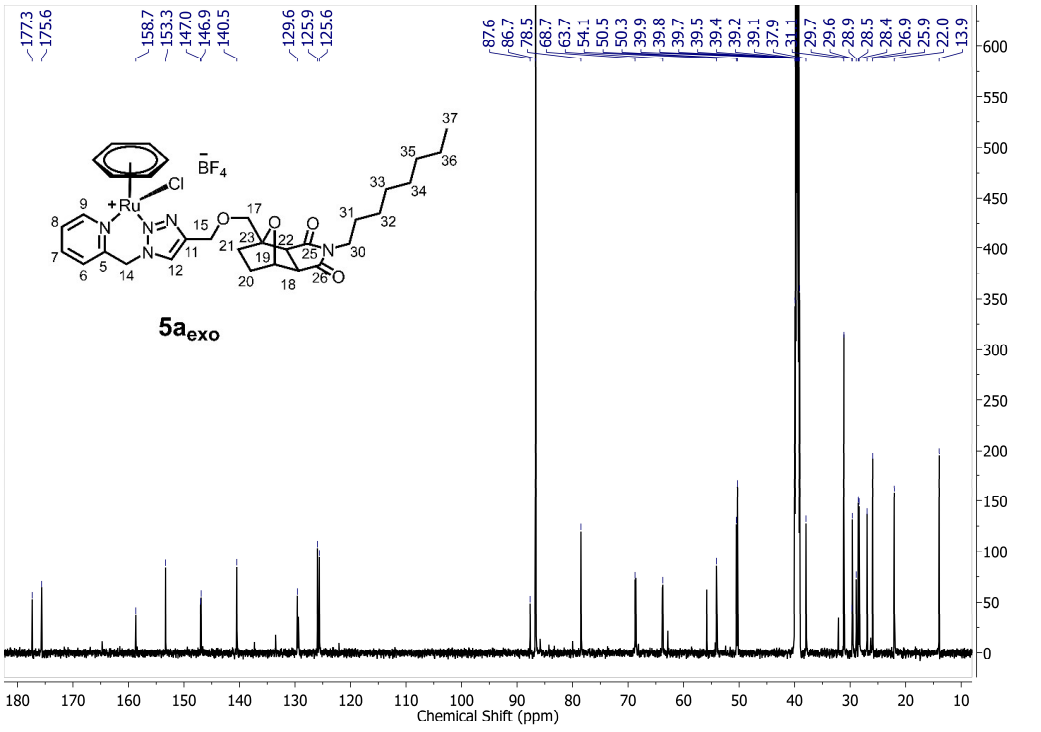

^{13}C{^{1}H} NMR spectrum of **5a$_{exo}$** (DMSO-d_6).

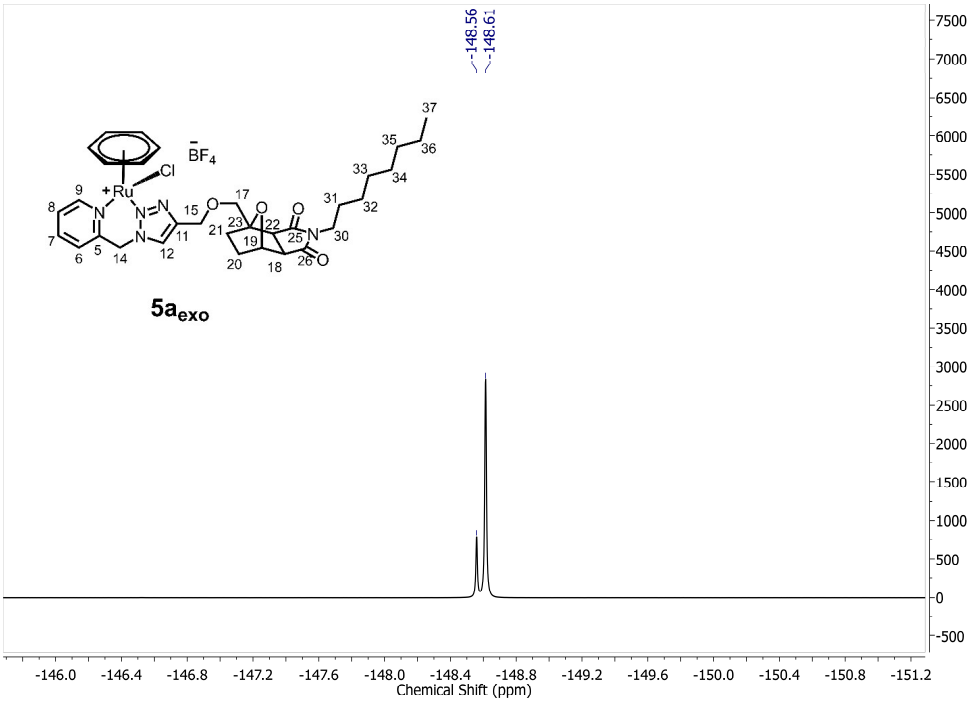

$^{19}F\{^{1}H\}$ NMR spectrum of **5a$_{exo}$** (DMSO-d_6).

REFERENCES

1. G. Scheldrick, *Acta Crystallogr., Sect. A: Found. Adv.*, 2015, **71**, 3-8.
2. G. Sheldrick, *University of Göttingen, Göttingen, Germany*, 2016.
3. I. V. Tetko, J. Gasteiger, R. Todeschini, A. Mauri, D. Livingstone, P. Ertl, V. A. Palyulin, E. V. Radchenko, N. S. Zefirov and A. S. Makarenko, *J. Comput. Aided Mol. Des.* , 2005, **19**, 453-463.
4. VCCLAB, *Journal*, 2005.
5. J. J. Wilson and S. J. Lippard, *J. Med. Chem.*, 2012, **55**, 5326-5336.
6. M. Bennett and T. Matheson, *J. Organomet. Chem.*, 1979, **175**, 87-93.
7. A. S. Kalgutkar, B. C. Crews and L. J. Marnett, *J. Med. Chem.*, 1996, **39**, 1692-1703.
8. M. Sortino, V. Cechinel Filho, R. Corrêa and S. Zacchino, *Bioorg. Med. Chem.*, 2008, **16**, 560-568.
9. L. Cao and L. Isaacs, *Org. Lett.*, 2012, **14**, 3072-3075.
10. M. D. Ogden, C. L. Hoch, S. I. Sinkov, G. P. Meier, G. J. Lumetta and K. L. Nash, *J. Solution Chem.*, q2011, **40**, 1874-1888.
11. V. Vichai and K. Kirtikara, *Nat. Protoc.*, 2006, **1**, 1112.